Manifestation of Quantum Fluctuations in Strongly Correlated Systems

A Dissertation
Presented to the Faculty of the Graduate School
of
Yale University
in Candidacy for the Degree of
Doctor of Philosophy

by
Anatoli Polkovnikov

Dissertation Director: Subir Sachdev

December 2003

ProQuest Information and Learning Company
300 North Zeeb Road
P.O. Box 1346
Ann Arbor, MI 48106-1346

Abstract

Manifestation of Quantum Fluctuations in Strongly Correlated Systems

Anatoli Polkovnikov

2003

The work underlying the thesis is an attempt to study possible signatures of quantum fluctuations in strongly correlated systems and relate them to some existing and future experiments. There are two basic parts. The first one focuses on static properties of high temperature superconductors. In particular, we study the scattering of quasiparticles on magnetic impurities and on dynamical collective spin fluctuations. We show that if the spin-spin interaction strength between quasiparticles and defects is large enough then quantum fluctuations lead to the Kondo effect. The Kondo screening strongly renormalizes the scattering matrix of the electrons on the impurity and results in the appearance of low energy resonances detectable by tunneling microscopy. We show that near the critical coupling the impurity behaves as a scatterer in the unitarity limit. The second part of the work focuses on nonequilibrium dynamics of interacting bosons confined in a periodic lattice. We examine the range of validity of the classical evolution for some experimentally relevant situations . We discuss dynamical restoration of coherence in such a system after a sudden increase of the tunneling amplitude and in the absence of energy relaxation. We also describe behavior of the condensate near the point of classical instability and argue that quantum fluctuations can drive the system into a macroscopically entangled state. At the end we show how to generalize classical Gross-Pitaevskii dynamics systematically including quantum fluctuations.

Contents

List of Figures

Acknowledgments

First of all I would like to thank my advisor Subir Sachdev for his guidance, collaboration and support in all stages of my research. Hardly any of the presented results would ever be possible without his advices or direct involvement.

I am extremely grateful to Steven Girvin, collaboration with whom on the work related to the second part of the thesis was crucial for understanding the physical picture.

I benefited a lot from collaboration with Matthias Vojta on the work related to high-temperature superconductors.

I acknowledge numerous discussions related to this dissertation, which I was fortunate to have during my research. In particular, I would like to thank I. Aleiner, H. Alloul, E. Altman, W. Atkinson, I. Carusotto, A. Clerk, S. Davis, E. Demler, M. Kasevich, A. Melikidze, V. Oganesyan, K. Park, D. Scalapino, K. Sengupta, and A. Tuchman.

I am very grateful to the staff and faculty at the department of physics at Yale University for giving me the opportunity to study here. These were wonderful years of my life.

And last, but not the least, I want to thank my wife Irina and my son Ilya for the love, tolerance and inspiration, which they have constantly given to me.

Chapter 1

Introduction

Throughout several decades, the effects of quantum fluctuations on various properties of many-body systems at low temperatures have been particularly attractive for both theoretical and experimental studies, especially in the case of strong interactions, where it is particularly hard to deal with the problems. Among the topics which were extensively studied recently we mention various quantum phase transitions [131], fractional quantum hall effect [126], high-temperature superconductivity [111], transport through quantum dots [56], problems of quantum measurements [27], equilibrium and non-equilibrium properties of Bose-Einstein condensates [92], quantum entanglement and applications to quantum computing [149], and many more. The main obstacle in addressing all these issues is the importance of both interactions and quantum effects. So except for a very limited class of exactly solvable problems, approximate methods have to be used. Some of the most successful approaches to equilibrium problems include various mean-field theories with possible lowest order corrections in fluctuations (see e.g. [99]), quantum Monte-Carlo algorithms [30], renormalization and numerical renormalization group theories [96, 164], and dynamical mean field theory [55]. Various methods are usually designed for

specific kinds of the problems. For example, renormalization group analysis is particularly suitable for studying continuous phase transitions, where the properties are universal and can be described by few renormalized coupling constants. On the other hand, appropriate mean field theories usually capture very well key aspects of the possible phases of the system, but fail to describe fluctuations near phase transitions. Besides it is usually extremely hard to check the validity of the mean field results. The situation becomes even more complicated and much less studied for the case of nonequilibrium problems. Very well understood linear response theory is appropriate only for systems close to the thermal equilibrium [42]. Quantum-kinetic equations can successfully deal with some out of equilibrium problems but are very complicated and restricted to the systems close to some kind of steady state [99]. The Keldysh technique proves to be very powerful for many different situations [76]. However, ultimately this approach, like any diagrammatic technique, is limited by smallness of interactions and complexity of the computations. Among recently developed methods it is worth mentioning the reformulation of quantum evolution in terms of classical stochastic equations [21]. So far such a mapping exists only for a limited number of hamiltonians, but this field is intensively developed at present. Somewhat similar stochastic methods are also very useful for studying open systems interacting with bath degrees of freedom [53].

After this brief overview let us describe in some more detail the main motivation for the work presented here. It consists of two main parts. In the first one we study scattering of quasiparticles in high temperature superconductors by isolated defects. Quantum effects manifest themselves through Kondo screening and through possible coupling to the virtual dynamical fluctuations of other collective degrees of freedom. In the second part we focus on the non-equilibrium temporal behavior of strongly correlated Bose systems. There we study how quantum scattering affects semiclas-

sical (Gross-Pitaevskii) dynamics and develop a perturbation theory in powers of Planck's constant. In both parts we will describe in some detail experimental consequences of the theoretical analysis and emphasize the difference between classical and quantum results.

1.1 Defects in high temperature superconductors

Since their discovery in 1986 [14], high temperature superconductors (HTSCs) have attracted lots of theoretical and experimental activity. However, apart from a few well established facts, there is still a lot of controversy about them. At present there is no fully consistent and accepted theoretical framework, which would describe their properties. The only thing which is clear about cuprates is that their phase diagram is extremely complicated and contains a number of conventional and unconventional phases. In this prospect local defects can become a very important probe of the underlying electronic structure of HTSC materials. Indeed, a number of recent scanning tunneling microscopy (STM) experiments discovered interesting properties of the quasiparticle behavior near isolated defects. Thus imaging of the electron density of states (DOS) near Ni [71, 72] and Zn [114] impurities as well as unidentified local defects [168] showed the presence of the low energy resonance states with Friedel-like oscillations. It turns out that for gapless quasiparticles, e.g. nodal fermions in d-wave superconductors, it is possible to obtain low energy resonances in the presence of a very strong potential scatterer [12, 137, 138]. So it was quite natural to assume that those resonances were the ones experimentally observed [100, 101]. However, it turns out that the direct potential or magnetic scattering give spatial pattern which is complementary to what was observed in experiments [48]. The only way to reconcile this with the simple theory is to assume some kind of extra d-wave mixing of

the electronic orbitals in the copper layer with the Bi atoms on the surface of the superconductor [101]. There are no independent verifications of this idea so far. On the other hand, a different group of experiments using nuclear magnetic resonance detected a Kondo-like effect in cuprates doped by Zn, Ni or Li impurities both above and below T_c [15, 16, 97, 98, 103], and an uncompensated spin $S = 1/2$ was observed near the Zn impurity [75]. The Kondo screening was also a very likely explanation of the specific heat data in Zn-doped $YBa_2Cu_3O_{6.95}$ compounds [145]. Moreover the characteristic Kondo scale was very close to the low energy resonance observed in STM experiments. The emergence of an uncompensated moment near a spinless impurity was also predicted in a number of theoretical papers [84, 107, 129, 162] due to proximity to the antiferromagnetic state and enhancement of the spin fluctuations near the defect. These all led us to believe that the Kondo physics should play a very important role in the observed STM data [118, 122]. Later a number of other theoretical papers addressed the same issue [155, 175]. Besides experimental motivation, the study of the Kondo effect in d-wave superconductors has some purely theoretical interest. It is well known that in conventional metals, even infinitesimal antiferromagnetic coupling of electrons with a single impurity causes the Kondo effect at sufficiently low temperatures [62]. However, this is not necessarily true if the density of quasiparticle states vanishes at the Fermi level [23, 24, 73, 165, 173, 176], which is the case in cuprates below T_c. In particular, there is no Kondo phase if the coupling constant is relatively small so the impurity remains effectively free. If the DOS vanishes at the Fermi surface slower than the square root of energy: $\rho(\varepsilon) \propto |\varepsilon|^r$ with $r < 1/2$, then it is possible to develop a perturbation theory in r [165], which predicts the Kondo transition at a spin-spin coupling larger than a certain critical value proportional to r. However if $r \geq 1/2$ this simple picture doesn't work. Both numerical renormalization group (NRG) [57, 155, 156] and dynamic large N multi-

channel approach [157] showed that the Kondo phase exists only if the Hamiltonian does not respect particle-hole symmetry. In the symmetric case, the spin-spin coupling always flows to zero. In our work [118, 122], which will be presented below, we attempt to describe the Kondo physics within a simple analytically tractable model and discuss its implications on the experimentally observable quantities.

Recently another series of beautiful STM experiments was performed in the cuprates. A four unit cell periodic DOS modulation was observed near isolated magnetic vortices [64]. Later, similar modulations with the same periodicity were discovered without magnetic field near isolated defects [65, 67, 68, 102]. The periodicity four is quite remarkable because it can not be explained by simple antiferromagnetic fluctuations. On the other hand neutron scattering experiments on lanthanum cuprates clearly showed the existence of period eight spin fluctuations, which can either coexist or be gapped in the superconducting phase [82, 83, 89, 90]. The general phenomenological theory of competition between superconducting and spin-density wave (SDW) order was developed in [36, 174]. On symmetry grounds [170], collinear SDW correlations are always accompanied by charge order correlations at precisely doubled wavevectors (or half period). Assuming that this is not simply a coincidence, we developed a phenomenological model describing scattering of quasiparticles on dynamical SDWs pinned by isolated defects [119, 120, 121]. We will give a detailed discussion of the results in this thesis. There has been a different related work suggesting that the spin or charge density order is responsible for the period four oscillations [86]. There is again some controversy about interpreting the experimental data. Based on a simple analysis of the quasiparticle scattering from a point defect [161, 172], it was claimed [102] that one can reconstruct the quasiparticle Fermi surface from the STM data alone. However, as will be discussed below, the simple scattering model may be not adequate to explain the data and we discuss

how the future experiments may address this issue.

Because of unusual properties, the multiple scattering of quasiparticles on defects at low temperatures brings a lot of new interesting results. Thus it was shown that depending on the symmetry of the underlying hamiltonian, the quasiparticle density of states in the presence of multiple unitary scatterers may diverge [116], vanish [11, 140] or remain finite [177]. Unusual diffusion of quasiparticles was studied in [167]. However, all those predictions are very hard to confirm partly because the cuprate semiconductors are very inhomogeneous [69]. Therefore we believe that the single defect probes are the most effective in extracting some intrinsic electronic structure of HTSCs. Here we briefly mentioned only few experimental and theoretical results concerning high temperature superconductors. We intentionally avoided any references to numerous specific microscopic theories aiming to describe the cuprates. So far, there is no accepted view on which one is correct. The present work mostly relies on phenomenological models which contain few unknown parameters, so that the theoretical predictions can be easily compared with experiments. There are many other experimental results which are beyond the scope of this thesis. Unfortunately it seems now impossible to address all of them within one even purely phenomenological theoretical framework simply because of the complexity of different phases emerging in HTSCs. Nevertheless, even clear and unambiguous understanding of some parts of the phase diagram would be great progress in this field.

1.2 Interacting bosons in optical lattices

In the second part of the thesis we will focus on a different subfield of strongly correlated systems. While d-wave superconductors are widely believed to emerge from the fermion Hubbard model [6], very interesting physics also arises from the boson Hub-

bard model. The huge interest to interacting bosons was stimulated by experimental advances in realization of ultra-cold Bose-Einstein condensates (BECs) [5, 33, 58, 59, 112]. If the atoms are subject to an additional periodic potential coming from optical standing waves, then they form perfect bosonic crystals with no dislocations, impurities or other defects. Also, contrary to conventional condensed matter systems, one can vary the hopping amplitude between the adjacent sites of this crystal by orders of magnitude, simply by tuning intensity of the laser beam [58, 112]. Moreover, even the sign and the strength of interaction can be changed using an external magnetic field [29, 150]. Hence, one can experimentally address various phenomena without worrying about complications arising from unwanted degrees of freedom. For example, at equilibrium, the bosons can undergo a transition from a superfluid to an insulator as the strength of the optical potential is increased [4, 41, 46, 52, 74, 131]. This transition was directly tested [58], and there is no controversy in interpreting this experiment as in the case of high temperature superconductors. The simplicity of the system and relatively slow decoherence suggest possible use of interacting bosons in quantum computations [35, 95]. A very appealing idea is to encode quantum information in different sites of the optical lattice rather than in different internal atomic states [113]. In this way the measurement process and the manipulation of the information seem to be very straightforward.

Another huge advantage of the cold atomic systems is that one can address dynamic properties of the interacting atoms both theoretically and experimentally. In conventional many-body systems, strong and non-adiabatic perturbations generically lead to fast damping due to various degrees of freedom. So if one is interested in quantum effects, it is extremely hard to work far from the equilibrium. There are no such limitations, however, in the atomic systems. Indeed, in order to obtain extremely low temperatures where the atomic de Broglie wavelength becomes com-

parable with the inter-particle spacing, it is necessary to isolate the system to such an extent that it can be really thought of as completely closed. One of the examples of the strongly out of equilibrium behavior occurs when the sign of interactions changes from repulsive to attractive using Feshbach resonance [37, 77, 80]. The important issue for this class of problems from the theoretical point of view is how to take into account quantum fluctuations. The classical or Gross-Pitaevskii (GP) equations of motion can not adequately describe dynamical properties near the instabilities simply because the classical wavepacket spreads very fast. The obvious generalization comes from Bogoluibov approach [92]. However, it is good only if the instabilities are weak. There were some attempts to generalize GP equations including the interaction of the condensate with excited bosons which are produced during collapse of condensate [39, 148]. However, these approaches are not very general because they rely on specific assumptions about the evolution. Recently, there was developed another class of methods based on stochastic wavefunctions [21, 22]. These ideas look very promising, but so far the theory is applicable to a particular class of two-body interactions and it is not completely clear (at least to this author) how to generalize them. So at the moment, out of equilibrium dynamics is certainly a theoretical and experimental challenge. Feshbach resonances allow switching interaction from large positive to large negative values. Such a sudden change usually causes a collapse of the condensate, while a slow, adiabatic tuning is required to manipulate the condensates in a reversible way which preserves the coherence. Fortunately this difficulty can be easily overcome in optical lattices. The trick consists in changing the relative phase of the condensates confined in particular lattice sites [127, 146, 166]. [1] Thus in a periodic lattice the relative π phaseshift from the point of view of the dynamics is

[1] If each site contains relatively large number of bosons in the same state then they can be treated as condensates.

equivalent to the switch of the interaction sign from positive to negative [123, 124]. Moreover, it turns out that in a finite lattice a sufficiently small attractive interaction does not cause collapse of the condensate. In this way it becomes possible to drive the system adiabatically to the point of instability and check how it evolves. Then the role of quantum fluctuations becomes especially emphasized since they are responsible for initiating the wavepacket spread. We consider this process in detail in this thesis (see chapter 5). Another interesting set of experiments corresponds to the quite opposite limit, where some parameters, e.g. tunneling, change abruptly. For example, it is possible [154] to start in the insulating phase with no phase coherence and suddenly increase the hopping amplitude by orders of magnitude so that the ground state becomes superfluid. The resulting evolution, however, is quite different from what is generally expected in conventional condensed matter systems because there is no energy relaxation. It turns out that the emerging dynamics can be still described within a GP approach but only for a finite amount of time [123]. The evolution and arising limitations are described in this work (see chapter 4).

The dynamic and static properties of interacting bosons rise a very important issue of developing some generic approach to include quantum fluctuations in the classical picture. This is fairly well understood for equilibrium problems where the Bogoluibov's approximation and perturbative treatment of the interactions between quasiparticles give a consistent expansion near the classical ground state. On the other hand, such an approach is not adequate for many nonequilibrium problems simply because it is valid for a limited amount of time and it heavily relies on the stability of the classical motion. Let us give a simple intuitive example illustrating this. Suppose that there is a macroscopic ball located right on the top of the hill with a finite height, which has for example a Mexican hat like shape. Further suppose the system is isolated from any sort of external noise. Classically, the ball will stay on

the top forever. However, because of the zero point motion, it will go down along different classical paths. The quantum effects will be manifested only in certain phase relations between these paths but will not affect the motion itself. Clearly neither classical nor Bogoliubov's approach (which is equivalent to approximating the hill with an inverted paraboloid) will work in this case. Also the conventional Keldysh diagramatic technique is not very useful, as it is hard to sum all the diagrams which would contribute to a nonlinear classical dynamics. This is an extreme example, but one can think of many more where the classical approach is not sufficient, Bogoliubov's does not work, Keldysh's is very complicated, and still intuitively it is clear the motion is quite close in some sense to the classical limit. The problem with the ball is somewhat artificial, because one can just solve the Schrödinger equation exactly. On the other hand, if this ball represents some collective degree of freedom of a many-particle system, the problem becomes much harder. Here we will suggest a method showing how to include quantum fluctuations to the noneqilibrium semiclassical evolution [125]. In spirit it is somewhat similar to that developed in a series of works by Filinov *et. al.* [43, 44, 45] for interacting fermions. Another generic reason for disturbing the semiclassical equations of motion is the coupling to other degrees of freedom, which are usually represented as a thermal bath. Though as we mentioned before, the notion of the bath is not particularly useful for condensates because of their isolation, this coupling is certainly a strong mechanism of decoherence in most of condensed matter systems. A standard approach to this problem uses a representation of the bath as a set of harmonic oscillators satisfying certain physical properties. Then after integrating out environment degrees of freedom one derives Langevin equations, which are essentially classical equations of motion with extra dissipative and random force terms [19]. In thermal equilibrium both random forces coming from environmental fluctuations and dissipation are necessary.

Moreover there is a ceratin relation between them which constitutes the fluctuation-dissipation theorem [91]. The main drawback of the Langevin equations is that they can be rigorously derived only for the harmonic potential linearly coupled to the bath, i.e. in the noninteracting limit where there are no corrections to the classical equations of motion. There were some attempts to generalize these equations [70] but they did not yield a simple and tractable picture of the resulting evolution. One can think that if the classical dynamics gives a fairly good description in the isolated system then the effects of environment can be taken into account in the same spirit as described in [19]. However, it turns out to be wrong close to equilibrium and at sufficiently low temperatures [28] where the quantum effects become important at long time scales. In the last chapter of this thesis we will argue about a possible way to generalize Langevin equations to the interacting system and how to access asymptotically the zero temperature limit.

1.3 Outline of the work

- **Chapter 2**

This chapter is based on papers [118, 122]. Here we consider Kondo screening in d-wave superconductors and describe possible experimental manifestations of this effect. A simple mean-field (or large N) approximation is employed for this purposes. It gives a picture consistent with that obtained using numerical renormalization group methods. The advantage of the approach used here is that it yields transparent analytical results, which can be easily generalized to include the effects of screening by nonlocal spins, which is relevant to the experiments with Zn impurities [114]. The emerging structure of the electron density of states modulations is consistent with available experimental results and does not need extra assumptions about the

tunneling as required in the pure potential scattering model [101].

- **Chapter 3**

This chapter is entirely devoted to the discussion of the possible manifestation of the dynamic spin-density order in STM experiments performed recently by two different groups [65, 67, 68, 102]. Using a simple phenomenological model it is argued what are the main distinctions between scattering of quasiparticles on the order parameter and simple potential scattering on isolated defects. Some confusion existing in the literature on this account is discussed and further possible experiments which can distinguish the two scenarios are suggested. The results of this chapter are based on papers [119, 120, 121].

- **Chapter 4**

In this chapter we consider nonequilibrium evolution of the bosons in a lattice which were initially in the insulating (incoherent) state and were then subject to a sudden increase in the hopping amplitude. This work was motivated by yet unpublished experimental results [154]. Classical dynamics and its limitations are discussed. Surprisingly it appears that the coherence between the sites develops even in the absence of energy relaxation. We discuss the importance of the interaction strength and of the shape of the smooth confining potential profile on the dynamics. We argue that in the classical limit the system evolves towards the microcanonical ensemble satisfying initial energy and number of particles constraints. This chapter is mostly based on Ref. [123].

- **Chapter 5**

Here we focus on the evolution of the many-particle "Schrödinger cat" state. We develop a theoretical description suitable to take into account both quantum

fluctuations and highly unstable classical evolution. This approach is equivalent to the truncated Wigner approximation used in quantum optics, where one can work with classical equations of motion corresponding to a family of initial conditions distributed according to a Wigner transform of the initial density matrix. Possible limitations due to coupling to the environment are discussed at the end. This chapter relies on the results of [123, 124].

- **Chapter 6**

In this chapter we develop a general framework for the dynamics of the bosonic systems close to the classical limit. A consistent perturbation theory in $\hbar$ is suggested here. The approach goes beyond Bogoliubov's approximation and accesses the regime of arbitrary interactions, which is very hard to achieve using standard Keldysh technique. Contrary to the latter, the initial density matrix of the system in our approach is completely isolated from the dynamics and enters only as a distribution of the initial conditions. The corrections to the classical equations of motion are shown to be in the form of nonlinear response to the infinitesimal transformation of the bosonic field along the classical trajectory. Such corrections can be thought of as quantum scattering events and in diagrammatic technique, they correspond to quantum vertices. At the end of this chapter we briefly describe how to generalize Langevin equations based on this analysis.

Chapter 2

Kondo effect in d-wave superconductors

It is well known [62] that in ordinary metals any local moment antiferromagnetically coupled to quasiparticles gets screened at low temperatures below:

$$T_K \sim \frac{1}{\rho} e^{-\frac{1}{\rho J}}, \tag{2.1}$$

where ρ is the quasiparticle density of states at the Fermi level and J is the spin-spin coupling between the impurity and quasiparticles. On the other hand this effect does not occur in dielectrics or semiconductors where band electrons are gapped, simply because at low temperatures there are no free carriers. Therefore the situation with vanishing density of states becomes particularly interesting. Essentially two effects compete: the available quasiparticles try to screen the impurity as temperature is lowered, but the number of the free carriers goes to zero as $T \to 0$.

If the density of states vanishes as a small power of energy:

$$\rho(\varepsilon) \propto |\varepsilon|^r \tag{2.2}$$

with $r << 1$, it is possible to give a perturbative argument of resulting low energy

behavior of the impurity similar to "poor-man's-scaling" [7]. This has been done in [165] where it was shown that a third unstable fixed point for the interaction J appears. So that when $J < J_c$ the coupling flows to zero and there is no Kondo effect, otherwise it flows to infinity and the impurity spin gets screened. The critical coupling itself is proportional to the exponent r and vanishes if the density of states is constant. However, as we already mentioned in the introduction, if $r \geq 1/2$ this simple picture doesn't work. Both numerical renormalization group [57, 155, 156] and dynamic large N multichannel approaches [157] showed that the Kondo phase exists only if the hamiltonian does not respect the particle-hole symmetry. In the symmetric case the spin-spin coupling always flows to zero. The main difficulty of the NRG approach is that it is hard to generalize to realistic band structure and to the case of nonlocal magnetic moment. It is also restricted only to the low energy scales and does not give access to high energies, which might be important at e.g. finite temperatures. On the other hand these difficulties do not arise in simple mean field or large N theories, where both screened and unscreened phases can be easily studied. The large N approximation was first successfully applied to the Kondo problem in ordinary metals by Read and Newns [128].

The model hamiltonian of a pure superconductor to be exploited in the present work is:

$$H_0 = \sum_{\mathbf{k}} \psi_i^\dagger(\mathbf{k}) \left(\varepsilon_{\mathbf{k}} \tau_z^{ij} + \Delta_{\mathbf{k}} \tau_x^{ij}\right) \psi_j(\mathbf{k}), \tag{2.3}$$

where $\varepsilon_{\mathbf{k}} = -\varepsilon_0(\cos k_x + \cos k_y) - \mu$ and $\Delta_{\mathbf{k}} = \Delta_0(\cos k_x - \cos k_y)$ are the hopping energy and superconducting gap respectively, and $\psi(k)=(c_\uparrow(k), c_\downarrow^\dagger(-k))$ is the Gor'kov-Nambu spinor. For simplicity we will keep only the nearest neighbor hopping terms. Second nearest neighbor tunneling is necessary to explain the actual Fermi surface and we will include this term in the numerical calculations. The interaction

with a single impurity can be expressed in the Coqblin-Schrieffer form [62]:

$$H_{int} = U\psi_i^\dagger(\mathbf{r}_0)\tau_z^{ij}\psi_j(\mathbf{r}_0) - \frac{J}{2}(\psi_\uparrow^\dagger(\mathbf{r}_0)F_\uparrow - F_\downarrow^\dagger\psi_\downarrow(\mathbf{r}_0))(F_\uparrow^\dagger\psi_\uparrow(\mathbf{r}_0) - \psi_\downarrow^\dagger(\mathbf{r}_0)F_\downarrow), \qquad (2.4)$$

where U and J are the potential and spin-spin coupling constants, F is the effective impurity spinor in the Nambu representation (related to the creation and annihilation operators by $F_\uparrow = f_\uparrow,\ F_\downarrow = f_\downarrow^\dagger$). The single impurity occupancy corresponds to the condition:

$$f_i^\dagger f_i = 1 \quad \Leftrightarrow \quad F_i^\dagger\tau_z^{i,j}F_j = 0. \qquad (2.5)$$

In fact, there is an additional potential like scattering term proportional to J in (2.4), however, it disappears in the path-integral formulation of the problem [23]. If chemical potential $\mu = 0$ then the hamiltonian (2.3) respects the particle hole symmetry, i.e. under the transformation $k_x \to k_x + \pi,\ k_y \to k_y + \pi$ both the hopping energy ε_k and the pairing amplitude Δ_k change their signs. This additional symmetry is not generic, it disappears if either μ or the second neighbor hopping become non zero. However this notion is very useful, since in many cases the particle-hole asymmetry can be treated as a perturbation. The model above but without the potential scattering term was already examined by C. Cassanello and E. Fradkin in [23, 24]. The authors concluded that there is a Kondo phase transition above some critical spin-spin coupling J_c. They found that for the linear DOS, the Kondo temperature vanishes exponentially near the phase transition. Also it was argued that in the Kondo phase the impurity susceptibility vanishes at $T \to 0$ as $T \ln 1/T$. However, these results were obtained even in the particle-hole symmetric case. We find similar dependences of the Kondo temperature and susceptibility only if the particle-hole symmetry is broken, e.g. by non-zero potential scattering. The reason for this discrepancy is that the symmetrization of the action with respect to positive and negative frequencies used in [23, 24] is not valid, and resulted in essential

inconsistencies there. We come back to this point in the next section. The other difference between our approaches is that we start from the hamiltonian (2.3) instead of its linearized nodal version. This is important for the analysis because (i) the particle-hole asymmetry ($U \neq 0$ or $\mu \neq 0$) is a high energy effect, i.e. it does not come from nodal quasiparticles only, but rather is determined by contributions from the whole Brillouin zone, (ii) the spatial structure of the scattering can not be correctly reproduced from the nodal version of the hamiltonian, (iii) the expressions for the T-matrix and Green functions are much more transparent in the original Gor'kov-Nambu representation than in that of the nodal quasiparticles.

We also study in detail the phase diagram of an isolated impurity at finite temperature, where the effects of particle hole asymmetry become crucial. The model is generalized to the case of an arbitrary exponent r larger than $1/2$, where the simple Withoff-Fradkin picture [165] is not valid. We would also mention that the problem addressed here but for the Anderson magnetic impurity was studied in [176] using the slave-boson mean field approach. The impurity potential was chosen in such a way that only zero or single occupancy was allowed. As a result the hamiltonian was strongly particle-hole asymmetric from the beginning. It was found that this model predicts the Kondo effect and that the particle hole symmetry of the pure superconductor is not important. The model also results in a low-energy resonance in the DOS and is consistent with the experimental spatial dependence.

This chapter is organized as follows. In Section 2.1 we solve the saddle point equations and study the phase diagram in the space of the potential and spin-spin couplings U and J. It is found that the transition to the Kondo phase occurs only in the particle-hole asymmetric case. At zero temperature the critical spin-spin coupling J_c saturates as $U \to 0$ if $r \leq 1$ and diverges as $1/\sqrt{U}$ if $r > 1$. In the case of a d-wave superconductor ($r = 1$), the Kondo temperature is found to vanish

exponentially near $J = J_c$ in agreement with [24]. At fixed temperature and for $r \leq 1$ the crossover from the high temperature ($T \gg T_K$) to the low temperature ($T \ll T_K$) limit occurs at J diverging as $U \to 0$.

In section 2.2 we examine the expressions for the local and total magnetic susceptibilities of the impurity and the quasiparticle density of states. It is shown that in the particle-hole symmetric case for $r \leq 1$ and $J > J_c$ the local susceptibility, which includes only the magnetic response of the impurity spin, diverges as $T \to 0$, but $T\chi_{loc} \to 0$, while the total impurity susceptibility, which is defined as the difference between the susceptibilities of the superconductor with and without impurity, has the usual Curie-like behavior: $T\chi_{imp} \to$ const. In the Kondo phase χ_{loc} saturates and $\chi_{imp} \to 0$. Both χ_{loc} and χ_{imp} as functions of temperature have a maximum at $T \approx T_K$. At the end of the section we derive the expression for the induced quasiparticle DOS near the impurity. It is shown that in the Kondo phase the effective scattering matrix has a pole at a frequency close to the Kondo temperature ($\Omega \approx T_K$). The crucial difference between this model and simple potential scattering [12, 137] is that the unitary limit here occurs at finite magnitude of the spin-spin coupling $J \approx J_c$, which does not have to be large.

Section 2.3 is devoted to the discussion of the modifications of the model for the case of a non-magnetic impurity, which induces a staggered magnetization nearby. This study is motivated by the nuclear magnetic resonance (NMR) experiments [15, 75] unambiguously showing existence of the magnetic moments in the vicinity of the Zn atom, which substitutes for Cu. From the theoretical point of view, this issue is interesting since the spin-spin interaction becomes non-local. Assuming that the effective spin is induced on the first Cu neighbors of Zn we show that the action has four different saddle points, and for the whole range of coupling constants the configuration with the D symmetry of the order parameter corresponds to the lowest

energy. The critical spin-spin coupling for the non-local spin is found to decrease with U as opposed to the local spin case. The spatial dependence of the induced DOS is also different. It is characteristic for the scattering on four rather than a single site and gives an excellent agreement with the data from STM experiments [114].

In section 2.4 we present numerical results for the electron density of states near the Zn-impurity using the realistic band structure of the $Bi_2Sr_2CaCu_2O_{8+\delta}$. We compare the emerging spatial structure of the DOS modulations with that coming from a pure potential scattering model and discuss the main differences. Unfortunately, using STM data alone it would not be possible to distinguish quasiparticle scattering from a Kondo screened impurity from simple potential scattering. We will briefly argue what possible experiments can be further performed to determine which mechanism is responsible for the observed low energy resonance.

2.1 Saddle point approximation for a single magnetic impurity

After performing a standard Hubbard-Stratonovich decoupling and integrating out fermion fields, the partition function for the system with the hamiltonian given by (2.3) and (2.4) becomes a functional integral over the auxiliary fields ϕ and ϵ with the action:

$$S = -\mathrm{Tr}\ln\left(\frac{\partial}{\partial\tau} + \epsilon(\tau)\tau_z - \phi(\tau)G\left(\frac{\partial}{\partial\tau}\right)\phi(\tau)\right) + \frac{2}{J}\int_0^\beta \phi(\tau)^2 d\tau,$$

where trace is taken over all antiperiodic functions of τ: $f(\tau+\beta) = -f(\tau)$;

$$G(\partial/\partial\tau) \equiv G(\mathbf{r}_0, \mathbf{r}_0, \partial/\partial\tau)$$

is the quasiparticle Green's function in the presence of the potential scattering on the impurity:

$$G(\mathbf{r},\mathbf{r}',\omega) = G^0(\mathbf{r}-\mathbf{r}',\omega) - G^0(\mathbf{r}-\mathbf{r}_0,\omega)U\tau_z\left(1+U\tau_z G^0(0,\omega)\right)^{-1} G^0(\mathbf{r}_0-\mathbf{r}',\omega), \quad (2.7)$$

and G^0 is the free electron Green's function, which in the momentum space is equal to:

$$G^0_{\mathbf{k}}(\omega) = \left(-i\omega\tau_0 + \varepsilon_{\mathbf{k}}\tau_z + \Delta_{\mathbf{k}}\tau_x\right)^{-1}. \quad (2.8)$$

The Lagrange multiplier field ϵ in (2.6) enforces the single occupancy constraint. In general ϕ is a complex field, however its phase can be reabsorbed into ϵ by a simple gauge transformation [128].

It is not hard to show that in a d-wave superconductor the free particle Green's function at $\mathbf{r} = 0$ is expressed as:

$$G^0(0,\omega) = G^0_0(\omega) + G^0_1(\omega)\tau_z \quad (2.9)$$

with G^0_0 and G^0_1 being even and odd functions of frequency, respectively. If the free hamiltonian is also invariant under the particle-hole transformation then $G^0_1 \equiv 0$ [63]. For simplicity we assume this is the case. In fact, it can be shown that the models with $U \neq 0$ and $G^0_1 \neq 0$ can be mapped onto each other. Explicitly $G^0_0(\omega_n)$ is given by

$$G^0_0(\omega_n) = \sum_{\mathbf{k}} \frac{i\omega_n}{\omega_n^2 + \varepsilon_{\mathbf{k}}^2 + \Delta_{\mathbf{k}}^2}. \quad (2.10)$$

At small frequencies the main contribution to G^0_0 comes from the wavevectors close to the nodes, so we can do the summation over $\mathbf{k}$ and obtain:

$$G^0_0(\omega_n) \approx \frac{i\omega_n}{\pi v^2} \ln \frac{\omega_n^2 + \Lambda^2}{\omega_n^2}, \quad (2.11)$$

where $v = \sqrt{v_F v_\Delta}$ is the geometrical mean velocity near the nodes and Λ denotes the upper cutoff of the order of Δ. For the hamiltonian (2.3) with $\mu = 0$ we have $v_F = \varepsilon_0\sqrt{2}$, $v_\Delta = \Delta_0\sqrt{2}$.

From equation (2.9) we see that the action (2.6) splits into two identical terms for the spin up and spin down polarizations so that:

$$S = -N \,\mathrm{Tr}\, \ln\left(\frac{\partial}{\partial\tau} + \epsilon - \phi^{\dagger}(\tau)\, G_{\uparrow}\left(\frac{\partial}{\partial\tau}\right)\phi(\tau)\right) + \frac{N}{J}\int_0^{\beta} d\tau |\phi(\tau)|^2 - \frac{N}{2}\epsilon\beta, \quad (2.12)$$

where $N = 2$ is the number of the spin channels,

$$G_{\uparrow}\left(\frac{\partial}{\partial\tau}\right) = G_0^0\left(\frac{\partial}{\partial\tau}\right)\left(1 + UG_0^0\left(\frac{\partial}{\partial\tau}\right)\right)^{-1}. \quad (2.13)$$

Note that there is an additional term "$-N/2\,\epsilon\beta$" in (2.12), which enforces the symmetry $\epsilon \longrightarrow -\epsilon$ in the absence of the potential scattering. In (2.12) we find it more convenient to use a gauge, where ϕ is complex, but ϵ is time independent. In the large N limit, the action can be evaluated in the saddle point approximation [128]. Thus it is necessary to find the stationary point with respect to the auxiliary fields ϵ and ϕ. Let us start with ϵ:

$$\frac{2}{N}\frac{\partial S}{\partial\epsilon} \equiv I(\epsilon) = -\beta - \sum_{\omega_n} \frac{2}{\frac{e^{-i\omega_n\delta}-1}{\delta} + \epsilon - G_{\uparrow}(\omega_n)|\phi|^2}, \quad (2.14)$$

where δ is an infinitesimal parameter showing the correct procedure for closing the Wick's contour. If $U = 0$ then for any ϕ:

$$I(\epsilon) = \beta(-1 + 2g_F(\epsilon)) \quad \Longleftrightarrow \quad I(\epsilon) + I(-\epsilon) = 0, \quad (2.15)$$

where g_F is the Fermi function. In fact this identity is just a consequence of the particle-hole symmetry. If $U \neq 0$ the relation above generalizes to

$$I(\epsilon, U) + I(-\epsilon, -U) = 0. \quad (2.16)$$

So in the absence of the potential scattering, $\epsilon = 0$ at the saddle point. With the help of (2.15), we write the saddle point condition as follows:

$$\begin{aligned} &\sum_{\omega_n} \frac{-\epsilon}{(i\omega_n - \epsilon + |\phi|^2 G_{\uparrow}(\omega_n))\,(i\omega_n + |\phi|^2 G_0^0(\omega_n))} \\ = \quad &\sum_{\omega_n} \frac{U|\phi|^2 G_0^0(\omega_n) G_{\uparrow}(\omega_n)}{(i\omega_n - \epsilon + |\phi|^2 G_{\uparrow}(\omega_n))\,(i\omega_n + |\phi|^2 G_0^0(\omega_n))}, \end{aligned} \quad (2.17)$$

so that both sums become convergent at $\omega_n \to \infty$. Clearly $\epsilon = 0$ as long as $|\phi| = 0$. Near the phase transition, the order parameter $|\phi|$ is small and therefore ϵ is also small. After introducing dimensionless parameters

$$\epsilon \to \frac{\epsilon}{\Lambda},\ \beta \to \Lambda\beta,\ U \to \frac{\Lambda U}{\pi v^2},\ J \to \frac{\Lambda J}{\pi v^2},\ |\phi|^2 \to \frac{|\phi|^2}{\pi v^2} \tag{2.18}$$

and using $\epsilon \ll 1$ we can simplify (2.17) to:

$$\tanh \frac{\epsilon\beta}{1 + 2|\phi|^2 \ln \frac{1}{|\epsilon|}} \approx 2\left(1 + 2|\phi|^2 \ln \frac{1}{|\epsilon|}\right) F(\phi, U), \tag{2.19}$$

where

$$F(\phi, U) = \int_0^\infty \frac{dx}{\pi} \frac{U|\phi|^2}{\left[\ln^{-1}\left(1 + \frac{1}{x^2}\right) + |\phi|^2\right]^2 + U^2 x^2}. \tag{2.20}$$

The function F increases linearly with U at small U and saturates at $1/2$ at $U \to \infty$. At finite temperature and small U or $|\phi|$, (2.19) shows that $\epsilon \propto T$ up to logarithmic corrections, i.e. instead of (2.19) we can write:

$$\tanh \frac{\varepsilon\beta}{1 + 2|\phi|^2 \ln \beta} \approx 2\left(1 + 2|\phi|^2 \ln \beta\right) F(\phi, U). \tag{2.21}$$

As long as temperature is not too small we can ignore the weak logarithmic dependence of the RHS of (2.21) on T, and ϵ is a decreasing function of temperature. This picture is valid down to $T = T_K$, where

$$T_K(\phi, U) \approx \exp\left(-\frac{1 - 2F(\phi, U)}{4|\phi|^2 F(\phi, U)}\right). \tag{2.22}$$

At this temperature ϵ saturates becoming

$$\epsilon_0 \approx T_K\left(1 + 2|\phi|^2 \ln \frac{1}{T_K}\right). \tag{2.23}$$

The quantity T_K gives the low-energy scale of the problem and further will be identified with the Kondo temperature. Note that it depends exponentially on the order parameter $|\phi|$.

The second equation defining the saddle point is obtained by differentiating (2.12) with respect to ϕ. There is always a trivial solution $\phi = 0$, the second one is found from:

$$\frac{1}{J} = \int_0^\infty \frac{d\omega}{\pi} \Re \left\{ \frac{G_\uparrow(\omega)}{i\omega - \epsilon + |\phi|^2 G_\uparrow(\omega)} \right\}, \tag{2.24}$$

where the sum over discrete ω_n was transformed into the integral, which is justified in the low temperature limit. Assuming $\epsilon \ll 1$ and $\epsilon U \ll 1$, i.e. the system is in the vicinity of the phase transition, (2.24) becomes:

$$\frac{1}{J} = \int_0^\infty \frac{dx}{\pi} \frac{\left(1 + |\phi|^2 \ln(1+\frac{1}{x^2})\right) \ln\left(1+\frac{1}{x^2}\right)}{\left(1+ |\phi|^2 \ln(1+\frac{1}{x^2})\right)^2 + x^2 U^2 \ln^2(1+\frac{1}{x^2})}, \tag{2.25}$$

The RHS of (2.25) is bounded from above with the value 1 corresponding to $\phi = 0$ and $U = 0$. We see that if J is less than the critical value J_c given by

$$\frac{1}{J_c(U)} = \int_0^\infty \frac{dx}{\pi} \frac{\ln\left(1+\frac{1}{x^2}\right)}{1 + x^2 U^2 \ln^2(1+\frac{1}{x^2})}, \tag{2.26}$$

then $\phi = 0$ at the saddle point and the impurity is decoupled from quasiparticles. The critical coupling is an increasing function of U. In particular

$$\begin{aligned} J_c(U) &\approx 1 + \frac{1}{3}U^2 \quad \text{at } U \ll 1, \\ J_c(U) &\approx U \qquad\quad \text{at } U \gg 1. \end{aligned} \tag{2.27}$$

As J increases and becomes larger than J_c, the nontrivial solution of (2.25) becomes relevant, since it defines the minimum of the action as a function of $|\phi|^2$. Near the critical point $J \approx J_c$ we have:

$$\begin{aligned} |\phi|^2 &\approx \frac{J - J_c}{4 J_c^2 \ln 2} \left(1 + \frac{U^2}{2 \ln 2}\right) \qquad \text{at } U \ll 1, \\ |\phi|^2 &\approx \frac{J - J_c(U)}{J_c(U)} \qquad\qquad\qquad\quad \text{at } U \gg 1, \end{aligned} \tag{2.28}$$

At the transition $T_K = 0$ and according to (2.22) its asymptotics are:

$$T_K(J,U) \approx \exp\left(-\frac{J_c^2(U)\ln 2}{2(J-J_c(U))^2 U}\right) \quad \text{at } U \ll 1,$$
$$T_K(J,U) \approx \exp\left(-\frac{J_c^2(U)}{4(J-J_c(U))^2 \ln U}\right) \quad \text{at } U \gg 1. \tag{2.29}$$

These expressions show that close to the phase transition, T_K is exponentially small and as long as $T_K < T \ll 1$, the system is in the regime where the effective impurity energy ϵ is a temperature dependent quantity (see (2.21)):

$$\epsilon \approx \frac{1}{\beta}\left(1+\frac{J-J_c}{J_c^2 2\ln 2}\ln\beta\right)^2 \frac{(J-J_c)U}{J_c^2} \quad \text{at } U \ll 1,$$
$$\epsilon \approx \frac{1}{\beta}\left(1+2\frac{J-J_c(U)}{J_c(U)}\ln\beta\right)^2 \frac{2(J-J_c(U))\ln U}{J_c(U)+2(J-J_c(U))\ln U} \quad \text{at } U \gg 1. \tag{2.30}$$

In the regime, where $T \ll T_K$, ϵ saturates at the value proportional to T_K (2.23). The exponential behavior of the Kondo temperature and the effective impurity energy have been already predicted in [24]. However, we note that this is the case only if the particle-hole symmetry is broken. In the particle-hole symmetric case ϵ and T_K are identically equal to zero for the whole range of the magnetic coupling constant.

As we noted in the introduction, our results are quite different from those derived in [23, 24]. We believe there are several weak points in those treatments. In particular, the action (2.28) in [23] clearly doesn't give a zero saddle point for the effective impurity energy ϵ_f in the particle-hole symmetric case $Q_f = N_c/2$ (we use the notation of [23] in this paragraph). As a result the action in that form does not predict the Curie law for the susceptibility even when the impurity is free. On the other hand this symmetrization is appropriate for finding the order parameter ϕ and the critical coupling g_c (J_c in our notation). That is why we find completely different expressions for the Kondo temperature as compared to [23], while the critical cou-

pling J_c remains the same. In their second paper [24], the authors considered only the linear density of states (see (3.33) therein) and treated the action more carefully. However the saddle point equation (5.3) in [24] is still incorrect. It gives the nonzero value of ϵ_f in the particle-hole symmetric case (see e.g. (5.9) with $x = 1/2$). It seems that there was lost a contribution to (5.3) from the residue at $|\epsilon| > |\Delta_0|$, and hence an implicit particle-hole asymmetry was introduced.

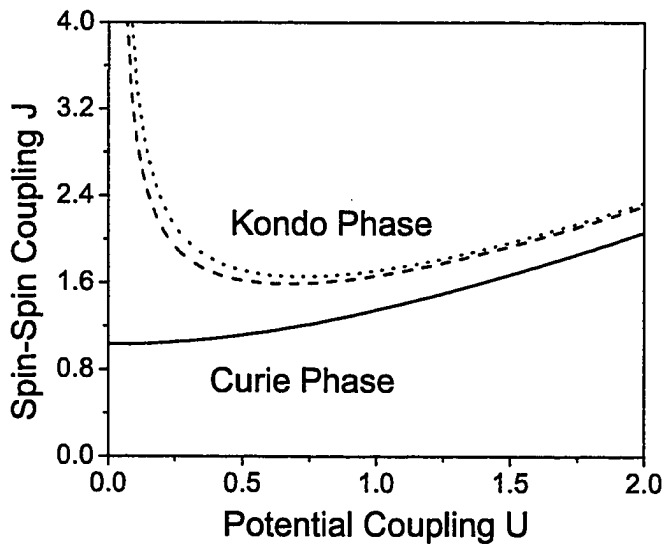

Figure 2.1: Phase diagram in the J–U plane. The solid line ($J = J_c$) corresponds to the Kondo transition at zero temperature. The dot and the dashed lines are the contours of constant Kondo temperature $T_K(J, U) = 10^{-4}$ and $T_K = 10^{-5}$ respectively. The critical spin-spin coupling J_c remains finite at $U = 0$, however in this case there is no real transition to the Kondo phase since at any finite temperature the crossover value of J (dashed and dot lines) diverges as $U \to 0$. For $r < 1$ the phase diagram is similar to this, while for $r > 1$ the zero temperature boundary between the Kondo and Curie phases is analogous to the dashed line.

Figure 2.1 illustrates the phase diagram in the $J - U$ plane. The solid line corresponds to the phase transition, while the dashed and dot lines show the contours of the constant T_K. At fixed T the latter lines separate the high-temperature ($T_K < T$) and the low-temperature ($T_K > T$) regions. Here we would like to emphasize

that the phase diagram with the dashed line being a boundary is reminiscent of that obtained by NRG [57]. This probably indicates that the large N-theory is not very reliable in the zero temperature limit. It is also important to note that the curve $J(U)$, corresponding to T_K =const is very insensitive to the variations of the latter. Thus the dot and the dashed lines corresponding to $T_K = 10^{-4}$ and $T_K = 10^{-5}$ almost coincide.

Generalization to the nonlinear density of states

Before we proceed further with d-wave superconductors, let us generalize the expressions obtained in the large N limit to the case of vanishing density of states with an arbitrary exponent:

$$\rho(\epsilon) = \begin{cases} \frac{r+1}{2}|\epsilon|^r & |\epsilon| < 1 \\ 0 & |\epsilon| \geq 1 \end{cases} \tag{2.31}$$

i.e. the action is still given by the equation (2.12), but the unperturbed Green function $G_0^0(\omega_n)$ is now as follows:

$$G_0^0(\omega_n) = i\int_{-1}^{1} \frac{\omega_n \rho(\epsilon)}{\omega_n^2+\epsilon^2} d\epsilon = i\frac{r+1}{2} \frac{\mathcal{F}\left(1, \frac{1+r}{2}, \frac{3+r}{2}, -\frac{1}{\omega_n^2}\right)}{\omega_n}, \tag{2.32}$$

where $\mathcal{F}$ is the hypergeometric function. High and low frequency asymptotics of G_0^0 are

$$G_0^0(\omega_n) \approx \begin{cases} i\omega_n^r \frac{r+1}{2} \frac{\pi}{\cos\frac{\pi r}{2}} - i\omega_n \frac{r+1}{r-1} & \omega_n \ll 1 \\ i\omega_n^{-1} & \omega_n \gg 1. \end{cases} \tag{2.33}$$

For $r < 1/2$ the problem was studied in detail in [73, 165]. Both the consequent analysis and numerical results [57] show that the effects of the particle-hole asymmetry become crucial for $r > 1/2$. Here only this situation will be considered. Doing

the same steps as before we find the critical J, where $|\phi|$ first becomes nonzero, is

$$\begin{aligned} J_c &\sim \frac{r(r+1)}{2} && \text{at } U \to 0 \\ J_c &\sim U \max\left(\frac{2r}{r+1}, 1\right) && \text{at } U \to \infty. \end{aligned} \tag{2.34}$$

In the case of small potential scattering U, the order parameter near the phase transition is:

$$|\phi|^2 \sim \frac{J - J_c}{J_c^2} \frac{4r-2}{(r+1)^2} \left(\psi\left(\frac{r+1}{2}\right) - \psi\left(\frac{1}{2}\right)\right)^{-1}, \tag{2.35}$$

where ψ is the digamma function. Note that regardless of r, $|\phi|^2$ is proportional to $J - J_c$. However, when ϵ is considered, it is necessary to distinguish between $r < 1$ and $r > 1$. In the former case one can define the Kondo temperature:

$$T_K \approx \left[\frac{2\cos\frac{\pi r}{2}}{\pi^r(1-r)} + \frac{4^r - 1}{4^{r-1}} \frac{\cos\frac{\pi r}{2}\zeta(2r)}{\pi^{1+r}|\phi|^4 F_r(U)}\right]^{-\frac{1}{1-r}}, \tag{2.36}$$

where ζ is the Riemann zeta function,

$$\begin{aligned} F_r(U) &\sim \frac{U}{2} \frac{(r+1)^2}{2r-1} \left(\psi\left(\frac{1+r}{2}\right) - \psi\left(\frac{r}{2}\right)\right) && \text{for } U \ll 1 \\ F_r(U) &\sim \frac{U^{\frac{1-r}{r}} - 1}{\left(\cos\frac{\pi r}{2}\right)^{\frac{1}{r}}} \frac{\pi^{\frac{1}{r}}(1+r)^{\frac{1}{r}}}{r\, 2^{\frac{1+r}{r}} \sin\frac{\pi}{2r}} && \text{for } U \gg 1. \end{aligned} \tag{2.37}$$

For $r < 1$ near the phase transition we have:

$$T_K \propto (J - J_c)^{\frac{2}{1-r}} \tag{2.38}$$

Above the Kondo temperature ϵ increases with T, while for $T < T_K$ it saturates at the value:

$$\epsilon \sim |\phi|^2 \frac{\pi^{1+r}(1+r)}{2\cos\frac{\pi r}{2}} T_K^r \left(1 - \frac{2\cos\frac{\pi r}{2}}{\pi^r(1+r)} T_K^{1-r}\right). \tag{2.39}$$

It is easy to check that the expressions for $r = 1$ obtained earlier are consistent with these formulas.

The picture becomes quite different for $r > 1$. If the order parameter is sufficiently small, ϵ can be found from:

$$\tanh\left(\frac{\beta\epsilon}{1+\frac{r+1}{r-1}|\phi|^2}\right)=2|\phi|^2\left(1+\frac{r+1}{r-1}|\phi|^2\right)F_r(U). \tag{2.40}$$

Provided the RHS of (2.40) is less than 1, this equation has a solution with $\epsilon \propto T$, i.e. vanishing as T goes to zero. On the other hand if the RHS becomes larger than 1, this equation has no solution and at zero temperature at this point there is a phase transition to the Kondo phase. Thus for r slightly greater than 1 and $U \ll 1$ the new critical coupling $\tilde{J}_c$, which gives the actual transition to the Kondo phase, is

$$\tilde{J}_c \sim J_c + 0.35\sqrt{\frac{r-1}{U}}. \tag{2.41}$$

For $U \gg 1$ we have $\tilde{J}_c \approx J_c$. The diverging behavior of $\tilde{J}_c$ at $U \to 0$ is in fact very similar to that of the crossover value of the spin-spin coupling for $r = 1$ at finite temperature (see dashed line in Fig. 2.1). However, for $r > 1$ this divergence exists even in the zero temperature limit.

At this point we obtain an additional evidence that the large-N theory might be not reliable at small temperatures for $r \leq 1$. Namely, the NRG analysis shows that $r = 1$ is not a special point in the phase diagram [155]. On the other hand, the saddle point approximation predicts that the curve similar to the dashed (not solid) line in figure 1 corresponds to the transition to the Kondo phase for $r > 1$. At the same time at finite temperature, the mean field results are qualitatively similar to those given by NRG [73, 155]. Moreover, for r close to 1 the contours $T_K(J, U)$ =const are very insensitive to the magnitude of T_K (see Fig. 2.1).

2.2 Magnetic susceptibility and quasiparticle density of states.

We start this section by calculating the local magnetic susceptibility at zero field. In the saddle point approximation it is given by:

$$\chi_{loc} = -\frac{1}{4\beta}\frac{\partial^2 S_{eff}(h)}{\partial h^2} = -\frac{1}{4\beta}\frac{\partial^2 S_{eff}(\epsilon)}{\partial \epsilon^2}. \tag{2.42}$$

Using (2.14) we immediately get:

$$\chi_{loc} = \sum_{\omega_n} \frac{N}{4\beta\left(\omega_n - i\epsilon - i|\phi|^2 G_\uparrow(\omega_n)\right)^2}. \tag{2.43}$$

This expression becomes particularly simple if there is no potential scattering and $\epsilon = 0$ (we always assume that the temperature is small compared to the cutoff, i.e. $\beta \gg 1$):

$$\chi_{loc} \approx \frac{N\beta}{16}\left(1 + 2|\phi|^2 \log\frac{\beta}{\pi}\right)^{-2}. \tag{2.44}$$

It is not surprising that for $\phi = 0$ in the physical case $N = 2$, (2.44) gives one half of the usual Curie constant. This feature is an artifact of the large N techniques applied here. For $r < 1$ instead of (2.44) we have

$$\chi_{loc} \approx \frac{N\beta}{16} \quad 1 \ll \beta \ll \beta_0 \equiv \pi\left[\frac{2\cos\frac{\pi r}{2}}{\pi(r+1)\phi^2}\right]^{\frac{1}{1-r}} \tag{2.45}$$

$$\chi_{loc} \approx \frac{2N\beta^{2r-1}\cos^2\frac{\pi r}{2}}{\phi^4\pi^{2(r+1)}(r+1)^2}\frac{4^r-1}{4^r}\zeta(2r) \quad \beta \gg \beta_0. \tag{2.46}$$

On the other hand for $r > 1$ the local susceptibility in the particle-hole symmetric case is completely described by the Curie law.

The formulas above are valid as long as $\epsilon \ll T$. For $r \leq 1$ this is equivalent to $T \gg T_K$. Below the Kondo temperature χ_{loc} saturates at:

$$\chi_{loc} \approx \frac{N|\phi|^2}{4T_K(1 - 2|\phi|^2\ln(T_K))^3} \qquad \text{for } r = 1, \tag{2.47}$$

$$\chi_{loc} \approx \frac{N}{4|\phi|^4 T_K^{2r-1}}\frac{2(1-r)\cos^2\frac{\pi r}{2}}{r^2\pi^{2r-1}(r+1)^2} \quad \text{for } r < 1. \tag{2.48}$$

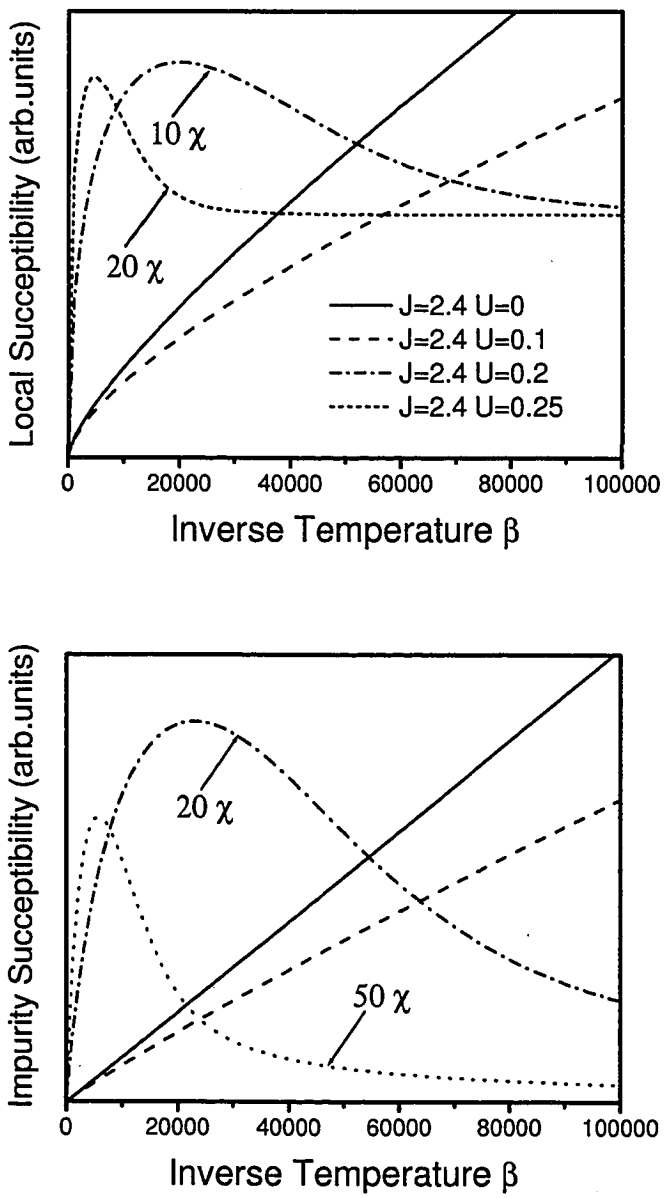

Figure 2.2: Temperature dependence of local (top) and impurity (bottom) susceptibilities in the Kondo phase for different values of U. For $U = 0$ and $U = 0.1$ (see figure 2.1) the Kondo temperature is much smaller than $T = \beta^{-1}$ for all plotted values of β. So both susceptibilities increase with β. Note that χ_{loc} is clearly a sublinear function of inverse temperature even in the particle-hole symmetric case. For $U = 0.2$ and $U = 0.25$ the Kondo temperature becomes large enough and both susceptibilities have a maximum at $\beta T_K \approx 1$. The local susceptibility saturates at $\beta \to \infty$, while $\chi_{imp} \to 0$.

The temperature dependence of χ_{loc} for $r = 1$ is plotted on the top graph on figure 2.2. This function is non-monotonic with the maximum occurring at $T \approx T_K$.

Using equation (2.43), it is not hard to calculate a correction to $\chi_{loc}(T = 0)$ for $T \ll T_K$:

$$\chi_{loc}(T) - \chi_{loc}(0) \approx \frac{9\zeta(3)|\phi|^2 T^3}{\pi\epsilon^4}\left(1 + 2|\phi|^2 \ln\frac{1}{T}\right), \tag{2.49}$$

showing that χ_{loc} decreases at $T \to 0$ for $T < T_K$.

The local susceptibility is the response function to the magnetic field coupled only to the impurity. We will also consider here the impurity susceptibility which additionally includes the contribution from the nearby electron cloud .

Assuming that the g-factors of band and impurity electrons are the same, we see that the only effect of the magnetic field h on the action (2.12) is the shift of the imaginary frequency $\omega_n \to \omega_n + ih$ for the spin up states and $\omega_n \to \omega_n - ih$ for the spin down states. Therefore, the impurity susceptibility at zero field is:

$$\chi_{imp} = \frac{N}{4\beta}\sum_n \frac{\left(1 - i|\phi|^2 \frac{\partial}{\partial\omega_n} G_\uparrow(\omega_n)\right)^2}{\left(\omega_n + i\epsilon - i|\phi|^2 G_\uparrow(\omega_n)\right)^2} - \frac{N}{4\beta}\sum_n \frac{|\phi|^2 \frac{\partial^2}{\partial\omega_n^2} G_\uparrow(\omega_n)}{i\omega_n - \epsilon + |\phi|^2 G_\uparrow(\omega_n)}. \tag{2.50}$$

If $\epsilon = 0$, the expression above reduces to:

$$\chi_{imp} \approx \frac{N\beta}{16}\left(1 - \frac{2|\phi|^2}{1 + 2|\phi|^2 \ln\beta}\right). \tag{2.51}$$

Note that χ_{imp} asymptotically approaches the Curie law at $T \to 0$, contrary to (2.44) where $T\chi_{loc} \to 0$. This peculiarity was already predicted in [26], however in the later work [57], χ_{loc} was found to be proportional to the inverse temperature without any logarithmic corrections. The discrepancy between the mean-field and NRG results can not be resolved considering the next terms in the $1/N$ expansion near the saddle point. In fact, it is easy to show, that for $U = 0$ at each order of the perturbation series for χ_{loc}, a multiplier $(1+2|\phi|^2 \ln\beta)^2$ is generated in the denominator. Therefore the sublinear dependence of $\chi_{loc}(T)$ is generic for the large N approach. Probably

the reason for the discrepancy between this work and [57, 155] is that the large N expansion is asymptotic in the particle-hole symmetric case and for $r \leq 1$, and it does not converge as temperature goes to zero.

For $r > 1$ near $J = J_c$, $\chi_{imp} = \chi_{loc} = N\beta/16$. While for $r < 1$ there is a crossover between

$$\chi_{imp} \approx \frac{N\beta}{16} \tag{2.52}$$

and

$$\chi_{imp} \approx \frac{Nr\beta}{16}, \tag{2.53}$$

for $T\beta_0 \gg 1$ and $T\beta_0 \ll 1$ respectively, with β_0 defined in (2.45). Hence the impurity is partially screened. We note again that these results are valid only for $r > 1/2$, otherwise there is a transition to Kondo phase even in the particle-hole symmetric case.

Below the Kondo temperature χ_{imp} goes to zero in agreement with [24] . For example, at $r = 1$:

$$\chi_{imp} \approx \frac{T|\phi|^2 N \ln 2}{T_K^2 (1 - 2|\phi|^2 \ln T)}. \tag{2.54}$$

The impurity susceptibility as a function of temperature is plotted in the bottom graph of Fig. 2.2.

Another manifestation of the coupling between quasiparticles and the impurity is the change of the electron density of states, which is given by the imaginary part of the effective Green function:

$$\rho(\Omega, \mathbf{r}) = \Im \mathrm{Tr} \frac{1 + \tau_z}{2} \tilde{G}(\mathbf{r}, \mathbf{r}, \Omega), \tag{2.55}$$

where Ω is a real frequency with an infinitesimal positive imaginary part,

$$\tilde{G}(\mathbf{r}, \mathbf{r}', \Omega) = G(\mathbf{r}, \mathbf{r}', \Omega) + G(\mathbf{r}, \mathbf{r}_0, \Omega)\, \mathcal{T}_K(\Omega)\, G(\mathbf{r}_0, \mathbf{r}', \Omega). \tag{2.56}$$

The scattering matrix $\mathcal{T}_K(\Omega)$, corresponding to the Kondo contribution is equal to:

$$\mathcal{T}_K(\Omega) = \frac{|\phi|^2}{-\Omega + \epsilon\tau_z - |\phi|^2\tau_z G(\mathbf{r}_0, \mathbf{r}_0, \Omega)\tau_z}. \tag{2.57}$$

Note that a similar form for $\mathcal{T}$ was found in [173] for the case of an Anderson impurity below the Kondo temperature. Using (2.9), (2.55) can be simplified further:

$$\rho(\Omega, \mathbf{r}) = \Im\, G^0_+(\mathbf{r}, \Omega)\mathcal{T}_+(\Omega)G^0_+(-\mathbf{r}, \Omega) + G^0_x(\mathbf{r}, \Omega)\mathcal{T}_-(\Omega)G^0_x(-\mathbf{r}, \Omega). \tag{2.58}$$

We have adopted the notation:

$$G^0_+(\mathbf{r}, \Omega) = \mathrm{Tr}\,\frac{1+\tau_z}{2}G_0(\mathbf{r}, \Omega), \quad G^0_x(\mathbf{r}, \Omega) = \mathrm{Tr}\,\frac{\tau_x}{2}G_0(\mathbf{r}, \Omega), \tag{2.59}$$

$$\mathcal{T}_\pm(\Omega) = -\frac{1}{1 \pm UG^0_0(\Omega)} + \left(\frac{1}{1 \pm UG^0_0(\Omega)}\right)^2 \frac{1}{-\Omega \pm \epsilon - |\phi|^2 \frac{G^0_0(\Omega)}{1 \pm UG^0_0(\Omega)}}. \tag{2.60}$$

The spatial dependence of the DOS coincides with that obtained earlier for the case of pure classical scattering [137, 138]. We note that at small frequencies ($\Omega \ll \Delta$), there is a maximum at the nearest neighbors of the impurity and at $r \to \infty$ the asymptotic behavior of the DOS is r^{-2}. Also it is easy to show that if the resonance frequency is much smaller than the superconducting gap, the spatially integrated DOS remains particle-hole symmetric. It is determined by the momenta in the vicinity of the nodes and therefore this result is valid regardless the microscopic details of the model such as chemical potential, existence of second-neighbor hopping matrix elements, etc.

Clearly the $\mathcal{T}$-matrix for the Kondo scattering channel has a pole at the frequency $\Omega \approx T_K$. If $T_K \ll \Delta$, i.e. $J \approx J_c$, the resonant levels corresponding to the poles in $\mathcal{T}_+$ and $\mathcal{T}_-$ become very narrow and they have roughly Lorentzian shape. In the opposite limit $\Delta \ll T_K$, the resonance corresponding to $\mathcal{T}_-$ disappears and (2.58) results in the Fano lineshape in agreement with [171].

We would like to emphasize that the scattering in a strong classical magnet gives two identical peaks at positive and negative frequencies and additional weak potential

coupling results in the weak splitting of those [138]. In the Kondo case, even at small U the spatial structure of the resonances at positive and negative frequency is highly asymmetric.

2.3 Non-magnetic impurity in a d-wave superconductor

In this section we focus on the situation, where the spin is not located on the impurity site, but rather it is a staggered moment distributed nearby. The main motivation for this study comes from the NMR experiments [15, 16, 75, 97, 98, 103] with non-magnetic Zn or Li impurities in BiSCCO superconductors. The effective strength of the induced moments rapidly decreases with the distance [75], therefore it is reasonable to assume that the spins are located only on the first nearest neighbors.

In this way the new interacting part of the hamiltonian becomes:

$$H_{int} = U\psi_i^\dagger(\mathbf{r}_0)\tau_z^{ij}\psi_j(\mathbf{r}_0) - \frac{J}{2}\sum_{s\in O}(\psi_\uparrow^\dagger(\mathbf{r}_s)F_\uparrow - F_\downarrow^\dagger\psi_\downarrow(\mathbf{r}_s))(F_\uparrow^\dagger\psi_\uparrow(\mathbf{r}_s) - \psi_\downarrow^\dagger(\mathbf{r}_s)F_\downarrow), \quad (2.61)$$

where O denotes the subset of the sites closest to the $\mathbf{r}_0$. Contrary to the spin-spin coupling which is strongest on the nearest neighbors of the impurity, the potential scattering is dominated by the local term, therefore its form is unchanged as compared to (2.4). Repeating the same steps as before and using the static approximation we obtain:

$$S = -\mathrm{Tr}\,\ln\left(\frac{\partial}{\partial\tau} + \epsilon\tau_z - \sum_{s,s'\in O}\phi_s\, G\left(\mathbf{r}_s, \mathbf{r}_{s'}, \frac{\partial}{\partial\tau}\right)\phi_{s'}\right) + \frac{2\beta}{J}\sum_{s\in O}\phi_s^2, \quad (2.62)$$

This action can be also evaluated in the saddle point approximation. The important difference with the local spin case is that there are four nontrivial saddle points corresponding to S ($\phi_{10} = \phi_{01} = \phi_{\bar{1},0} = \phi_{0,\bar{1}}$), D ($\phi_{10} = -\phi_{01} = \phi_{\bar{1},0} = -\phi_{0,\bar{1}}$), and

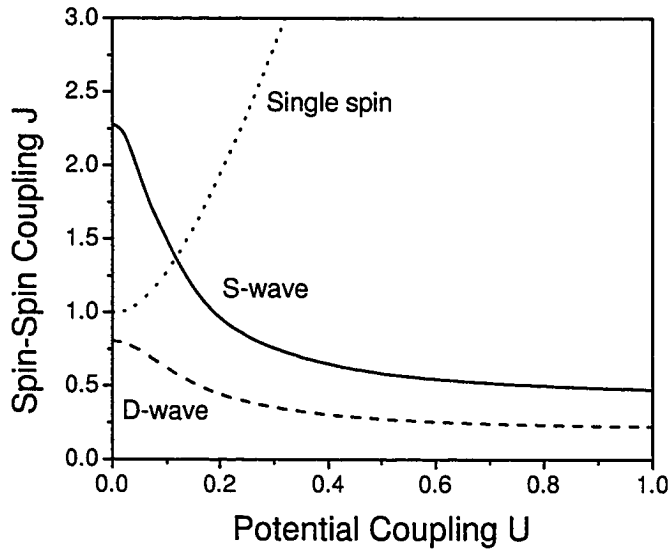

Figure 2.3: Critical spin-spin coupling as a function of potential scattering for the non-local spin case. The D-wave configuration of the order parameter ϕ always has a lower critical coupling J_c and thus corresponds to the Kondo phase transition. Contrary to the local spin case $J_c(U)$ is a decreasing function.

P ($\phi_{10} = -\phi_{\bar{1},0}$; $\phi_{0,1} = \phi_{0,\bar{1}} = 0$) symmetry of the order parameter, the latter case being doubly degenerate. In Fig. 2.3 we show the dependence of the critical coupling J_c on the potential scattering for the order parameter of the S and D symmetry (P case is always in between), and for the local spin. Clearly, for the whole range of U, D-order has a lower J_c and as a result a smaller action. Also, contrary to the local spin case, J_c decreases with U. This phenomenon is readily understood since the potential scattering increases the quasiparticle density of states on the nearest neighbors [137, 138], where the magnetic moments are located, and hence enhances the effective spin-spin coupling. It is interesting to note that the effective DOS of the "bath" electrons for the D-wave saddle point in the absence of potential scattering term is proportional to ω^3, and not ω, due to Green's functions cancellation near the nodes. However this feature is not important for the subsequent analysis.

Qualitatively, both the local and impurity magnetic susceptibility do not change as compared to the local spin case, since they are sensitive to the value of the impurity spin and not to its distribution. The situation is quite different for the density of states . In particular, for the spin scattering part and D-wave order parameter (2.58) generalizes to

$$\rho(\Omega,\mathbf{r}) = \Im\left[G^d_+(\mathbf{r},\Omega)\mathcal{T}_+(\Omega)G^d_+(-\mathbf{r},\Omega) + G^d_x(\mathbf{r},\Omega)\mathcal{T}_-(\Omega)G^d_x(-\mathbf{r},\Omega)\right], \tag{2.63}$$

where:

$$\mathcal{T}_\pm(\Omega) = \frac{-1}{\Omega \mp \epsilon + |\phi|^2\left(G^d_0(\Omega) + \frac{G^{d^2}_x(\mathbf{r}_0,\Omega)U^2G^0_0(\Omega)}{1-U^2G^{0^2}_0(\Omega)}\right)}, \tag{2.64}$$

$$G^d_{+,x}(\mathbf{r},\Omega) = \sum_{s\in O}(s_x^2 - s_y^2)\,G_{+,x}(\mathbf{r},\mathbf{r}_s,\Omega),$$
$$G^d_0(\Omega) = \sum_{s,s'\in O}(s_x^2 - s_y^2)(s_x'^2 - s_y'^2)\,G^0_0(\mathbf{r}_s - \mathbf{r}_{s'},\Omega),$$

with $s_i = 0, \pm 1$. The resonance frequency is approximately equal to the Kondo temperature as in the local spin case. If the potential scattering is not too large $UG^0_0(T_K) \ll 1$, then the spatial dependence of the DOS is determined by the interference from the scattering on the four nearest neighbor sites of the impurity. In particular, for the D (S) order parameter, the resonance corresponding to the $\mathcal{T}_-$ ($\mathcal{T}_+$) matrix gives the largest DOS at the impurity site $\mathbf{r} = \mathbf{r}_0$, a local maximum at the second neighbors and very small signal at the first neighbors. This behavior is in the excellent agreement with the experiments, where the spatial distribution of the DOS near a Zn impurity was directly observed [114]. Also at $r \to \infty$ the density of states vanishes as r^{-4}, i.e. much faster than for the the local scattering. The spatially integrated induced DOS is generically particle-hole asymmetric. In particular, it can be shown that if $UG^0_0(T_K) \ll 1$ and $T_K \ll \Delta$ then at the resonance frequency

the integrated DOS is:

$$\rho_+(\Omega) \approx \frac{4}{\Delta_0^2}\int \frac{\varepsilon_k^2\Delta_k^2}{(\varepsilon_k^2+\Delta_k^2)^2}\frac{d^2k}{(2\pi)^2}\Im\mathcal{T}_+(\Omega) \tag{2.65}$$

$$\rho_-(-\Omega) \approx \frac{4}{\Delta_0^2}\int \frac{\Delta_k^4}{(\varepsilon_k^2+\Delta_k^2)^2}\frac{d^2k}{(2\pi)^2}\Im\mathcal{T}_-(-\Omega) \tag{2.66}$$

Simple power counting shows that (2.65) and (2.66) converge near the nodes. Therefore the ratio of the spatially integrated DOS is nonuniversal and while for particle-hole symmetric spectrum $\rho_-/\rho_+ \sim 2.5$, it decreases with the doping, crossing 1 at some level. For comparison we will give the results for the local spin:

$$\tilde{\rho}_+(\Omega) \approx \int\limits_{\varepsilon_k^2+\Delta_k^2>\Omega^2} \frac{\varepsilon_k^2}{(\varepsilon_k^2+\Delta_k^2)^2}\frac{d^2k}{(2\pi)^2}\Im\mathcal{T}_+(\Omega) \tag{2.67}$$

$$\tilde{\rho}_-(-\Omega) \approx \int\limits_{\varepsilon_k^2+\Delta_k^2>\Omega^2} \frac{\Delta_k^2}{(\varepsilon_k^2+\Delta_k^2)^2}\frac{d^2k}{(2\pi)^2}\Im\mathcal{T}_-(-\Omega) \tag{2.68}$$

These expressions logarithmically diverge when ε and Δ become small, and therefore it is necessary to put a low energy cutoff of the order of the frequency. The integrals mainly sit on the nodes and $\rho_+ \approx \rho_-$ if Ω is small. Physically these differences are related to the slow $(1/r^2)$ dependence of the DOS on the distance for a single spin, while for the nonlocal scattering, the DOS rapidly decreases away from the impurity and the main contribution to the spatial integrals comes from the short distances or high momenta.

Let us say a few words about the strong potential scattering case $U \gg 1$. As we see from Fig. 2.3, the critical Kondo coupling J_c goes to zero as $1/U$ up to logarithmic corrections. Therefore for most values of J the system is in the Kondo phase. If J is not too large, then the order parameter $|\phi|$ and the Kondo temperature are small enough so that the condition $UG_0^0(T_K) \ll 1$ is fulfilled. As a result, the spatial structure of the DOS remains the same, as if there is no potential scattering. This contradicts the naive idea of the "hard-wall" impurity, which prohibits a large

DOS at $\mathbf{r} = \mathbf{r}_0$. The reason why this argument is not correct is that if the energy scale T_K is too small then the potential scattering is irrelevant. If both conditions $U \gg 1$ and $J \gg J_c$ are satisfied then $UG_0^0(T_K)$ might be greater than 1. In this case, the Kondo scattering occurs on the almost frozen density of states created by the potential scatterer and apart from small variations, the spatial structures of the Kondo and potential resonances coincide. But we emphasize again, that in order to have this situation, U should be very large.

2.4 Numerical results

In this section we will present numerical results based on the analysis given above, but using realistic parameters describing the band structure of $Bi_2Sr_2CaCu_2O_{8+\delta}$. For the hamiltonian (2.3) we will include first, second and third nearest neighbor hopping amplitudes to correctly reproduce details of the Fermi surface. We ignore the potential scattering term U to see the results coming from the Kondo effect only. As we argued above, only very strong values of U may qualitatively change the actual picture at low energies. Although the calculations can be done only numerically, the qualitative analysis remains the same as described before. Thus at magnetic coupling larger than some critical value, which we determine to be about 0.1eV at optimal doping, the impurity gets Kondo screened, resulting in a resonant feature in the scattering matrix. The energy and spatial dependence of the local DOS for a typical set of parameters at 14% hole doping are shown in Fig. 2.4. Most significant is the pronounced peak at $\mathbf{r}_0$ (on the Zn site) at a bias, $\omega = -\omega_0$. This was a robust feature of our results: the peak retained a small negative bias and width for a wide range of $J > J_c$. Away from the central site, the peaks were much weaker, and varied slightly depending upon U and doping. At optimal doping (and more robustly at

lower doping) we obtained the alternating intensity pattern in Fig. 2.4b. The spatial integral of the spectrum at negative bias is larger than that at positive bias, and the ratio is quoted in Fig. 2.4. In Fig. 2.5 we show the comparison between the spatial structures of the resonances obtained within the present model and for pure potential scattering in the unitarity limit. Note, it is necessary to choose a very large value of $|U|$ to make the peak sharp and occur at a small bias. Both these features are sensitive to variations in the values of the doping, the band structure parameters and U. Another important observation, which is clear from the graphs, is that the spatial decay of the induced DOS oscillations is much faster in the Kondo case than for the single impurity scattering, which is also in agreement with experiments [114].

Let us make a few remarks on the spatial dependencies in Fig. 2.4. The dominant contribution at peak energy comes from the normal (τ^z - at positive bias) and anomalous (τ^x - at negative bias) components of G (2.63). These two terms result in complementary spatial structure of the DOS modulations in agreement with STM data [114]. Using the location of the four sites in O and the d-wave structure of both the superconducting gap function $\Delta_{\mathbf{k}}$ and the ϕ fields, we see that at $\mathbf{r}_0$ the normal (anomalous) Green's functions destructively (constructively) interfere leading to a vanishing (large) peak at $-\Omega_0$. This interference is also responsible for the asymmetry of the spatially integrated spectrum. (We note that for an s-wave pattern in the ϕ fields the interference mechanism is similar, with the difference that the peak at $\mathbf{r}_0$ appears at $+\Omega_0$.) An analogous discussion [137] can be applied to the potential scattering case, where such interference does not occur. So in order to explain the spatial structure (both peak maximum at the impurity site and the fast decay of the DOS modulations with distance), one has to introduce by hand an extra interference mechanism as was suggested in [138]. We also note that the coherence peaks, appear-

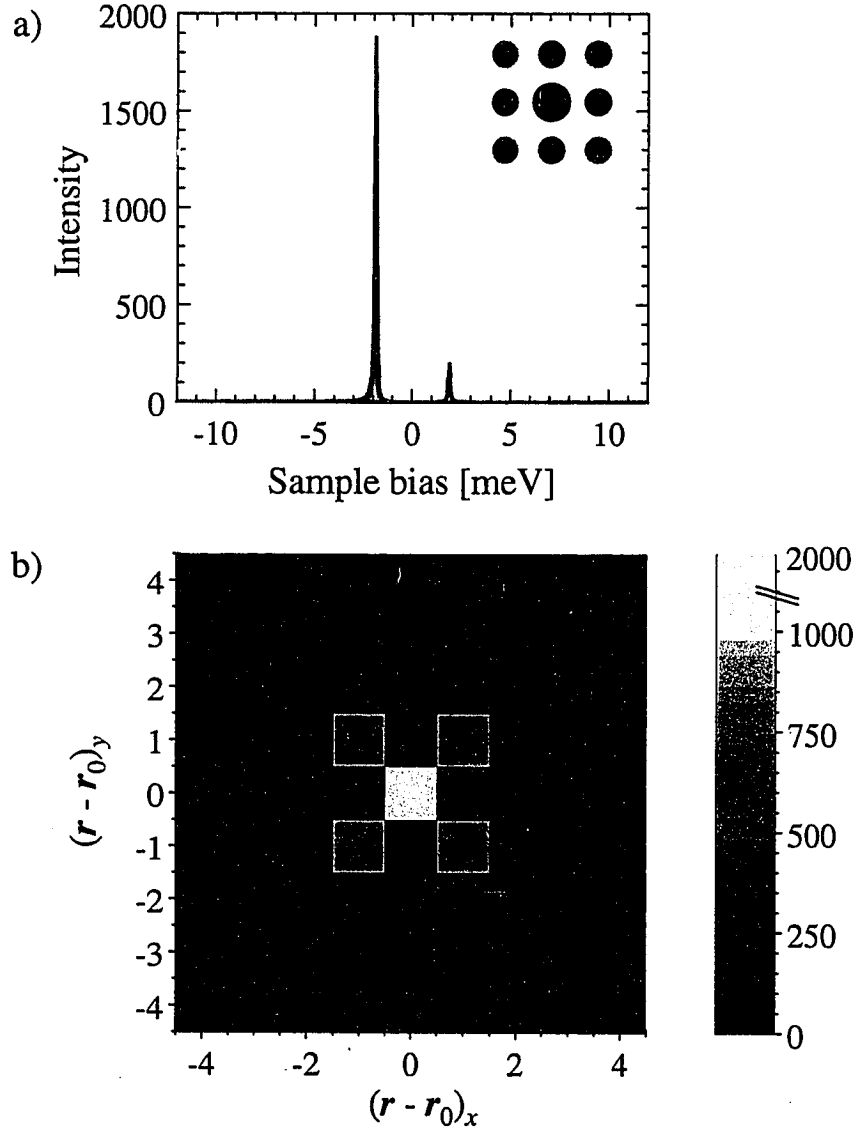

Figure 2.4: Tunneling density of states for the Kondo impurity model at 14% hole doping with a realistic band structure ($t = 0.1$ eV, $t' = -t/4$, $t'' = t/8$), $\Delta_0 = 0.04$ eV, $J = 0.21$ eV, $\mu = -0.09$ eV and $U \approx 0$. For these parameters $J_c = 0.1$ eV. (a) Tunneling spectrum versus sample bias for the impurity site, the nearest and second neighbor sites. (b) Spatial dependence of the differential conductance at the bias $\Omega = -1.9$ meV ($= -\Omega_0$). The ratio of the spatial integrals at $\pm\omega$ is 1.5, and this value increases with decreasing doping.

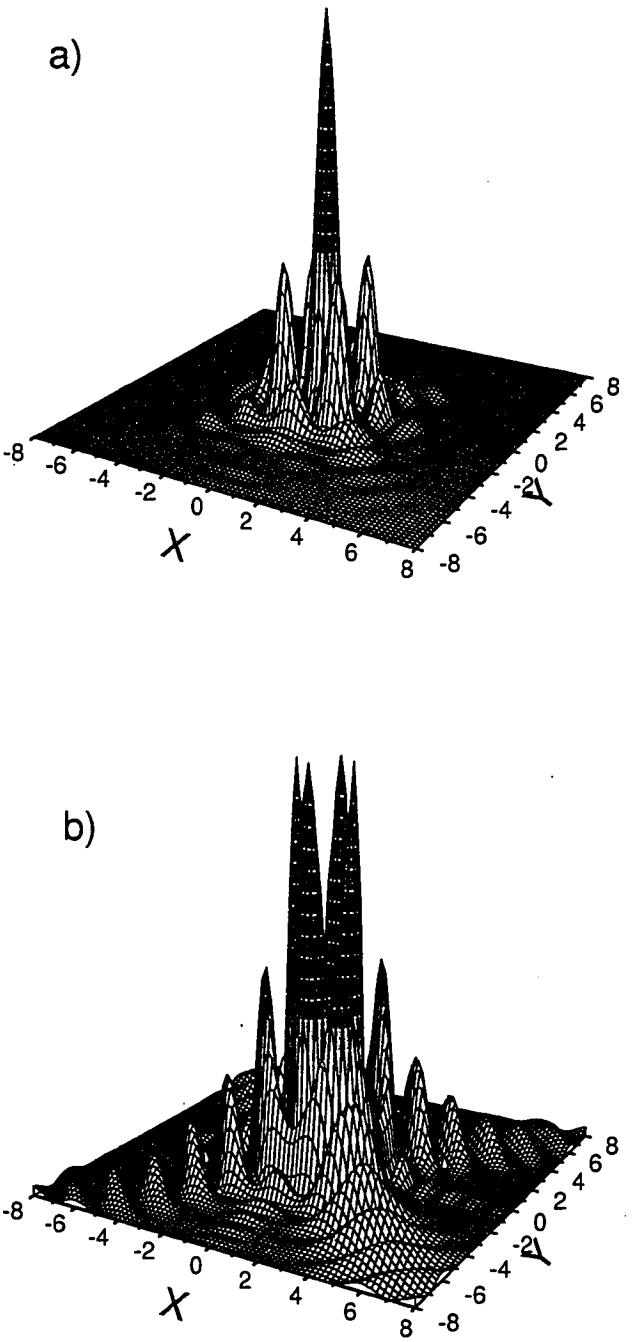

Figure 2.5: Comparison between spatial structures of the low energy resonances for the Kondo model (a) and unitarity limit of the potential scattering (b). The graph (a) agrees with experimental results. In order to reconcile (b) with them, it is necessary to introduce a filtering mechanism [101], which has not been independently verified.

ing in the DOS at the gap energy, are much suppressed at the impurity site and its neighbors, although we did *not* include a spatial variation of the pairing amplitude. Furthermore, upon moving to the metallic state by setting $\Delta_0 = 0$, our approach is closely related to that of [171], and then the large DOS around the Fermi level leads to a Fano lineshape.

2.5 Conclusions

In this chapter we studied the screening of a magnetic impurity in d-wave superconductors. It was found that there is a Kondo transition, which occurs only if the particle-hole symmetry is distorted, e.g. by potential scattering. The Kondo temperature is exponentially small near the critical coupling. However, at finite but small temperature, the crossover from the regime $T \gg T_K$, where the impurity spin is not screened to $T \ll T_K$ occurs at qualitatively different values of the magnetic coupling J (see Fig. 2.1), in particular the crossover $J \to \infty$ if the potential coupling $U \to 0$. In the particle-hole symmetric phase it was found that the impurity susceptibility behaves in a Curie-like fashion: $T\chi_{imp} \to$const as $T \to 0$, while the local susceptibility has multiplicative logarithmic corrections, so that: $T\chi_{loc} \to 0$. This result, which holds in any order of the $1/N$ expansion, agrees with [26], however it contradicts later NRG investigations [57, 155]. It is possible that the logarithmic corrections are beyond the accuracy of the large N expansion in the particle-hole symmetric case. On the other hand, the resulting phase diagram at finite temperature is qualitatively similar to that, obtained by NRG [57, 155] and dynamic multichannel [157] methods. Moreover the contours of constant T_K change very slowly (logarithmically) with T_K (see Fig. 2.1). Therefore, we expect that the conclusions about the Kondo phase are reliable.

We also examined the situations with $1/2 < r < 1$ and $r > 1$. The former appears to be analogous to the $r = 1$ case with the only difference that exponential (logarithmic) behavior is substituted by a suitable power law. For $r > 1$ the picture is different in the sense that the phase diagram is qualitatively consistent with NRG results even in the zero temperature limit.

Finally we studied the behavior of a non-magnetic impurity in a d-wave superconductor, which creates a staggered magnetization on the nearest copper neighbors. It was found that the saddle point corresponding to the true minimum of the action always has d symmetry. The resulting spatial structure of the quasiparticle density of states near the impurity for this saddle point is consistent with the experimental data. It was also shown that contrary to the single spin case, the critical magnetic coupling corresponding to the Kondo transition decreases as U increases.

The developed model appears to be required to explain NMR [15, 16, 47, 75, 98, 103] and neutron scattering measurements [49, 134, 141, 158] on the same system. It is therefore satisfying that our model also leads to a low bias peak in the STM; the measured bias of this peak (1.5 meV) suggests that the Kondo screening of the moment (as can be measured directly in NMR) occurs at a temperature of order 15 K. We note, that density of states measurements alone can not distinguish between the purely potential and the Kondo scattering mechanisms. Indeed, the Kondo screened impurity behaves as a spin singlet and thus is equivalent to a spinless defect. The main difference for the Zn impurity case comes from the fact that local moments are induced on the neighboring sites and thus the scattering occurs from four points and results in a particular interference pattern consistent with experimental observations. On the other hand there are no natural reasons to assume anything like that if the impurity is treated as a simple single site defect. Therefore additional filtering mechanisms between the Cu layer and the STM tip were advocated to rec-

oncile that model with experiments [101]. It is difficult to argue what is the actual information, which is obtained from the STM measurements. On the other hand, further experiments may show which of these scenarios is indeed true. The potential scattering should not be sensitive at all to the applied magnetic field. On the other hand, the Kondo resonance should be destroyed by moderate fields corresponding to the Zeeman splitting comparable to the Kondo resonance energy ($\Omega_0 \approx 1.5$meV). Also possible temperature dependence of the DOS can shade the light because again at $T \sim 15$K, which is still much below T_c at optimal doping in $Bi_2Sr_2CaCu_2O_{8+\delta}$, the Kondo effect would be destroyed, while the potential scattering would survive.

Chapter 3

Pinning of dynamic spin density waves in HTSCs

Many studies of the cuprates assume that high temperature superconductivity is best understood by a theory of doping mobile charge carriers into a Mott insulator which is paramagnetic [8] *i.e.* a Mott insulator with no static spin moment on any site and dynamic antiferromagnetic spin density wave (SDW) correlations. Studies of paramagnetic Mott insulators on the square lattice of Cu ions [136, 159] showed that the most promising candidates have broken translational symmetry associated with the appearance of spontaneous bond charge order. The term "charge order" can be defined very generally: there is a periodic spatial modulation in observables which are invariant under spin rotations and time reversal, such as local electron/hole density of states (LDOS), the spin exchange energy, the pairing amplitude, or the electron kinetic energy contained in a link of the square lattice; the modulation in the total charge density may well be unobservably small because of screening by the long-range Coulomb interactions.

Ref [159] studied the doping of the charge-ordered paramagnetic Mott insulator:

superconductivity co-existed with charge order for a finite range of carrier concentrations (δ), and a d-wave superconductor with the full square lattice symmetry appeared above a critical δ. This, and other theoretical and experimental studies have concluded that the low temperature properties of this d-wave superconductor at optimal δ are qualitatively identical to those of a BCS superconductor obtained by the Cooper instability of a metallic Fermi liquid. This conclusion raises the question of whether the connection to the Mott insulator is even necessary in a description of the low temperature properties of the superconductor at or above optimal δ.

A number of works [10, 50, 61, 85, 108, 132] have argued that memory of the Mott insulator should survive in and around vortices in superconducting order: the suppression of superconductivity in the vortex core implies that the Cooper pairs are not condensed, but the electrons should still strive to retain the exchange correlation energy of the Mott insulator. This reasoning, and the studies of the doped paramagnetic Mott insulator [159], led to the suggestion that the static charge order, along with dynamic SDW correlations, should appear near vortex cores.

Hoffman *et al.* [64] introduced a novel scanning tunnelling microscopy (STM) technology of atomically registered spectroscopic mapping. Applied to slightly overdoped $Bi_2Sr_2CaCu_2O_{8+x}$, they detected LDOS modulations around the vortex cores at wavevectors $\mathbf{K}_{cx} = (\pi/2, 0)$ and $\mathbf{K}_{cy} = (0, \pi/2)$ (the square lattice spacing has unit length and this modulation has a period of four lattice spacings), co-existing with well established superconductivity [36, 174].

Bulk charge order with this, and related, periods has been discussed in insulating/superconducting paired hole states from a number of different theoretical perspectives [2, 17, 25, 87, 115, 153, 159, 163, 169]. Neutron scattering studies of the optimally doped cuprates have not (so far) seen dynamic or static charge order, but do see collinear SDW fluctuations at wavevectors $\mathbf{K}_{sx} = (3\pi/4, \pi)$ and $\mathbf{K}_{sy} = (\pi, 3\pi/4)$

and at energies above a spin gap Δ. On symmetry grounds [170], collinear SDW correlations are accompanied by charge order correlations at wavevectors $2\mathbf{K}_{sx,y}$, which equal the values of $\pm\mathbf{K}_{cx,y}$, modulo reciprocal lattice vectors. As we will show below, this connection can be used to describe the spatial envelope of the charge order in the doped Mott paramagnet by the pinning of a 'sliding' degree of freedom of the SDW by imperfections, such as vortex cores.

3.1 Phenomenological model

We assume the cuprate superconductor has a dominant spin collective mode near the wavevectors $\mathbf{K}_x = (3\pi/4, \pi)$ and $\mathbf{K}_y = (\pi, 3\pi/4)$, and so write for the spin operator on the lattice site $\mathbf{r}$ at imaginary time τ

$$S_\alpha(\mathbf{r}, \tau) = \mathrm{Re}\left[e^{i\mathbf{K}_x\cdot\mathbf{r}}\Phi_{x\alpha}(\mathbf{r}, \tau) + e^{i\mathbf{K}_y\cdot\mathbf{r}}\Phi_{y\alpha}(\mathbf{r}, \tau)\right],$$

where $\Phi_{x,y\alpha}$ are the spin density wave (SDW) order parameters which are assumed to be smooth functions of spacetime.

We use a Gaussian action for $\Phi_{x,y\alpha}$ fluctuations:

$$\mathcal{S}_\Phi = T\sum_{\mathbf{q},\omega_n,\alpha} \chi_x^{-1}(\mathbf{q}, \omega_n)|\Phi_{x\alpha}(\mathbf{q}, \omega_n)|^2 + (x \to y); \tag{3.1}$$

we have Fourier transformed from $(\mathbf{r}, \tau)$ to wavevectors $\mathbf{q}$ and Matsubara frequencies ω_n at a temperature T. The dynamic spin susceptibilities $\chi_{x,y}$ will be inputs from which we will deduce the dynamic structure of the pinned charge order. However, this should not be interpreted as a causal connection from the SDW fluctuations to the charge order; rather, our method relies on the assumed proximity of the superconductor to a quantum transition to a superconducting state with long-range SDW order [36, 159, 174]. The presence of such a quantum critical point, and the values of $\mathbf{K}_{sx,y}$ near it, are determined by a complicated interplay between spin and charge

correlations in the superconductor and the proximate Mott insulator. We will take a simple functional form for $\chi_{x,y}$ (see below), with a spectral weight which vanishes below a spin gap energy Δ (a more accurate form can, in principle, be extracted from neutron scattering experiments). Sachdev, Demler, and Zhang [36, 174] argued that the value of Δ can be tuned by an applied magnetic field perpendicular to the square lattice layers, and its primary effect is a reduction in Δ.

Invariance under translation by n_x lattice spacings in the x direction (for arbitrary integer n_x) leads to the symmetry $\Phi_{x,\alpha} \to e^{in_x\pi/4}\Phi_{x\alpha}$ obeyed by $\mathcal{S}_\Phi$ (and similarly for $\Phi_{y\alpha}$). As long as this symmetry is preserved, no observable will exhibit static charge order at wavevectors $\mathbf{K}_{cx,y}$. However, this sliding translation symmetry is broken by any imperfection (vortex core or impurity) that may be centered near $\mathbf{r} = \mathbf{r}_0$, provided the spatial extent of the imperfection is not much larger than the charge order period (4 lattice spacings). We account for such an imperfection by adding a pinning term to the action

$$\mathcal{S}_{\rm pin} = -\sum_\alpha \int d\tau \left[\zeta_x \Phi^2_{x\alpha}(\mathbf{r}_0,\tau) + (x \to y) + c.c.\right], \tag{3.2}$$

where $\zeta_{x,y}$ are complex coupling constants representing the pinning potential. Note that $\mathcal{S}_{\rm pin}$ contains the simplest terms which break the $\Phi_{x,\alpha} \to e^{in_x\pi/4}\Phi_{x\alpha}$ symmetry, but preserve spin rotation invariance. Additional terms like $\Phi_{x\alpha}(\mathbf{r}_0,\tau)\Phi_{y\alpha}(\mathbf{r}_0,\tau)$ are also permitted but we will not include them for simplicity; such terms lead to a 90° turn in an SDW fluctuation and can be expected to have a small amplitude on physical grounds—their presence will lead to additional charge order at $\pm\mathbf{K}_{sx} \pm \mathbf{K}_{sy}$. We also note that the theory for the superconductor proximate to a charge ordering transition has a pinning term linear in the charge order parameter.

STM involves tunneling of single electrons, and so to compute the STM spectra we couple the Gaussian SDW fluctuations described by $\mathcal{S}_\Phi + \mathcal{S}_{\rm pin}$ to the electrons,

which we describe by a standard d-wave BCS model:

$$H_{\rm BCS} = \sum_{\mathbf{k}} \Psi^{\dagger}_{\mathbf{k}} \left[(\varepsilon_{\mathbf{k}} - \mu)\tau^z + \Delta_{\mathbf{k}}\tau^x \right] \Psi_{\mathbf{k}}. \tag{3.3}$$

Here $\Psi_{\mathbf{k}} = (c_{\mathbf{k}\uparrow}, c^{\dagger}_{-\mathbf{k}\downarrow})$ is a Nambu spinor at momentum $\mathbf{k} = (k_x, k_y)$, $\tau^{x,y,z}$ are Pauli matrices in particle-hole space, and μ is a chemical potential. For the kinetic energy, $\varepsilon_{\mathbf{k}}$ we have first (t) and second (t') neighbor hopping, while we assume a d-wave form for the BCS pairing function $\Delta_{\mathbf{k}} = (\Delta_0/2)(\cos k_x - \cos k_y)$. The full Hamiltonian for the conduction electrons reads

$$H = H_{BCS} + \gamma \sum_{\mathbf{r}} c^{\dagger}_{\mu}(\mathbf{r})\sigma^{\alpha}_{\mu\nu}c_{\nu}(\mathbf{r}) \left(\Phi_{x\alpha}(\mathbf{r})e^{i\mathbf{K}_x\cdot\mathbf{r}} + \Phi^{*}_{x\alpha}(\mathbf{r})e^{-i\mathbf{K}_x\cdot\mathbf{r}} + (x \rightarrow y) \right), \tag{3.4}$$

where σ^{α} are the Pauli spin matrices, and γ describes the scattering of the Bogoliubov quasiparticles of the superconductor off the SDW fluctuations. We note that Han [61] has used the same model, but used microscopic computations on the t-J model as input for χ.

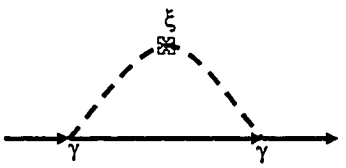

Figure 3.1: Feynman diagram corresponding to the LDOS modulation described by 3.5. Solid and dashed lines represent quasiparticle and SDW propagators respectively. The cross corresponds to the pinning of the SDW by a local defect.

In second order in the quasiparticle-collective mode coupling γ and in first order in the pinning strength ζ, described by the diagram 3.1, the model predicts the following density of states modulations:

$$\delta\rho(\mathbf{r},\omega) \approx \Im \mathrm{Tr} \frac{1+\tau_z}{2} \sum_{\mathbf{r}_1,\mathbf{r}_2} G_0(\mathbf{r}-\mathbf{r}_1,\omega)\Sigma(\mathbf{r}_1,\mathbf{r}_2,\omega)G_0(\mathbf{r}_2-\mathbf{r},\omega), \tag{3.5}$$

where G_0 is the electronic Green's function in a canonical translationally invariant BCS superconductor with kinetic energy $\varepsilon_{\mathbf{k}}$ and pairing amplitude $\Delta_{\mathbf{k}}$ (the momentum subscript on $\Delta_{\mathbf{k}}$ distinguishes it from the collective spin gap Δ), and τ_z is a

Pauli matrix in the Nambu particle-hole space. The self energy Σ arises from the coupling to the spin collective mode, and we focus only on the contribution which breaks translational invariance because of the pinning of the collective mode

$$\Sigma(\mathbf{r}_1, \mathbf{r}_2, \omega) \approx 12\xi\gamma^2 \int \frac{d\nu}{2\pi} \chi(\mathbf{r}_2, \nu)\chi(\mathbf{r}_1, \nu)G_0(\mathbf{r}_2 - \mathbf{r}_1, \omega - \nu)\cos(\mathbf{K}_x(\mathbf{r}_1 + \mathbf{r}_2) - \delta). \quad (3.6)$$

The parameter δ, which is the phase of the coupling ζ, distinguishes site centered SDWs ($\delta = 0$) and bond centered SDWs ($\delta = \pi/2$). Following the STM experiments [64, 65, 67, 68], we will compute the Fourier transform of the LDOS:

$$\delta\rho(\mathbf{q}, \omega) = \Im \mathrm{Tr} \frac{1 + \tau_z}{2} \int \frac{d^2k}{(2\pi)^2} G_0(\mathbf{k}, \omega)\Sigma(\mathbf{k}, \mathbf{k} + \mathbf{q}, \omega)G_0(\mathbf{k} + \mathbf{q}, \omega). \quad (3.7)$$

It is not difficult to see from (3.5-3.7) that in the limit of a large spin gap ($\Delta \to \infty$), the modulations in the LDOS predicted by (3.7) are identical to those predicted in a model of quasiparticle scattering off isolated, point-like static impurities or other imperfections considered in Ref. [161]. For a general scattering potential $u(\mathbf{q})$, and impurity-induced variation in the superconducting gap $v(\mathbf{q}_1, \mathbf{q}_2)$, the expression for the LDOS modulation due to *static* impurities in the Born approximation is:

$$\delta\rho_{\mathrm{st}}(\mathbf{q}, \omega) = \Im \mathrm{Tr} \frac{1 + \tau_z}{2} \int \frac{d^2k}{(2\pi)^2} G_0(\mathbf{k}, \omega)(u(\mathbf{q})\tau_z + v(\mathbf{k}, \mathbf{k} + \mathbf{q})\tau_x)G_0(\mathbf{k} + \mathbf{q}, \omega). \quad (3.8)$$

Below, we will compare the predictions of (3.8) to those in (3.7) of a pinned dynamic SDW with a finite Δ.

3.2 Numerical results

Sample results from the dynamic SDW model (3.7) are shown in figs 3.2-3.4. For small spin gap Δ, the LDOS shows the expected [170] modulations near $\mathbf{q} = 2\mathbf{K}_{x,y}$. The magnitude of this modulation depends strongly on the value of Δ, and the strong expected dependence of Δ on doping and applied magnetic field [36] (Δ decreases

with decreasing δ and increasing field) will lead to a corresponding variation in the LDOS peaks near $\mathbf{q} = 2\mathbf{K}_{x,y}$. This peak also disperses as a function of ω, with the dispersion being stronger for larger values of Δ as shown in fig. 3.4; the decrease in the $\mathbf{q}$ value of the peak with increasing ω is consistent with observations [65].

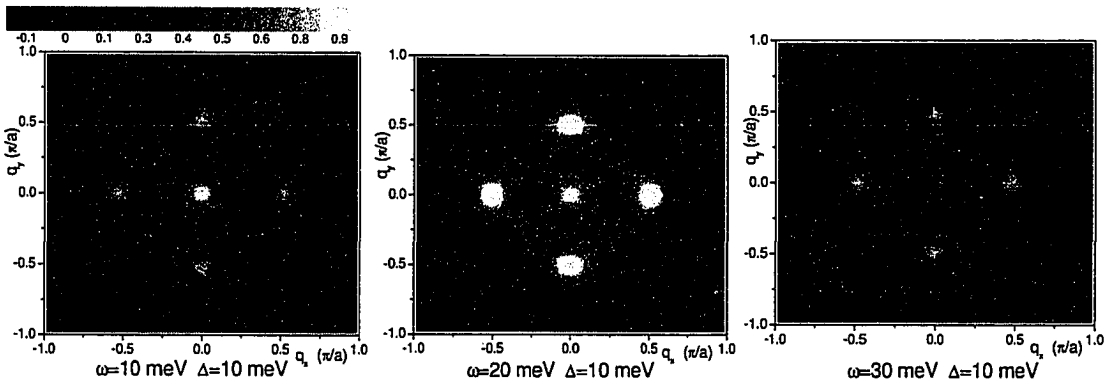

Figure 3.2: Fourier map of the LDOS $\delta\rho(\mathbf{q},\omega)$ in (3.7) for $\Delta = 10$ meV. The BCS superconductor is parameterized by $t = -0.15$ eV, $t' = -t/4$, $\mu = -0.135$ eV which gives a doping level of about 15%, and $\Delta_0 = 40$ meV. The spin wave velocity was assumed to be $c = 0.2$ eV. The maxima around $(\pi/2, 0)$ come mainly from scattering off a pinned SDW. The other peaks are due to details of quasiparticle spectrum.

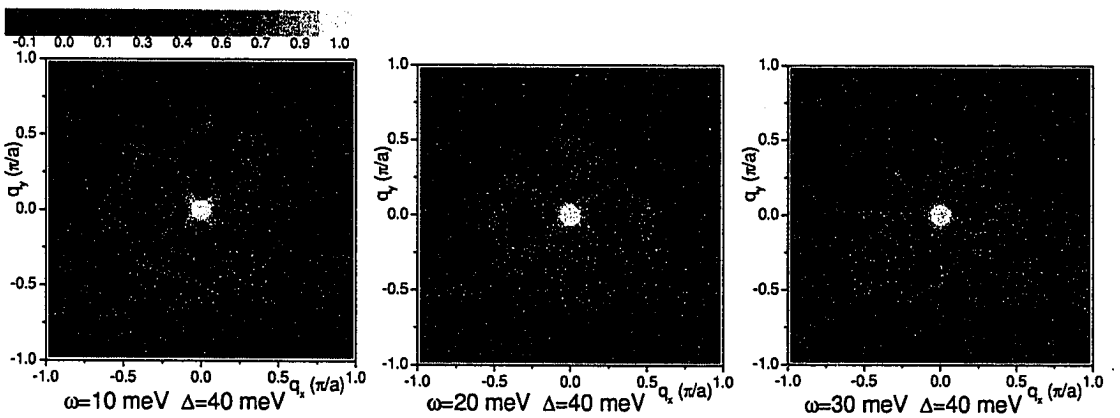

Figure 3.3: As in fig. 3.2 for $\Delta = 40$ meV.

As is clear from figs. 3.2 and 3.3, the LDOS also has peaks in its modulation at a number of other wavevectors. These arise from the two flanking quasiparticle Green's functions in (3.7), and are consequently sensitive to all details of the quasiparticle

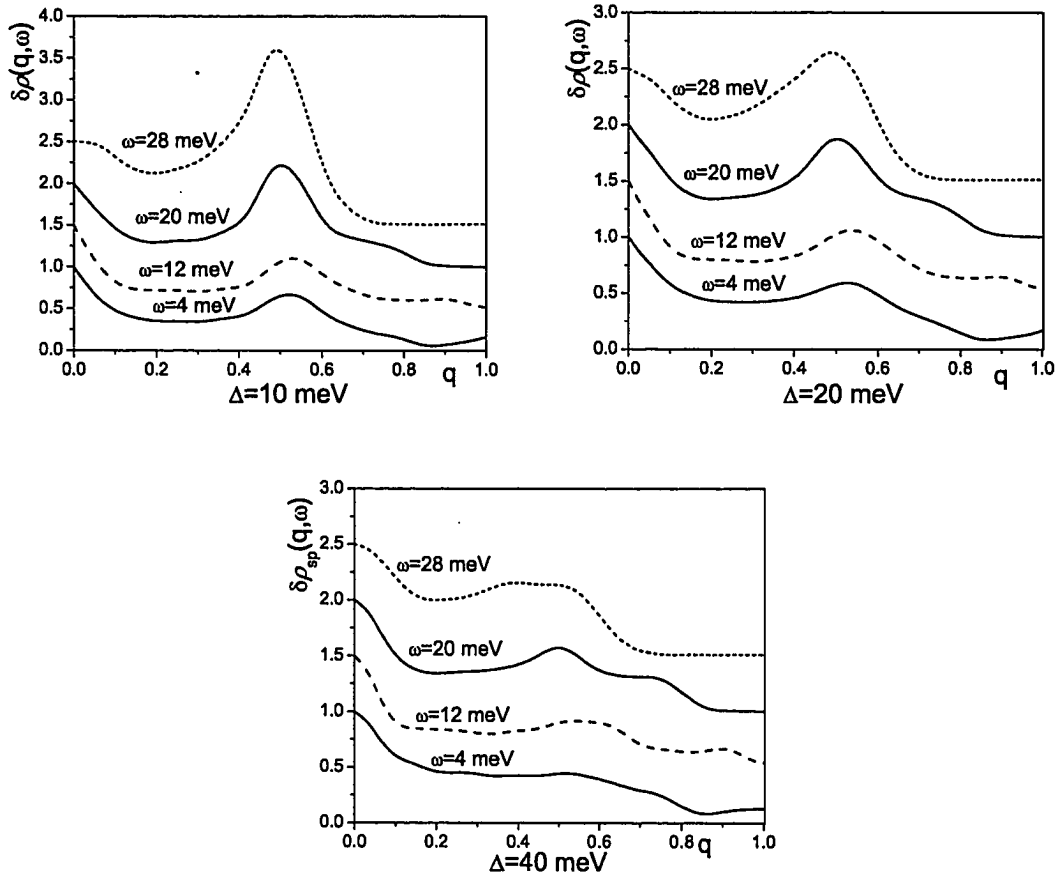

Figure 3.4: Dependence of the fourier component of LDOS on the wavevector along [1,0] direction for different energies.

spectrum. These additional features are also present in the static impurity model (3.8) whose results are shown in fig. 3.5

It is instructive to compare the static impurity scattering prediction in Fig 3.5 to the dynamic spin collective mode predictions in Figs. 3.2 and 3.3: apart from the strong contributions at $\mathbf{q} = \pm 2\mathbf{K}_{x,y}$ present in the latter, the former has the same general features as the large Δ cases of the latter. This is one of the main points of this paper.

The physics of the structure in the static impurity scattering LDOS modulation, $\delta\rho_{\rm st}(\mathbf{q},\omega)$ in (3.8), has already been discussed by several authors [161, 20, 86]. The

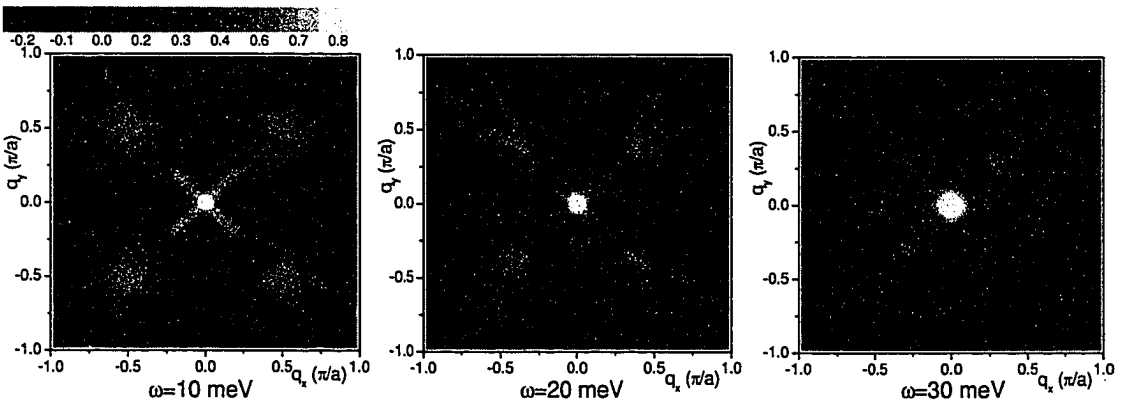

Figure 3.5: Fourier map of LDOS for scattering off a single localized defect, $\delta\rho_{\rm st}(\mathbf{q},\omega)$ in (3.8). We used a point defect with $u(\mathbf{q}) = v(\mathbf{k},\mathbf{k}+\mathbf{q}) = 1$.

expression (3.8) can be rewritten as:

$$\delta\rho_{\rm st}(\mathbf{q},\omega) = 2\int \frac{d^2k}{(2\pi)^2}\delta(-\omega^2+\varepsilon_{\mathbf{k}}^2+\Delta_{\mathbf{k}}^2)\left(u(\mathbf{q})\frac{(\omega-\varepsilon_{\mathbf{k}})(\omega-\varepsilon_{\mathbf{k+q}})-\Delta_{\mathbf{k}}\Delta_{\mathbf{k+q}}}{-\omega^2+\varepsilon_{\mathbf{k+q}}^2+\Delta_{\mathbf{k+q}}^2}-\right.$$
$$\left. v(\mathbf{k},\mathbf{k}+\mathbf{q})\frac{(\omega-\varepsilon_{\mathbf{k}})\Delta_{\mathbf{k+q}}+\Delta_{\mathbf{k}}(\omega-\varepsilon_{\mathbf{k+q}})}{-\omega^2+\varepsilon_{\mathbf{k+q}}^2+\Delta_{\mathbf{k+q}}^2}\right). \qquad (3.9)$$

We would like to point out, that this formula is not a convolution of the product of the density of states of quasiparticles at energy ω with momenta differing by $\mathbf{q}$, but rather the product of the density of states of one quasiparticle with the real part of the Green function of the other. It contains square root divergences [20] at wavevectors, where the contours of constant energies $\omega^2 = \varepsilon_{\mathbf{k}}^2 + \Delta_{\mathbf{k}}^2$ and $\omega^2 = \varepsilon_{\mathbf{k+q}}^2 + \Delta_{\mathbf{k+q}}^2$ are tangent to each other. These singularities form one-dimensional manifolds in the Fourer space. At special wavevectors there are local extremes, which look like isolated spots [20]. We show some of the wavevectors corresponding to these spots in Fig. 3.6. This singularities are quite weak in our plots; for strong impurity scattering it is necessary to go beyond the Born approximation, and then the structure at these (in fact at slightly different) wavevectors can be enhanced as discussed in Refs. [102, 161]. There are also other momenta giving large DOS modulations. For example, in Fig. 3.5, the main contributions for $\mathbf{q}$ along the Brillouin zone

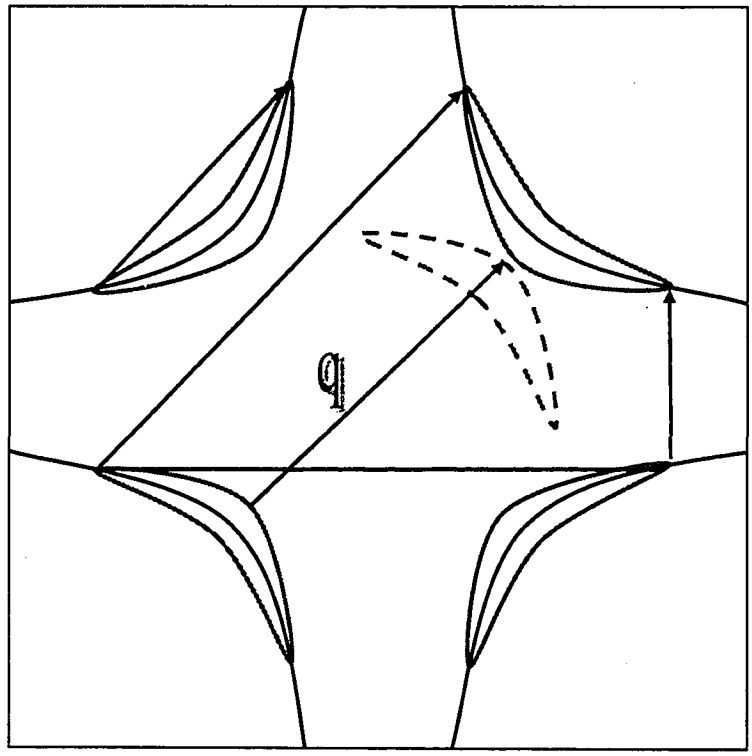

Figure 3.6: Fermi surface of a typical cuprate superconductor. Banana-like lines correspond to constant energy contours. The arrows identify some of the possible wavevectors giving local maxima in LDOS modulation. Without quasiparticle damping fourier component of LDOS would have a square root divergence whenever the contour of constant energy translated by vector q (dashed line) is tangent to a similar contour.

diagonals come from values of $\mathbf{k}$ and $\mathbf{k}+\mathbf{q}$ near the nodal points and the underlying Fermi surface near $\pm(\pi,0),\pm(0,\pi)$ respectively, presumably coming from Van Hove singularity . We emphasize that all these features of quasiparticle-scattering induced LDOS modulations also appear in our model of a pinned dynamic spin collective mode. In particular, as we noted earlier, if Δ is large, then the pinned SDW model is equivalent to an effective short-range static quasiparticle potential, along with additional weak modulations at $\pm 2\mathbf{K}_{x,y}$ (compare Figs. 3.3, and 3.5). For smaller Δ, the effective quasiparticle potential created by the SDW fluctuations is dynamic, but

the qualitative the picture at wavevectors different from $\pm 2\mathbf{K}_{x,y}$ remains the same.

3.3 Conclusions

In conclusion, we have shown that our model displays many of the features observed in recent STM experiments. Besides the modulations of the LDOS at wavevectors $\pm 2K_{x,y}$ arising from the spin collective mode, we find other features related to the spectrum of the fermionic Bogoliubov quasiparticles. The positions of the maxima at $\pm 2K_{x,y}$ have a relatively small (but not negligible) dependence on the tunnelling energy ω, while other features are more strongly dependent on ω and the details of the quasiparticle spectrum .

Whether the observed periodic modulation at the wavevector $(\pi/2, 0)$ is related purely to the details of the Fermi surface [102] or the period four modulations in the electron density of states can be attributed to the other collective degrees of freedom like static or dynamic SDWs as we discuss here or some other static charge density wave modulation [117] still remains an open question. It will be possible to resolve it doing further experiments. The spin fluctuations should drastically increase with the applied magnetic fields because of the strong field dependence of the anticipated spin gap Δ [36, 174]. Also, the details of the Fermi surface will strongly change upon doping. Thus, the period four modulation which is some kind of coincidence at some doping level in the simple scattering model, should be modified to completely different periodicity. On the other hand, the models which favor intrinsic order would still predict density of states modulations at the same wavevector. These issues are currently the subject of intense theoretical and experimental research and should be resolved in the next few years.

Chapter 4

Phase oscillations of BECs in optical lattices

As we already mentioned in the introduction, interacting bosons in an optical lattice have a number of spectacular properties. For example they can undergo a quantum phase transition from the superfluid to the insulating phase [46], and this was indeed experimentally observed [58]. The facile tunability and long characteristic time scales of these systems also offer an opportunity to investigate non-equilibrium dynamical regimes that have not been accessible before for other systems. In this context, there have been a few recent theoretical studies of the temporal behavior of bosons in a periodic potential [40, 51, 88, 151].

Motivation of the purpose of this chapter requires an understanding of the different parameter regimes of the boson system, which we will assume is well described by the single-band Hubbard model:

$$\mathcal{H} = \sum_j \left[-J(a_j^\dagger a_{j+1} + a_{j+1}^\dagger a_j) + V_j a_j^\dagger a_j + \frac{U}{2} a_j^\dagger a_j (a_j^\dagger a_j - 1) \right]. \tag{4.1}$$

Here a_j is a canonical Bose annihilation operator on sites of the optical lattice ("wells") labeled by the integer j, J is the tunneling amplitude between neighboring

lattice sites, $U > 0$ is the repulsive interaction energy between bosons in the same lattice minimum, and V_j is a smooth external potential due to the magnetic trap which is usually parabolic. We will mainly consider the case of a one-dimensional optical lattice, relevant to the experiments of Ref. [112], but generalization to higher dimensions is straightforward. There is another important parameter in the model: N, which is the typical number of bosons per site (in the case of nonuniform potential the more precise definition would be the number per central site, where V_j has a minimum). The importance of N becomes apparent if we consider two opposite regimes of the model. For simplicity let us ignore for the moment V_j. Then clearly in the limit $U \to \infty$ the ground state would be a Mott insulator with precisely N bosons per site. The elementary excitation would be a transfer of a single particle by one lattice spacing. The corresponding increase of the interaction energy will be:

$$\delta E_{int} = U\frac{(N+1)^2}{2} + U\frac{(N-1)^2}{2} - UN^2 = U. \tag{4.2}$$

On the other hand, because of the uncertainty relation $\delta N \delta\phi \geq 1/2$, it is clear that if $\delta N = 1$ then the phase fluctuations are also of the order of one and the gain in the hopping energy will be:

$$-\delta E_{hop} \approx 2JN\langle\cos\phi\rangle \sim JN. \tag{4.3}$$

If we equate these two energies we will get a qualitative estimate for the boundary of the superfluid - Mott insulator phase transition. Indeed if the hopping is zero, there is clearly a gap in the excitation spectrum, and small tunneling can not immediately destroy it. On the other hand if JN becomes larger than U, the gap disappears and the bosons can hop. The ground state then becomes superfluid. Let us now look into hamiltonian (4.1) from the opposite limit of vanishing interaction $U \to 0$. Then the energy associated with hopping is still the same as before:

$$E_{hop} \approx -2JN \tag{4.4}$$

while the interaction energy reads

$$E_{int} \approx U\frac{N^2}{2}. \tag{4.5}$$

Equating these two energies gives another scale for the interaction:

$$U \approx J/N. \tag{4.6}$$

It determines the crossover from the noninteracting to strongly interacting superfluid. Note that if $N \gg 1$ then there is a wide range of parameters:

$$\frac{J}{N} \ll U \ll JN, \tag{4.7}$$

where interactions are important but the quantum fluctuations are still relatively weak. This gives an additional motivation for studying the regime $N \gg 1$.

Instead of U, it is convenient to introduce a dimensionless measure of the strength of interactions between the bosons λ:

$$\lambda \equiv \frac{UN}{J}; \tag{4.8}$$

the different physical regimes of $\mathcal{H}$ are also conveniently delineated by the values of λ. The Mott insulator will correspond to $\lambda \geq \lambda_{SI} \sim N^2$, while the crossover from weakly to strongly interacting superfluid occurs at $\lambda \approx 1$. In this chapter we will be mostly interesting in the superfluid regime, i.e. $\lambda \ll N^2$. The discussion above is somewhat modified in the presence of external potential (see Appendix A). The phase transition is no longer there, but the scale for importance of quantum fluctuations λ_{SI} remains essentially unchanged.

For N large, and λ smaller than λ_{SI}, it is widely accepted [51] that the dynamics of $\mathcal{H}$ can be described by treating the operator a_j as a classical c-number. (We will investigate the conditions for the validity of this classical approximation more carefully in Section 4.1, where we will also discuss the time range over which it can be

applied.) More precisely, we introduce the dimensionless complex dynamical variable $\psi_j(t)$ whose value is a measure of $\langle a_j(t)\rangle/\sqrt{N}$; then its dynamics is described by the classical hamiltonian

$$H_{GP} = \sum_j \left[-(\psi_j^* \psi_{j+1} + \psi_{j+1}^* \psi_j) + \frac{V_j}{J}|\psi_j|^2 + \frac{\lambda}{2}|\psi_j|^4 \right], \tag{4.9}$$

and the Poisson brackets

$$\{\psi_j, \psi_j^*\} = \delta_{ij}. \tag{4.10}$$

Here, and henceforth, we measure time in units of $\hbar/J$. The resulting equations of motion are, of course, a discrete version of the familiar Gross-Pitaevskii (GP) equations. In the case of a parabolic confining potential

$$\frac{V_j}{J} = \frac{\xi}{2} j^2.$$

Nonuniform V_j also can lead to localization of bosons in separate wells; in particular, even without interaction ($\lambda = 0$), when $|V_{j+1} - V_j| \geq 2J$ the eigenmodes of (4.9) become localized. Note that this localization is a purely semiclassical effect, described by the GP equations. If V_j is smooth then for $\lambda > \lambda_{SI}$, the system undergoes a transition (or rather crossover) to a nonuniform insulating state driven entirely by quantum fluctuations [13, 78].

Describing the non-equilibrium quantum Bose dynamics for $\lambda < \lambda_{SI}$ is now reduced to a problem of integrating the classical equations of motion implied by (4.9,4.10). However, it remains to specify the initial conditions for the classical equations.

As an example, consider the physical situation (of current experimental interest [154]) where for $t \leq 0$ the bosons are in a Mott insulating state with $\lambda > \lambda_{SI}$, and at time $t = 0$ the optical lattice potential is suddenly reduced so that $\lambda < \lambda_{SI}$ for all $t > 0$. Clearly, the GP equations should apply for $t > 0$. On the other hand

the initial Mott insulating state can be never described using semiclassical theory. So we have to deal with the problem that the dynamics is classical but the initial conditions are not. In the next two chapters we will rigorously show how to deal with such situations in general. However for this particular example, the required initial conditions are readily deduced by a simple argument. Let us consider the full quantum Heisenberg equations of motion for $a_j(t)$ implied by $\mathcal{H}$. By integrating these equations, one can, in principle, relate any observable to the expectation values of products of powers of $a_j^\dagger(t=0)$ and $a_j(t=0)$. For the Mott insulator with $\lambda \gg \lambda_{SI}$ these expectation values have a very simple structure: they factorize into products of expectation values on each site, and are non-zero only if the number of creation and annihilation operators on each site are equal. Furthermore, for large N, we can also ignore the ordering of the a_j and $a_j^\dagger$ operators on each site, and *e.g.* we obtain to leading order in $1/N$:

$$\left\langle a_j^{\dagger n}(t=0) a_\ell^m(t=0) \right\rangle \approx \delta_{nm}\delta_{j\ell}\,(N_j)^n\,, \tag{4.11}$$

where we have accounted for a possible spatial inhomogeneity by introducing N_j (a number of order N), the number of bosons at site j in the Mott insulator. In terms of the classical variables ψ_j, the $t=0$ expectation values in (4.11) are easy to reproduce. We simply choose

$$\psi_j(t=0) = \sqrt{N_j/N}e^{i\phi_j} \tag{4.12}$$

where the ϕ_j are *independent random variables* which are uniformly distributed between 0 and 2π. The other intuitive way to get these boundary conditions is to note that the initial insulating state is essentially a number state with well defined number of bosons per site. On the other hand from the Heisenberg uncertainty principle, the phase in this state is completely undefined, i.e. randomly distributed. In this manner, we have mapped the fully deterministic quantum time evolution of

$\mathcal{H}$ to the classical evolution of H_{GP} with stochastic boundary conditions. In practice, the procedure is then as follows: choose a large ensemble of initial values of ϕ_j, and deterministically evolve H_{GP} for each such initial condition; the expectation value of any quantum observable at time t is then given by the average value of the corresponding classical observable at time t, with the average being taken over the random variables ϕ_j. In particular

$$\left\langle a_j^{\dagger n}(t) a_{j'}^m(t) \right\rangle_Q \approx N \left\langle \psi_j^{*n}(t) \psi_{j'}^m(t) \right\rangle_{\text{random } \phi_\ell}, \tag{4.13}$$

where we have indicated that the angular brackets on the left represent a traditional quantum expectation value, while those on the right represent an average over the independent variables ϕ_j specified by (4.12) at time $t = 0$. We will henceforth implicitly assume that all angular brackets have the meaning specified in (4.13), depending upon whether they contain quantum or classical variables.

An important property of (4.13) is that while we must have $j' = j$ for a non-zero result at $t = 0$, this is no longer true for $t > 0$. In particular, non-zero correlations can develop for large $|j' - j|$ as time evolves, corresponding to a restoration of phase coherence. Indeed the ground state for $\lambda < \lambda_{SI}$ is superfluid and thermalization must lead to increase of the phase correlations. However, in this paper we show, that even without relaxation the coherence can be restored dynamically. (Of course, as we are looking at one dimensional systems and the final state is expected to be thermalized at a non-zero temperature, the phase correlations cannot be truly long-range and must decay exponentially at large enough scales: however, guided by the experimental situation, we will look at relatively small systems for which this is not an issue.) Describing the dynamics of the restoration of this phase coherence is one of the central purposes of this chapter. We shall characterize the phase coherence by

studying the expectation value of

$$\mathcal{D}_g(t) = \frac{1}{M} \sum_{j \neq \ell} g(|j - \ell|) \left\langle \psi_j^*(t) \psi_\ell(t) \right\rangle \tag{4.14}$$

where M is the number of lattice sites (for a nonuniform external potential V_j, M is just the ratio of the total number of bosons to the number of bosons in central well), and g is some suitably chosen weight function. Observables closely related to $\mathcal{D}_g$ are measured upon detecting the atoms after releasing the trap so that each site serves as a source of matter waves and they interfere with each other if their phases are correlated. At time $t = 0$, $\mathcal{D}_g(0) = 0$, and we will be interested in the behavior of $\mathcal{D}_g(t)$ for $t > 0$, an increase would correspond to an enhancement of phase correlations characteristic to the superfluid phase. We note, in passing, that a closely related procedure was used earlier [31, 32] to describe the onset of phase coherence after a sudden quench from high temperature; here, we are always at zero temperature, and move into a superfluid parameter regime by a sudden change in the value of λ.

We will begin our analysis of the structure of $\mathcal{D}_g(t)$ by considering the case with two wells ($M = 2$) in Section 4.1. For the weakly interacting case ($\lambda \ll 1$), $\mathcal{D}_g(t)$ exhibits Josephson oscillations with a period of order unity; the weak interactions lead to a decay of oscillations with a slow ($t^{-1/2}$) saturation of the coherence at a steady-state value at a time scale $t \propto \lambda^{-1}$. For $\lambda \gg 1$ the oscillations are overdamped and $\mathcal{D}_g(t)$ saturates at $t \propto 1/\sqrt{\lambda}$, which is, in fact, shorter than a single tunneling time. For this two lattice site case we can also obtain a complete solution for $\mathcal{D}_g(t)$ for the quantum hamiltonian $\mathcal{H}$ (described in Section 4.1.2), and this allows a detailed analysis on the regime of validity of the semiclassical GP equations. We show that the semiclassical approach is valid for two lattice sites when N is large and $t < N/\lambda$. This is, in fact, a general result which implies that the quantum mechanics becomes

important when time exceeds inverse energy level spacing (or to be more precise difference between adjacent level spacings). For more than two lattice sites, the energy splitting scales as the inverse of the total number of particles and at $\lambda \ll 1$, the semiclassical conditions should be valid even for longer times. It is surprising that even with a small number of particles per site $N = 2$, and weak interactions, the GP equations give an excellent description of the system evolution, apart from overall numerical prefactor $(1 + 1/N)$, which is not small in this case. In the next chapter we will show that the classical dynamics is indeed asymptotically exact at small times for any number of bosons per well and we also explain the origin of the $(1 + 1/N)$ prefactor.

The restoration of coherence in a lattice with more than two sites is considered in Section 4.2. We discuss the case without an external potential in Section 4.2.1; with an equal number of particles initially in all the wells, phase correlations develop only in the interacting case ($\lambda > 0$). Similar to the two well case, in the weakly interacting regime phase correlations will oscillate in time. However these oscillations will be periodic only for particular number of wells: $M = 2, 3, 4, 6$ for periodic boundary conditions and $M = 2, 3, 5$ for open boundary conditions. For other numbers of wells, the oscillations are chaotic. As for the two wells, a stronger interaction results in decay of correlations in time, leading to a steady state, which as we will discuss, would correspond to a microcanonical thermodynamic ensemble.

Next, in Section 4.2.2, we consider the restoration of phase coherence for the experimentally important situation of a parabolic potential. The results are quite different for this case, and phase correlations develop even without interactions. In a weak potential, $\mathcal{D}_g(t)$ oscillates in time with a frequency which scales as the square root of the parabolicity, ξ. The period of oscillations is closely related to that discussed recently by Kramer *et al.* [88] in the context of the center of mass oscillations

of the atomic gas. In the present situation, there is no physical displacement of the condensate, but the same oscillation is excited upon a sudden change in the value of λ. The oscillations decay even at $\lambda = 0$; weak or intermediate interactions $\lambda \leq 1$ do not change the noninteracting picture much. The amplitude of the oscillations becomes even more pronounced for intermediate interactions $\lambda \approx 1$, but for $\lambda \gg 1$ the oscillations become much faster and strongly damped as for the flat potential.

Recent work of Altman and Auerbach also addresses the restoration of phase coherence in a Mott insulator [3]. However, there are some significant differences in the physical situations being addressed. Above, we have considered a system deep in the Mott insulating phase (with $\lambda \gg \lambda_{SI}$) taken suddenly to parameters for which the ground state was deep in the superfluid phase (with $\lambda \ll \lambda_{SI}$). In contrast, Ref. [3] considers the case when both the initial and final values of λ were not too far from λ_{SI}, but remained on opposite sides of it. For λ close to λ_{SI}, and at temperatures not too small, a "relativistic Gross-Pitaevski" equation had been proposed in Ref. [133] as a description of the "*Bose molasses*" dynamics of the order parameter. Altman and Auerbach [3] advocated that the same equations could describe the time evolution of the amplitude of the order parameter as it evolved from the Mott insulator (with zero amplitude) to the superfluid (with finite amplitude) at zero temperature. Altman and Auerbach also considered the situation without an external potential ($V_j \equiv 0$). We have noted above that such a potential changed our results significantly; in Appendix A we discuss the role of the external potential in the equilibrium properties for $\lambda \approx \lambda_{SI}$.

4.1 Semiclassical versus quantum dynamics of two coupled interacting Bose systems

We will start a general analysis of the semiclassical versus quantum dynamics from an exactly solvable case of two coupled Bose condensates. Although this problem was addressed earlier[51, 105, 127], we will give a complete analysis here trying to extract the results valid for the general case of multiple condensates.

First let us focus on the semiclassical description of the two well system. In this case, the Gross-Pitaevskii equations implied by (4.9) and (4.10) are

$$i\frac{\partial\psi_1}{\partial t} = -\psi_2 + \lambda|\psi_1|^2\psi_1, \tag{4.15}$$

$$i\frac{\partial\psi_2}{\partial t} = -\psi_1 + \lambda|\psi_2|^2\psi_2, \tag{4.16}$$

The total number of bosons $|\psi_1|^2 + |\psi_2|^2$ is a constant of the motion; with our normalization for ψ_j described above (4.9), we have $|\psi_1|^2 + |\psi_2|^2 = 2$. The above system with two integrals of motion (total energy and the number of bosons) is equivalent to a single second-order differential equation. To see this, let us use the parametrization:

$$\psi_{1,2} = \sqrt{1 \mp n}e^{i\theta \mp i\phi/2}. \tag{4.17}$$

Note that only the relative phase of ψ_1 and ψ_2 is an observable. Substituting (4.17) into (4.15) and (4.16) we obtain:

$$\frac{d^2n}{dt^2} + 4n + 4\lambda n\sqrt{1-n^2}\cos\phi = 0, \tag{4.18}$$

$$\frac{d\cos\phi}{dn} = \frac{n}{1-n^2}\cos\phi + \frac{\lambda n}{\sqrt{1-n^2}}. \tag{4.19}$$

After further manipulation this system reduces to a single differential equation for the continuous variable n:

$$\frac{d^2n}{dt^2} + 4n + 4\lambda n\sqrt{1-n_0^2}\cos\phi_0 + 2\lambda^2 n(n^2-n_0^2) = 0 \tag{4.20}$$

with initial conditions: $n(0) = n_0$, $dn(0)/dt = 2\sin\phi_0$. Similar equations were derived in [51, 127]. Without interaction ($\lambda = 0$) we have a situation equivalent to a single Josephson junction described by a free harmonic oscillator. The interaction is responsible for the anharmonicity. Note that for $\lambda \leq 1$ the solutions $n = 0$, $\phi = 0, \pi$ are stationary; *i.e.* the phase difference between the two wells can be either 0 or π. On the other hand for $\lambda > 1$ the solution with $\phi = \pi$ becomes unstable [51, 127], and instead the new minima appear at

$$n_{\min} = \pm\sqrt{\frac{2(\lambda - 1)}{\lambda^2}}. \tag{4.21}$$

This observation leads to interesting implications, which we are going to address in the next chapter.

Let us assume that initially the two condensates are completely uncoupled, i.e. that they are in product of number (Fock) states. We will consider their semiclassical and quantum evolution in turn:

4.1.1 Semiclassical theory

From the discussion above, we have $n_0 = 0$ and ϕ_0 is a uniform random variable. We will study the correlation between ψ_1 and ψ_2 as a function of time. It is easy to show that

$$\langle \psi_2^*(t)\psi_1(t) + \psi_1^*(t)\psi_2(t)\rangle = \frac{\lambda}{4}\langle n^2(t)\rangle, \tag{4.22}$$

where the average is taken over all possible initial phases ϕ_0. The correlator is proportional to the product of the coupling constant λ and the variance of n, reflecting the usual phase-number uncertainty relation.

Before proceeding with quantitative analysis let us argue qualitatively what happens with the system. Suppose $\lambda \ll 1$. Then (4.20) is equivalent to the motion of a particle in a harmonic potential with random initial velocity. Because the frequency

of the harmonic oscillator does not depend on the amplitude, $\langle n^2(t)\rangle$ is a periodic function of time with $T = \pi/2$. If λ is small but not negligible, then (4.20) still describes motion in a harmonic potential, which, however, depends on the initial conditions. As a result the oscillations of $\langle n^2(t)\rangle$ become quasiperiodic and decay with time. In the limit of large λ the oscillations become overdamped and the steady state solution develops during the time $t \sim 1/\sqrt{\lambda}$.

For weak coupling λ, equation (4.20) can be solved explicitly. Thus for $\lambda = 0$

$$\langle n^2(t)\rangle = \frac{1-\cos 4t}{4}. \tag{4.23}$$

For small λ the approximate analytical solution is also readily derived:

$$\langle n^2(t)\rangle \approx \frac{1}{4} - \frac{1}{2\pi}\int_0^{\pi} \sin^2\phi_0 \cos\left(4t\sqrt{1+\lambda\cos\phi_0}\right) d\phi_0. \tag{4.24}$$

It is easy to see that at large t we have the following asymptotic behavior:

$$\langle n^2(t)\rangle \approx \frac{1}{4} - \frac{1}{\sqrt{16\pi\lambda t}}\left[\cos\left(4t\sqrt{1+\lambda}+\frac{\pi}{4}\right)+\cos\left(4t\sqrt{1-\lambda}-\frac{\pi}{4}\right)\right], \tag{4.25}$$

so that the variance of n approaches the steady state value of one fourth. We note that the amplitude of oscillations decays with time as $t^{-1/2}$ and on top of that there are beats with the characteristic frequency $\omega_{beats} \approx 4\lambda$ (see Fig. 4.1). For large λ the oscillations decay very rapidly and $\langle n^2(t)\rangle$ quickly saturates at the steady state value, which decreases with λ.

4.1.2 Quantum theory

Let us now study the quantum case. The Heisenberg equations of motion are:

$$\frac{d\hat{a}_j}{dt} = i\,[\mathcal{H}, \hat{a}_j], \tag{4.26}$$

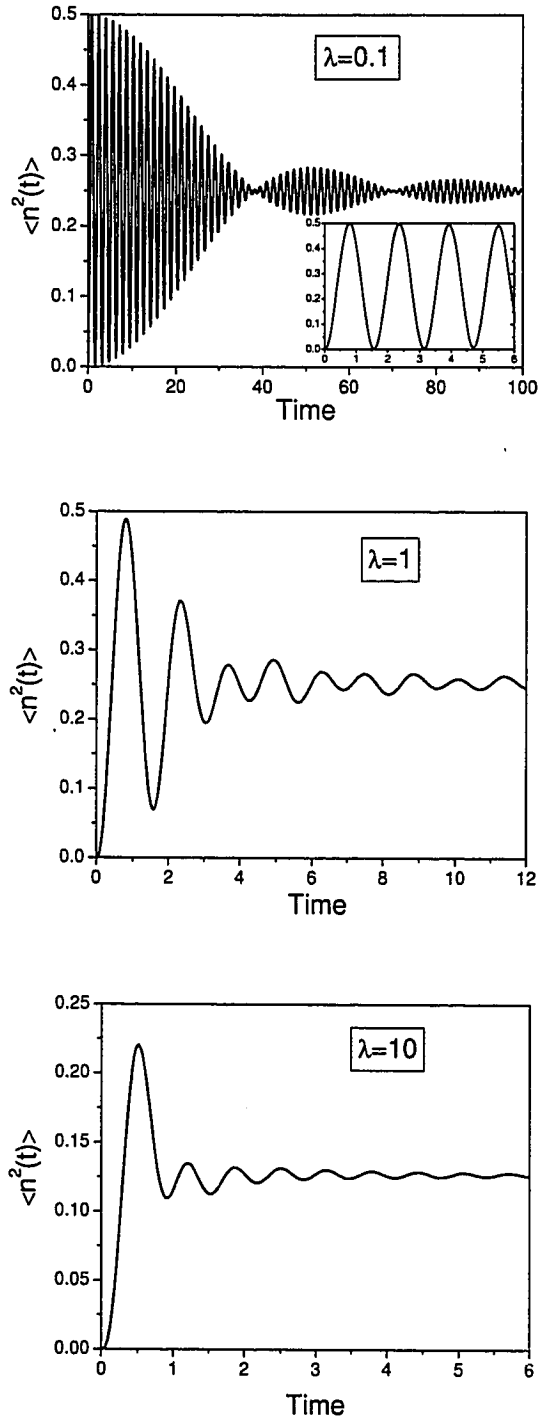

Figure 4.1: Semiclassical variance of n as a function of time. The insert on the top graph has a different time scale. We note again that hereafter time is measured in units of $\hbar/J$.

where square brackets denote commutator, $j = 1, 2$ and the hamiltonian $\mathcal{H}$ is given by (4.1). It turns to be convenient to use the following Heisenberg operators:

$$\begin{cases} \hat{\Phi} = \hat{a}_2^\dagger \hat{a}_1 - \hat{a}_1^\dagger \hat{a}_2, \\ \hat{\Psi} = \hat{a}_2^\dagger \hat{a}_1 + \hat{a}_1^\dagger \hat{a}_2, \\ \hat{n} = \hat{a}_2^\dagger \hat{a}_2 - \hat{a}_1^\dagger \hat{a}_1. \end{cases} \tag{4.27}$$

We introduce hats over the operators to distinguish them from numbers appearing in the semiclassical treatment and expectation values of the operators . It is easy to see that the following combination

$$\hat{\Psi} - \frac{\lambda}{4N}\hat{n}^2 \equiv \hat{\Psi} - \frac{U}{4J}\hat{n}^2 \tag{4.28}$$

commutes with the hamiltonian. Using this fact the system (4.26) can be reduced to a single differential equation:

$$\frac{d^2\hat{n}}{dt^2} + 4\hat{n} + \frac{2\lambda}{N}\left\{\hat{n}, \hat{\Psi}_s\right\}_+ + \frac{\lambda^2}{N^2}(2\hat{n}^3 - \left\{\hat{n}, \hat{n}_s^2\right\}_+) = 0 \tag{4.29}$$

with the initial conditions:

$$\hat{n}(0) = \hat{n}_s, \quad \left.\frac{d\hat{n}}{dt}\right|_{t=0} = -2i\hat{\Phi}_s. \tag{4.30}$$

In the equations above $\{\dots\}_+$ denotes the anticommutator, and the subindex s implies time-independent Schrödinger operators. We note that the second relation in (4.30) holds for all times if we use $\hat{\Phi}$ instead of $\hat{\Phi}_s$. In the noninteracting case ($\lambda = 0$) the solution of (4.29) is:

$$\hat{n}(t) = \hat{n}_s \cos 2t - i\hat{\Phi}_s \sin 2t. \tag{4.31}$$

The ground state for $\lambda \gg \lambda_{SI}$ is $|I\rangle \equiv |N/2, N/2\rangle$. Note that such a state is possible only if N is even. The generalization for N odd is straightforward, but we will not

do it here, since our major goal is to compare quantum and semiclassical pictures. Simple computation shows that

$$\frac{n^2(t)}{N^2} \equiv \frac{1}{N^2}\langle I|\hat{n}^2(t)|I\rangle = \frac{1-\cos 4t}{4}\frac{N+1}{N}. \tag{4.32}$$

Comparing (4.32) and (4.23) we see that the only difference between the semiclassical and quantum results in the noninteracting case is the presence of an extra numerical factor $1+1/N$ in (4.32). We will explain its origin in the next chapter.

In the weakly interacting regime ($\lambda \ll 1$) we can ignore terms proportional to λ^2. Then (4.29) simplifies to:

$$\frac{d^2\hat{n}}{dt^2} + 4\hat{n} + \frac{2\lambda}{N}\left\{\hat{n}, \hat{\Psi}_s\right\}_+ = 0. \tag{4.33}$$

It is very convenient to solve this equation in the eigenbasis of $\hat{\Psi}_s$:

$$|k\rangle = \frac{2^{-N}}{\sqrt{k!(2N-k)!}}(\hat{a}_{1s}^\dagger + \hat{a}_{2s}^\dagger)^k(\hat{a}_{1s}^\dagger - \hat{a}_{2s}^\dagger)^{2N-k}|0\rangle, \tag{4.34}$$

where $k = 0, 1, \ldots N$. After straightforward analysis one can show that the variance of n is:

$$\frac{n^2(t)}{N(N+1)} = \frac{1}{4} - \frac{2^{2-N}}{N(N+1)}\sum_{k=0}^{N-1}\frac{(2N-2k-1)!!\,(2k+1)!!}{(N-k-1)!\,k!} \times \cos 2t\left[\sqrt{1-\frac{\lambda}{2N}(4k+3-2N)} + \sqrt{1-\frac{\lambda}{2N}(4k+1-2N)}\right]. \tag{4.35}$$

Comparing (4.35) and (4.25) we see that in contrast to the continuous integral in the semiclassical case there is a discrete sum in the quantum case. One can formally obtain (4.25) from (4.35) in the limit $N \to \infty$ using Stirling's formula and transforming the summation over k to integration. If the number of particles per site $N = 1$, there is only one term in (4.35), so the oscillations are completely undamped. For $N = 2$, there are two terms and we expect perfect beats; *i.e.* the amplitude of oscillations first goes to zero then completely restores and so on. For

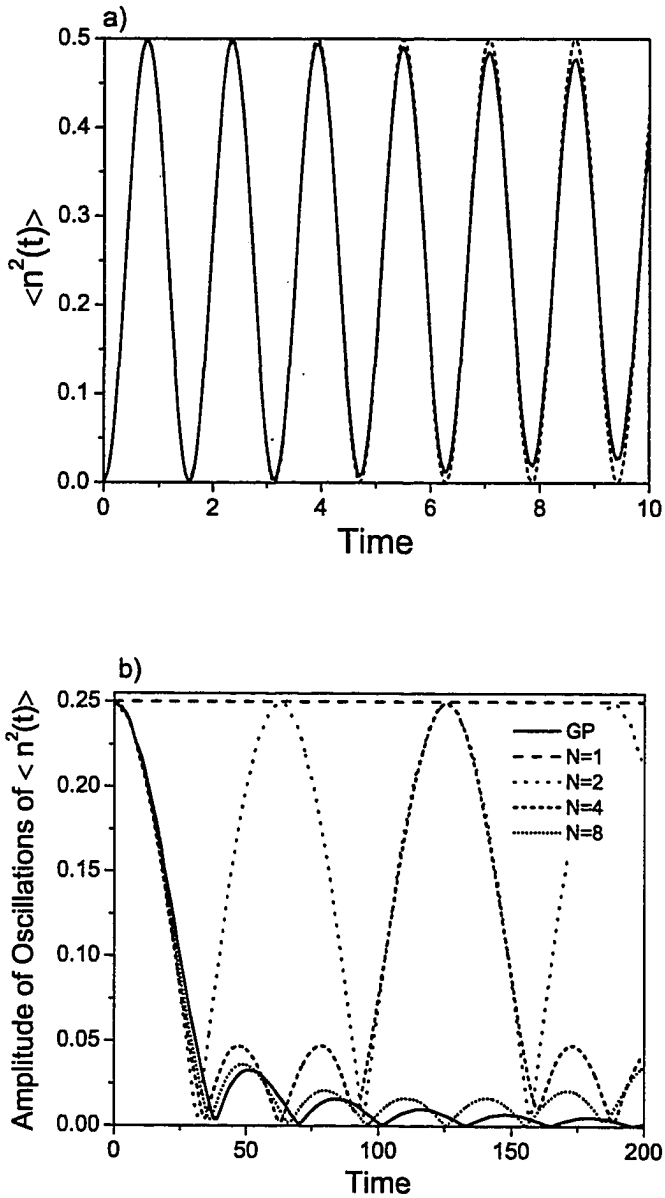

Figure 4.2: (a) Semiclassical (solid line) and quantum variance of n as a function of time for the weak coupling case $\lambda = 0.05$. Dash line and dot lines correspond to one and two bosons per site, respectively. Solid and dot line are indistinguishable on this plot. (b) Amplitude of the oscillations of the variance of n versus time.

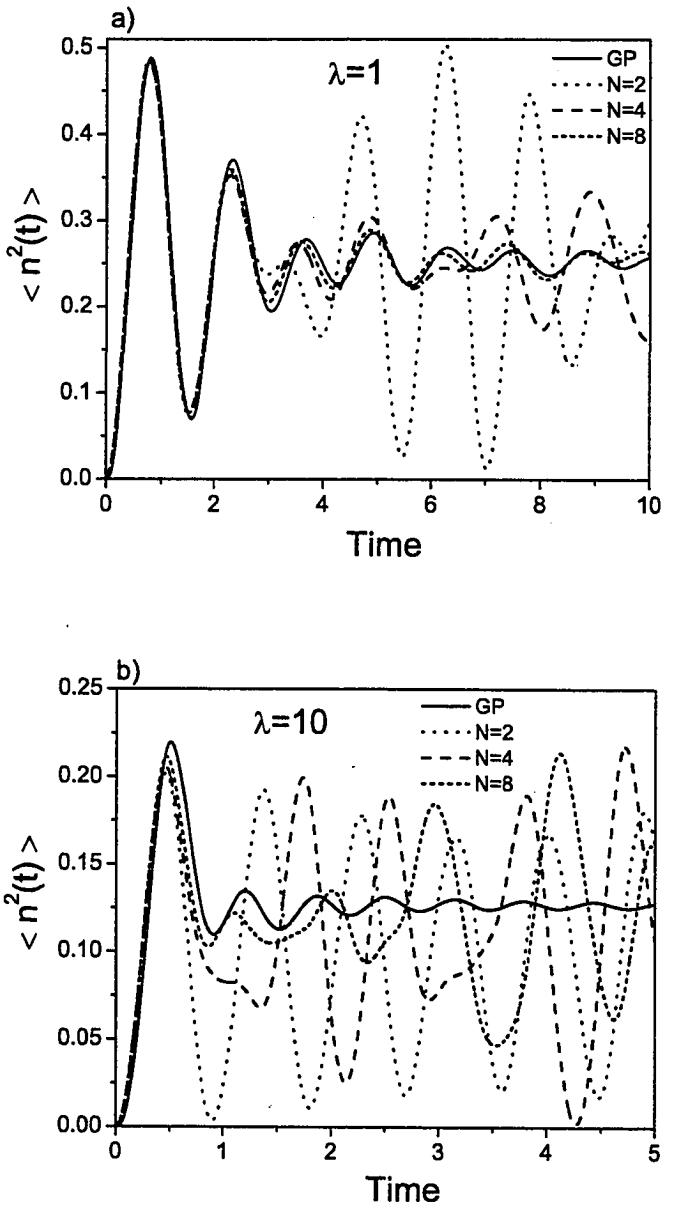

Figure 4.3: Variance of n as a function of time for intermediate (a) and large (b) coupling constants. Note that for larger N semiclassical approximation works well for a longer time scale, but eventually breaks down.

$N \geq 3$ there are several terms contributing to the sum. At relatively small time scale $\lambda^2 t/N \ll 1$ frequencies in different terms are approximately equidistant: $\Delta\Omega \approx 2\lambda/N$ so the amplitude of oscillations is a periodic function. However at a larger time scale the phases become random and periodicity disappears. Figure 4.2(a) shows the comparison of the variance of n for $N = 1$ and $N = 2$ with the semiclassical result. On short time scales already $N = 2$ gives an excellent agreement. In fact the semiclassical and the quantum curve (for $N = 2$) are almost indistinguishable. The behavior of the amplitude of oscillations of n^2 is plotted in Fig. 4.2(b). It is clear that with increasing N, the semiclassical approximation works for longer and longer time scales (see also Ref. [105]). However in a quantum system the recurrence time is always finite, so ultimately at $t > 1/\Delta\Omega$, the semiclassical description breaks down.

In Fig. 4.3 we present the numerical solution for the case of intermediate and strong couplings. As was discussed before for small N, the amplitude of oscillations fluctuates, being completely chaotic at large time scales. However, at sufficiently small time, the oscillations gradually decay, approaching the semiclassical result. At intermediate times the amplitude of the oscillations experiences beats (compare with Fig. 4.2). Note that for large coupling, the semiclassical description breaks down very early.

4.2 Semiclassical description of multi-well Bose gases

The full quantum solution of the many well case rapidly becomes numerically prohibitive with increasing N, and so we will confine our discussion in this section to the semiclassical GP equation. From (4.9) and (4.10) this is

$$i\frac{\partial \psi_j}{\partial t} = -(\psi_{j+1} + \psi_{j-1}) + \frac{V_j}{J}\psi_j + \lambda|\psi_j|^2\psi_j, \tag{4.36}$$

The equilibrium number of bosons in the central well ($j = 0$) is N, and so $|\psi_0|^2 = 1$ in the Mott insulating ground state.

We will compute the correlation function $\mathcal{D}_g(t)$ defined in (4.14) for two limiting possibilities for the weight function g: $g(j) = \delta_{j,1}$ and $g(j) = \text{const}$, where in the former (latter) case one finds the nearest neighbor (global) phase correlation. Using the GP equations (4.36) we can show that

$$\frac{d\mathcal{D}_g(t)}{dt} = i \sum_{j \neq \ell} \left(V_j + \lambda |\psi_j(t)|^2\right) g(|j-\ell|) \left(\psi_j^*(t)\psi_\ell(t) - \psi_\ell^*(t)\psi_j(t)\right). \tag{4.37}$$

Note that for uniform potential $\mathcal{D}_g(t)$ changes only due to the interaction. In this case, the ratio $\mathcal{D}_g(t)/\lambda$ has a finite limit at $\lambda \to 0$. We will consider the solution for $\mathcal{D}_g(t)$ with and without an external potential in the following subsections.

4.2.1 No external potential and periodic boundary conditions

Let us assume that the lattice forms a periodic array of quantum wells and there is no external potential ($V_j \equiv 0$). For the nearest neighbor correlation similarly to the two well case it is easy to show that

$$\mathcal{D}_g(t) \equiv \sum_j \psi_j^* \psi_{j+1} + \psi_{j+1}^* \psi_j = \frac{\lambda}{2} \sum_j (|\psi_j|^2 - 1)^2. \tag{4.38}$$

This equation shows that the nearest neighbor coherence is proportional to the product of the coupling constant and sum of the variances of number of bosons in each well. From the previous section we can expect that if the interaction is weak, then variances of n_j at short time scales will be fluctuating and governed by the noninteracting tunnelling hamiltonian. With increasing time the interaction will suppress the fluctuations leading to some steady state. In the noninteracting case,

(4.36) is just an ordinary Schrödinger equation. with eigenstates

$$\psi_k(j) = \frac{1}{\sqrt{M}} e^{2\pi i k j/N}, \tag{4.39}$$

corresponding to the eigenenergies

$$E_k = -2\cos\frac{2\pi k}{M}. \tag{4.40}$$

Here M is the number of wells. Expanding the initial insulating state in terms of the eigenstates defined above and propagating them in time we obtain

$$\sum_{j=1}^{N}(|\psi_j(t)|^2 - 1)^2 = M\left(1 - \sum_j |F(j,t)|^4\right), \tag{4.41}$$

where

$$F(j,t) = \frac{1}{M}\sum_{k=0}^{N-1} e^{2i(\pi kj/M + t\cos 2\pi k/M)}. \tag{4.42}$$

For several different values of M the function $\mathcal{D}_g^M(t)$ at vanishing λ is:

$$\mathcal{D}_g^2(t) = \frac{\lambda}{2}\sin^2 2t, \tag{4.43}$$

$$\mathcal{D}_g^3(t) = \frac{8\lambda}{9}(2+\cos 3t)\sin^2\frac{3}{2}t, \tag{4.44}$$

$$\mathcal{D}_g^4(t) = \frac{\lambda}{4}(7+\cos 2t)\sin^2 2t, \tag{4.45}$$

$$\mathcal{D}_g^5(t) = \frac{4\lambda}{25}(10 - 2\cos\sqrt{5}t - \cos\sqrt{5}t - 2\cos\frac{5}{2}t\cos\frac{3\sqrt{5}}{2}\cos\sqrt{5}t), \tag{4.46}$$

$$\mathcal{D}_g^6(t) = \frac{\lambda}{36}(63 - 8\cos t - 12\cos 2t - 24\cos 3t - 6\cos 4t - 12\cos 6t - \cos 8t), \tag{4.47}$$

$$\mathcal{D}_g^M(t) \to \frac{M\lambda}{2}\left(1 - J_0(t)^4 - 2\sum_{m=1}^{\infty} J_m(t)^4\right) \quad \text{at} \quad M \to \infty. \tag{4.48}$$

Clearly $\mathcal{D}_g^M(t)$ is a periodic function only for $M = 2, 3, 4, 6$ (this is, in fact true, not only for the nearest neighbor case). For many wells the number of harmonics contributing to the variance of n becomes large and oscillations become more chaotic and weaker in amplitude. In the limit $M \to \infty$, $\mathcal{D}_g^M(t)$ is a monotonically increasing

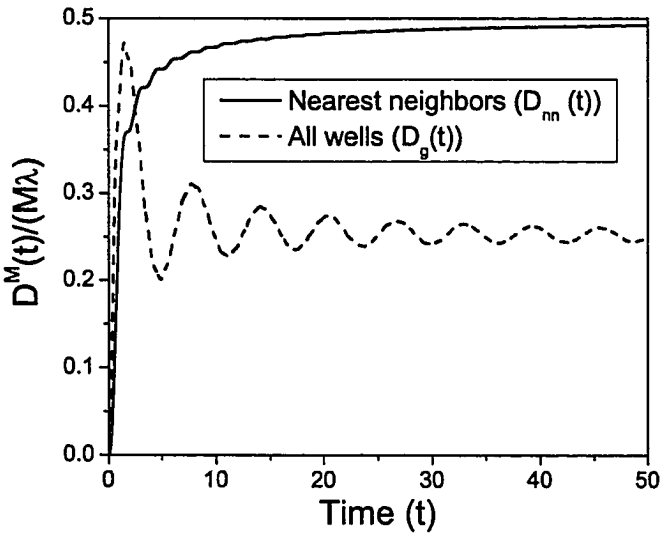

Figure 4.4: Time dependence of the coherence $\mathcal{D}_g(t)$ for the weakly interacting Bose gases at large number of wells ($M \to \infty$). Note that nearest neighbor correlation rapidly saturates, while the global coherence exhibits oscillations.

function. If we add the interaction, then the overall picture remains similar to the two well case. Namely, for small λ the amplitude of oscillations slowly decays in time. For strong interaction, the variance of n reaches steady state value in a very short time scale.

In the opposite to nearest neighbors limit $g(|j-\ell|) = \text{const}$ similar calculations give:

$$\mathcal{D}_g^2(t) = \frac{\lambda}{2}\sin^2 2t, \tag{4.49}$$

$$\mathcal{D}_g^3(t) = \frac{\lambda}{45}(3 - 2\cos 3t - \cos 6t), \tag{4.50}$$

$$\mathcal{D}_g^4(t) = \frac{\lambda}{160}(13 - 12\cos 4t - \cos 8t), \tag{4.51}$$

$$\mathcal{D}_g^6(t) = \frac{\lambda}{240}(33 + 16\cos t - 24\cos 2t - 8\cos 6t - \cos 8t), \tag{4.52}$$

$$\mathcal{D}_g^M(t) \overset{M\to\infty}{\longrightarrow} \frac{M\lambda}{2\pi^2}\int_0^{2\pi}\int_0^{2\pi} d\theta_1 d\theta_2 \frac{\sin^2 t(1+\cos\theta_1-\cos\theta_2-\cos(\theta_1-\theta_2))}{1+\cos\theta_1-\cos\theta_2-\cos(\theta_1-\theta_2)}. \tag{4.53}$$

The behavior of $\mathcal{D}_g(t)$ at large M is very different for nearest neighbor and global

correlations (see Fig. 4.4). While the former rapidly reaches a steady state value, the latter oscillates in time. Indeed the denominator in (4.53) selects only low frequency harmonics in $\mathcal{D}_g$, freezing out high frequency oscillations, especially at longer time scales. Another observation we can make from these graphs as well as from figure 4.5 is that the steady state values of the nearest neighbor and global correlators are comparable with each other, in fact they always lie within a factor of two from each other. This is clearly a characteristic of a short range phase coherence typical for thermal Bose gas rather than superfluid.

Figure 4.5 shows $\mathcal{D}_g(t)$ for six and twelve wells respectively. The former case gives periodic time dependence, while the latter corresponds to chaotic behavior. In all cases high frequency modes are suppressed for the case of global phase correlations. Note that according to formulas (4.44-4.48), (4.50-4.53) and figure 4.5, at small λ the steady state value of the correlator D is proportional to λ both for the nearest neighbor and the global cases. At large interaction $\lambda \gg 1$ it can be shown that D saturates and becomes independent of λ. This is a somewhat surprising result on the first sight. Indeed, we know that in the ground state the interactions are responsible for dephasing and here the situation is opposite. However, there is no paradox, because we deal with a strongly out of equilibrium problem. Without interactions there is no reason for the system to choose between positive and negative phases and it is the interaction which sets the preferred direction. To see this let us note that initially the interaction energy:

$$E_{int} = \sum_j \frac{U}{2}|\psi_j|^2 \tag{4.54}$$

had the minimum possible value, since we started from the ground state of the hamiltonian with no hopping. Any fluctuations can only increase E_{int} therefore decreasing the hopping energy. The latter is directly related to the nearest neighbor

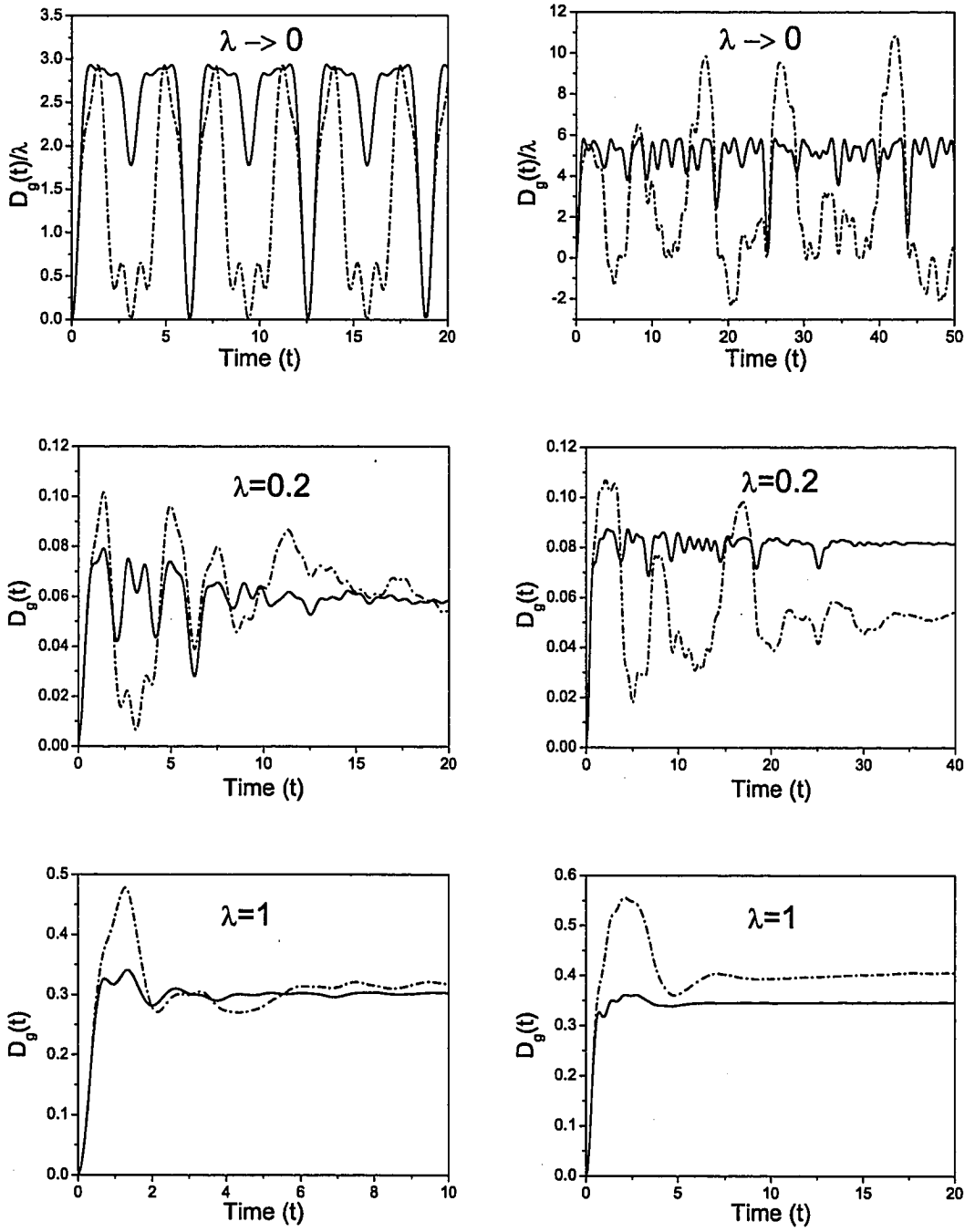

Figure 4.5: Time dependence of $\mathcal{D}_g(t)$ for 6 wells (left) and for 12 wells (right); solid and dashed lines correspond to nearest neighbor and global correlations respectively. Without interaction ($\lambda \to 0$) $\mathcal{D}_g(t)$ shows regular periodic behavior in time. Nonzero interactions leads to decay of oscillations. High frequency oscillations of global correlation function are effectively suppressed.

correlator D_g, which, therefore, must be positive. In fact, it is easy to check that the steady state corresponds to the microcanonical ensemble with fixed energy and the number of bosons defined by the initial conditions. If the interaction energy still dominates the hopping in the steady state, then there is no difference between the microcanonical and grand canonical ensembles, so the initial energy per boson, which is approximately $2J$ above the superfluid ground state will correspond to the temperature of the order of J. Clearly this is a high temperature phase from the point of view of superfluidity so the resulting statistical ensemble should correspond to fast decaying in space phase correlations and this can be also verified numerically. In other words, though the steady state develops phase correlations if the tunneling is quickly turned on, the system does not become superfluid.

It is interesting to check whether the semiclassical steady state is always a thermodynamic ensemble, i.e. it depends only on the energy and not on the other details characterizing different initial configurations. We would like to point out here that the true steady state can be achieved only if the number of bosons goes to infinity, so even for a finite number of wells we deal with infinite number of degrees of freedom. Instead of trying to give a complete proof, we consider a specific example, with different initial configurations having the same energy. Figure 4.2.1 illustrates

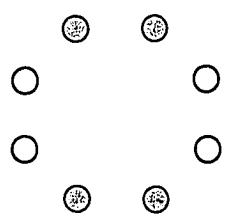

Figure 4.6: An example illustrating validity of the thermodynamic limit. The circles denote different sites. Initially all of them have the same number of bosons. The filled (empty) sites have the mean phase π (0). Besides there is a fluctuating component of the phase, which is randomly distributed within the interval $[-\theta, \theta]$. The states with different values of θ have *the same* energy.

a possible ensemble of such states, characterized by a continuous parameter θ. Note, that if $\theta = \pi$ (see figure caption) then we recover the usual number initial state

which is discussed elsewhere in this chapter. On the other hand $\theta = 0$ corresponds to some phase correlated state. All the configurations clearly have the same energy but different global correlator $D_g(0)$. The resulting time evolution for a number of different values of θ and different number of wells is plotted in Fig. 4.7. As seen from

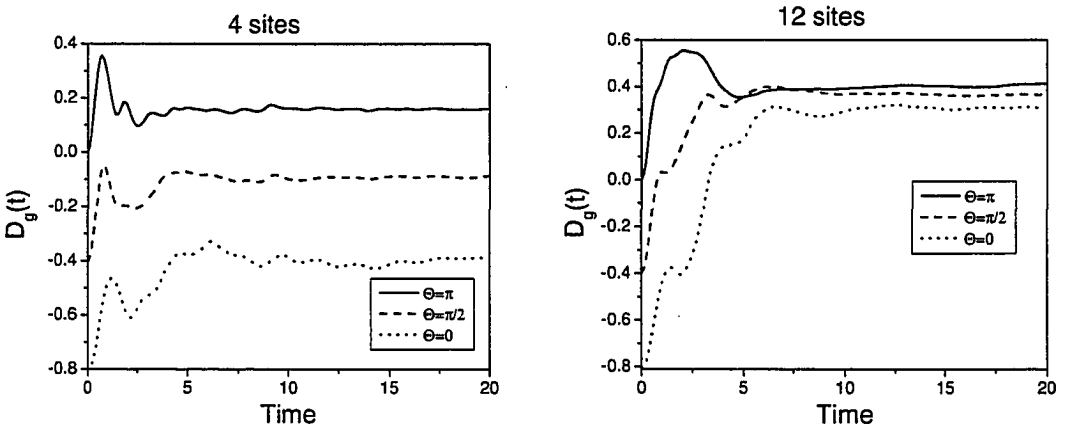

Figure 4.7: Evolution of the global phase correlations for different initial conditions corresponding to the same energy as described in Fig. 4.2.1. Clearly the steady state is the same only in for the infinite number of sites, i.e. in the thermodynamic limit.

the figure, the unique steady state develops only for the large number of sites, i.e. in the thermodynamic limit. This suggests that in this limit the details of the initial conditions are unimportant as long as the energy is specified. For example, the phase correlations are not entirely absent in the insulating state, they just exponentially decay with distance between the sites [131].

4.2.2 Parabolic confining potential

So far, we have considered the rather hypothetical situation of quantum wells sitting on a ring. However, usually the confinement is achieved using a magnetic trap, which is equivalent to a nonuniform external potential V_j in (4.36). The most common shape of this potential is harmonic ($V_j \propto j^2$) and we focus on this case, although the

analysis of other potentials is similar and straightforward. As before, we will first study the non-interacting system: ($\lambda = 0$).

$$i\frac{d\psi_j}{dt} = -(\psi_{j+1} + \psi_{j-1}) + \frac{\xi j^2}{2}\psi_j. \tag{4.55}$$

This is a linear Schrödinger equation with stationary states found from

$$E\psi_j = -(\psi_{j+1} + \psi_{j-1}) + \frac{\xi j^2}{2}\psi_j. \tag{4.56}$$

In the Fourier space the same equation looks more familiar:

$$E\psi(k) = -2\cos k\,\psi(k) - \frac{\xi}{2}\frac{d^2\psi(k)}{dk^2}, \tag{4.57}$$

describing the motion of an one-dimensional particle of mass ξ^{-1} living on a circle with the external potential $U(k) = -2\cos(k)$. Note that the same type of equation describes Josephson junctions with charging energy. If the curvature is small ($\xi \ll 1$), then the bosons form closely spaced extended states at low energies. In the Fourier space this is equivalent to having a heavy particle in the $-2\cos k$ potential. With a good accuracy one can describe the energy spectrum inside such a well using the WKB approximation. This is justified both for low energies, where $-2\cos k \approx -2+k^2$ and the WKB gives the exact energy spectrum and for high energies WKB works well for any potential. In fact there is a little subtlety near energy close to 2, since the potential there is almost flat and can not be approximated by a linear function, but this is just a minor detail. So the approximate WKB spectrum is given by

$$\begin{aligned}
&\int_{-\pi+\cos^{-1}E/2}^{\pi-\cos^{-1}E/2} \sqrt{\frac{2}{\xi}(E+2\cos k)}\,dk = \pi(n+1/2) \\
&\int_{-\pi}^{\pi} \sqrt{\frac{2}{\xi}(E+2\cos k)}\,dk = 2\pi n,
\end{aligned} \tag{4.58}$$

where the top (bottom) equation corresponds to $E < 2$ ($E > 2$). In the first equation even or odd n describes even and odd states (in both real and reciprocal space),

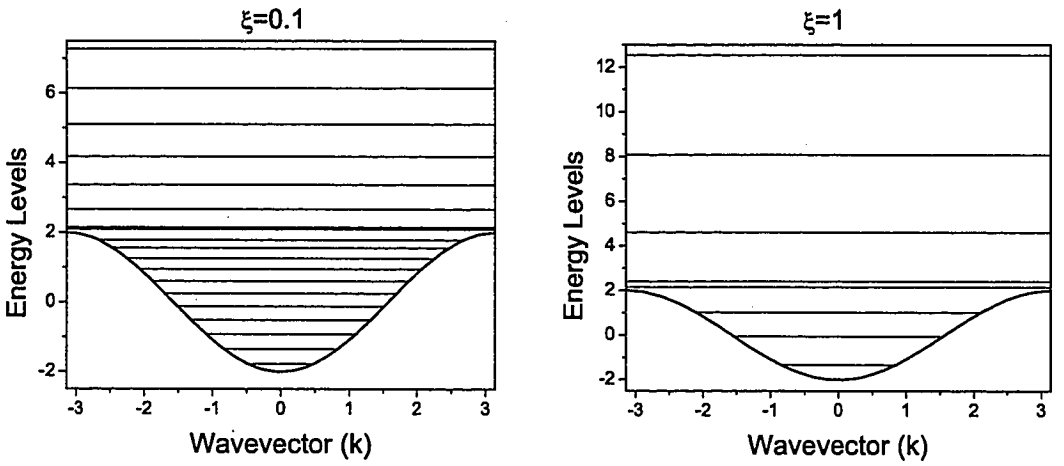

Figure 4.8: Energy spectrum of coupled noninteracting Bose gases in a weak (a) and intermediate (b) parabolic potential.

respectively. For energies $E > 2$, the second equation gives complete degeneracy between even and odd energy levels. In real space roughly all states with $E > 2$ are localized in individual wells, and degenerate while those with $E < 2$ are spread through many wells. Figure 4.8(a) briefly summarizes this discussion showing the exact spectrum for $\xi = 0.1$ (the WKB result is indistinguishable by eye from this graph). Clearly the low energy levels are approximately equally spaced, revealing the famous property of a harmonic potential, the spacing decreases as the energy approaches 2, and starts linearly increasing for $E > 2$ as in a usual square well. If $\xi \geq 1$ then bosons become localized within individual wells and their energies follow external potential. The crossover from weak to strong parabolicity is a finite system analog of the Anderson transition. It is important to note that this is a purely semiclassical transition in this case, because it is derived in the Gross-Pitaevskii picture. The "quantum mechanics" here originates from the wave nature of the classical field ψ. If the average number of bosons per well is much larger than one, then the semiclassical picture, where number of bosons and their phase commute,

holds until the typical fluctuations of ψ^2 becomes of the order of $1/N \ll 1$. This occurs deep inside the insulating regime, where the energy in GP approach is anyway almost phase independent.

After deriving the energy spectrum we can proceed with study of the dynamics of the condensate. Note that (4.37) yields that time derivative of $\mathcal{D}_g(t)$ is not equal to zero even without interaction ($\lambda = 0$). Therefore we anticipate that the results for the parabolic and flat potentials will be strongly different, at least in the weakly interacting regime. If the initial phases are uncorrelated then it is not hard to show that at $\lambda = 0$

$$\mathcal{D}_g(t) = 2\sum_{j\neq\ell} V(j)g(|j-\ell|)\sum_{p,\alpha,\beta} N_0^p \psi_\alpha^\star(j)\psi_\alpha(p)\psi_\beta^\star(p)\psi_\beta(\ell)\frac{\sin^2\frac{E_\beta - E_\alpha}{2}t}{E_\beta - E_\alpha}, \qquad (4.59)$$

where N_0^p is the initial number of Bosons in the well number p, ψ_α and E_α are the eigenfunction and energy of the level α respectively . If starting from the ground insulating state then

$$N_0^p = 1 - \frac{V_p}{\mu} \quad \text{for} \quad V_p < \mu, \qquad (4.60)$$

$$N_0^p = 0 \quad \text{for} \quad V_p > \mu, \qquad (4.61)$$

with μ being a chemical potential. Let us make few comments about (4.59). Levels β and α must have the same parity, meaning the lowest harmonic contributing to the sum will be $\omega_{\min} = 2\min_\alpha (E_{\alpha+2} - E_\alpha) > 0$. Because N_0^p is centered near the bottom of the well, only levels with delocalized wavefunctions will contribute to the sum. In particular, degenerate levels with $E > 2$ can be safely thrown away. If $g(|j-\ell|)$ is constant, then summation over m ensures that the major contribution comes from $\beta = 0$; therefore $\mathcal{D}_g(t)$ contains mostly harmonics with $\omega = E_2 - E_0$, $\omega = E_4 - E_0$, etc., with the strongest weight at the smallest frequency. Note that at small energies and weak parabolicity the lowest energy levels are approximately equally spaced, therefore

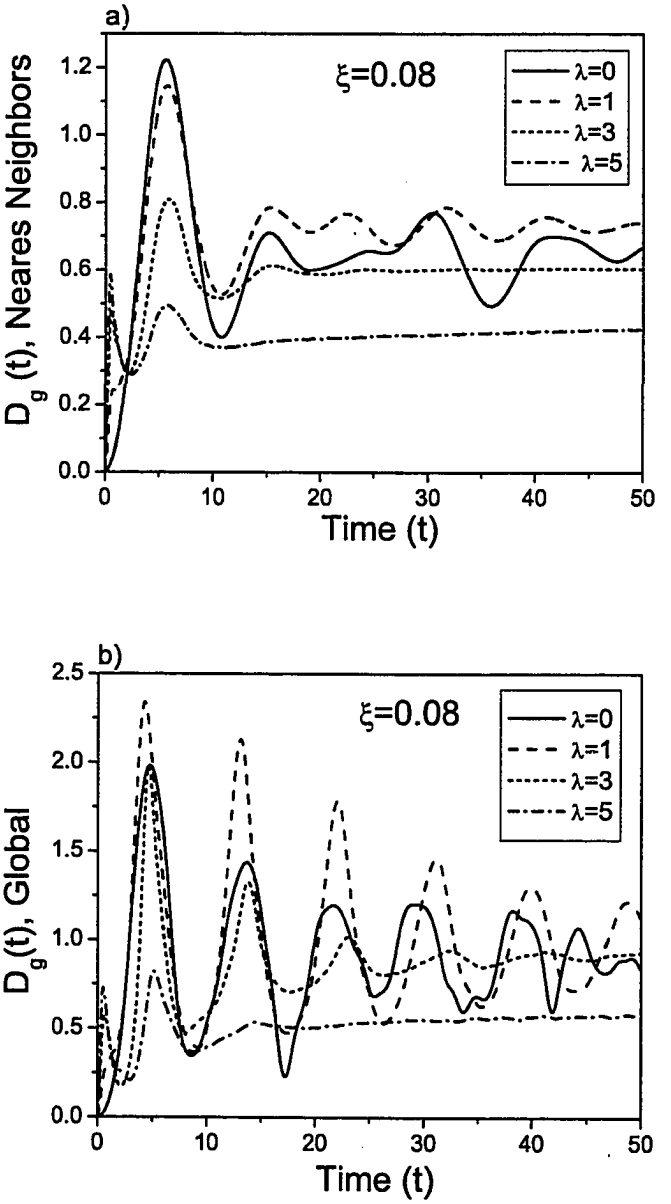

Figure 4.9: Time dependence of $\mathcal{D}_g$ for the nearest neighbor correlation (a) and global correlation (b). The period of oscillations scales as $1/\sqrt{\xi}$ and the amplitude is finite even without interaction $\lambda = 0$. At large λ, $\mathcal{D}_g(t)$ saturates very fast similarly to the flat potential. At intermediate coupling $\lambda \sim 1$, however, the oscillations become more pronounced than in the noninteracting regime.

the whole expression for $\mathcal{D}_g(t)$ will be a quasi-periodic function of a frequency $\omega \approx E_2 - E_0$. However, because this equidistance is not exact, the periodicity will be only approximate, and the amplitude of oscillations will slowly decay. On the contrary for the nearest neighbor phase coherence $g(|j-\ell|) = \delta_{j,\ell\pm1}$ neither β nor α are bounded to the ground state and we expect that all kinds of allowed frequencies $E_\alpha - E_\beta$ will give contributions. Clearly in this case dephasing occurs much earlier and the amplitude of oscillations is much weaker. Also the characteristic frequency of the oscillations for the nearest neighbor case will be somewhat larger than that for the global case since the level separation decreases with energy. Figure 4.9 shows time dependence of $\mathcal{D}_g$ for nearest neighbor and global correlations at the parabolicity $\xi = 0.08$. From the above analysis we should expect the major oscillations at the period

$$T = \frac{2\pi}{E_2 - E_0} \approx \frac{\pi}{\sqrt{2\xi}} \approx 8, \tag{4.62}$$

which is indeed very close to the numerical value. Relatively weak interaction does not qualitatively change the picture. In particular, if λ is of the order of one, the oscillations become much more pronounced and smooth compared to noninteracting case (see Fig. 4.9). This is at first quite an unexpected result, since we know that the interaction leads to decoherence and saturation of $\mathcal{D}_g$. However this is not the whole story. In the previous analysis we saw that at least for the $\mathcal{D}_g(t)$, interaction "kills" high frequency contributions first. But that is precisely what we need for harmonic behavior. So crudely speaking, small or intermediate interaction removes harmonics causing dephasing of the noninteracting function $\mathcal{D}_g$. If interactions become strong $\lambda \gg 1$, then the noninteracting picture is irrelevant and we come back to the usual behavior with fast saturation of $\mathcal{D}_g$. Notice from Fig. 4.9, that as interaction increases the other short time scale in the oscillations emerges and eventually becomes dominant. This can be understood from a simple qualitative analysis. Thus with

small or no interactions there is a collective center of mass degree of freedom which oscillates with a characteristic period given by (4.62). On the other hand stronger interactions lead to a fast damping of the center of mass mode. Instead, a new short time scale emerges, which is equal to the characteristic period of the Josephson oscillations between neighboring wells ($T \approx \pi/\sqrt{\lambda}$). Clearly in this limit of strong interactions details of the overall confining potential become unimportant.

4.3 Conclusions

We have studied the non-equilibrium temporal behavior of coupled bosons in a lattice. We predicted dynamical restoration of the phase coherence after a sudden increase of the tunnelling in a system initially in a Mott insulating state. In the strongly interacting case, $\lambda \gg 1$, the coherence reaches a steady state rapidly (within a Josephson time of plasma oscillations). On the other hand, time evolution in the weakly interacting regime $\lambda \lesssim 1$ depends strongly on the details of the confining potential. We predicted that in a parabolic potential $V_j = \xi j^2/2$ the coherence exerts decaying oscillations with period $T \propto 1/\sqrt{\xi}$ (see (4.62)). The period and the amplitude of oscillations only depend weakly on interaction in this case. On the other hand, if the confining potential is flat, then the oscillations are either periodic (for a particular number of wells in a lattice) or chaotic. Here the interaction leads to the decay of the oscillations with time. In both cases provided that the number of bosons is large and the semiclassical description is valid the system ultimately reaches steady state with nonzero short-range coherence.

For the two well case we explicitly tested the validity of GP approach. It was shown that the mapping of the deterministic quantum mechanical motion to the stochastic GP equations is essentially exact for time less than the characteristic in-

verse level spacing $t < N/\lambda$. Apart from the slight renormalization of the overall constant, the mapping is excellent in this time domain already for two bosons per well. For stronger interactions, the semiclassical and quantum mechanical trajectories start to depart faster, as expected.

Chapter 5

Evolution of a cat state in BEC

As we already mentioned several times BECs are particularly interesting because they provide a direct access to observing and manipulating various quantum effects in many-body interacting systems. Let us note again that in optical lattices the bosonic systems can undergo a quantum phase transition from superfuid to the insulating phase, which is entirely driven by the zero point motion. On the other hand, in the superfluid regime the quantum fluctuations are suppressed and either semiclassical (Gross-Pitaevskii) or Bogoliubov's approach is often adequate for the description of both static and dynamic properties of the condensates (see e.g. Refs. [92, 130]). However, there is another possibility, wherein the system is superfluid but neither of these approaches is good. Suppose that the condensate is driven to the regime of instability. This can be achieved either by applying a certain phase gradient to the superfluid with repulsive interactions [127, 146, 166] or by switching the sign of the interaction to the negative value using Feshbach resonance [77, 80]. The main difficulty arises because near the instability all the fluctuations including quantum exponentially diverge in time and cannot be treated perturbatively. To be more specific, suppose that for time $t \leq 0$ the periodic system of condensates in a lattice

was in a superfluid ground state, i.e. the interaction was relatively weak. Then a phase imprint, i.e. a certain phase difference between the adjacent wells, was imposed. Experimentally it can be achieved by e.g. applying a short (compared to a single tunneling time) pulse of external field to the system. A case of special interest will be when there is a relative π phase shift between neighboring wells:

$$\phi_j = j\pi. \tag{5.1}$$

For the two wells with equal number of bosons and relatively small interaction λ (see (4.8) for the definition), this state is metastable (this is also the case for even number of wells and periodic boundary conditions). However, if λ becomes larger than a critical value, this equilibrium becomes unstable and the bosons spontaneously form a "dipole" state [9, 51, 127] in which most of them occupy one of the two wells. Upon accounting for quantum fluctuations in a system with a finite number of bosons, the state obtained is a superposition of the two dipole states so that the inversion symmetry is preserved. Clearly in the case of infinite number of wells translational symmetry is always broken. For example in Ref. [135] a similar instability but for the case of a Mott insulator in a strong electric field was shown to drive the system into a dipole state.

Related to this instability is a very interesting possibility of forming a Schrödinger cat state [79]. If the interaction slowly increases in the π state, then at certain point the system becomes unstable. Classically the bosons will remain in this unstable state forever unless there is some noise present either dynamical or in the initial conditions. As we will show below such a noise will drive all the bosons into one spontaneously chosen well. However, apart from classical fluctuations, which are always present but relatively small in the condensates, there is a quantum zero point motion, which comes from the uncertainty relation between the number of bosons

and their phase. This quantum noise will also cause the classical trajectories to move apart from the unstable equilibrium. However, as we mentioned above, the quantum fluctuations do not break translational invariance so the resulting state must be macroscopically entangled. Let us give a simple analogy with a ball laying on the top of the hill. Without fluctuations it will remain there forever. However, because of the uncertainty principle this ball will move down along different classical paths. The quantum effects will be manifested only in certain phase relations between these paths but will not affect the motion itself. This analogy suggests that a good way to describe these situations is to take into account fluctuations yielding some probability distribution of the number and phase at initial time and evolve the fields according to the classical equations of motion. In the literature this approach is known as the truncated Wigner approximation [142, 143, 144, 94]. In this and the next chapters we will try to justify this approach both numerically and analytically and show how to go beyond.

5.1 Classical evolution of the phase modulated state

Recall, that in the classical description of the two coupled condensates the effective motion of the number difference is equivalent to that of a classical particle of unit mass in the effective potential (4.20):

$$U_{eff} = 2n^2(1 + \lambda\sqrt{1 - n_0^2}\cos\theta_0) + \lambda^2 n^2\left(\frac{n^2}{2} - n_0^2\right) = 0, \tag{5.2}$$

where the "coordinate" n represents the number difference between left and right sites, θ is the relative phase; $n_0 \equiv n(t = 0)$ and $\theta_0 \equiv \theta(t = 0)$ are the initial conditions. In particular, if $n_0 = 0$ and $\theta_0 = \pi$ then

$$U_{eff} = 2n^2(1 - \lambda) + \frac{\lambda^2 n^4}{2}. \tag{5.3}$$

Clearly the equilibrium $n = 0$ becomes unstable if $\lambda > 1$.

In a more general case of multiple wells a similar analysis can be done. Because there are now many degrees of freedom a simple representation of equations of motion as in (4.20) becomes impossible. Instead let us return to the GP version of the equations (4.36) with no external potential but with interaction being a function of time:

$$i\frac{d\psi_j}{d\tau} = -(\psi_{j+1} + \psi_{j-1}) + \lambda(t)\,\psi_j^*\psi_j^2, \tag{5.4}$$

where $\psi_j(t)$ is the semiclassical field corresponding to the expectation value of the operator a_j. We note again that we suppressed the tunneling amplitude J changing the units of time to $\hbar/J$. Clearly the π modulated state is a stationary solution:

$$\psi_j(t) = (-1)^j e^{i\Theta(t)}. \tag{5.5}$$

The unimportant global phase $\Theta(t)$ is given by:

$$\Theta(t) = -2t - \int_0^t \lambda(\tau)d\tau. \tag{5.6}$$

Similarly to the two well case this state becomes unstable when the interaction exceeds a certain critical value [146]:

$$\lambda_c = 2\sin^2\frac{\pi}{M}, \tag{5.7}$$

where M is the number of the lattice sites in the array. The origin of the instability becomes intuitively clear if use a dynamical symmetry which is obvious from (5.4): $\lambda \to -\lambda$, $\psi_j \to (-1)^j\psi_j^*$. So the strong repulsive interaction for the π state is equivalent to the strong attractive interaction for the symmetric state. And the instability for the attractive interaction is naturally expected [77, 80]. To get more quantitative results we consider a time evolution of fluctuations around the π state:

$$\psi_j(t) = (-1)^j\, e^{i\Theta(t)}(1 + \xi_j(t) + i\eta_j(t)), \tag{5.8}$$

with ξ_j and η_j being the small real deviations from the exact π solution found above. Substituting (5.8) into (5.4) and linearizing the resulting equations we obtain:

$$\frac{d\xi_j}{dt} = \eta_{j+1} + \eta_{j-1} - 2\eta_j \tag{5.9}$$

$$-\frac{d\eta_j}{dt} = \xi_{j+1} + \xi_{j-1} - 2\xi_j + 2\lambda(t)\xi_j. \tag{5.10}$$

In the Fourier space this system is equivalent to a set of decoupled second order differential equations:

$$\frac{d^2\xi_q}{dt^2} = -16\sin^4\frac{q}{2}\xi_q + 8\lambda(t)\sin^2\frac{q}{2}\xi_q, \tag{5.11}$$

and

$$\eta_q = -\frac{1}{4\sin^2\frac{q}{2}}\frac{d\xi_q}{dt}. \tag{5.12}$$

In the case of adiabatically changing interaction we can write:

$$\xi_q(t) = \xi_{0q}e^{i\phi_q(t)} \tag{5.13}$$

where ξ_{0q} is the initial amplitude of fluctuations and neglect by the second derivative of ϕ_q. Substituting (5.13) into (5.10) we get:

$$\frac{d\phi_q}{dt} = \pm 4\sin^2\frac{q}{2}\sqrt{1 - \frac{\lambda(t)}{2\sin^2\frac{q}{2}}}. \tag{5.14}$$

For simplicity we assume that the interaction increases as:

$$\lambda(t) = \frac{\lambda_0}{1-\delta t}, \tag{5.15}$$

where δ is a small parameter and λ_0 is the initial interaction, which we assume to be small . This type of $\lambda(t)$ dependence, in fact, corresponds to the tunnelling exponentially decreasing with time ($J(t) = J_0e^{-\delta t}$) with $t \to t/J(t)$. It is straightforward to solve (5.14) explicitly and the result is:

$$\phi_q(\lambda) = \pm\frac{2\sin^2\frac{q}{2}}{\delta}\left[\frac{\sqrt{4-\frac{2\lambda_0}{\sin^2\frac{q}{2}}}}{\lambda_0} - \frac{\sqrt{4-\frac{2\lambda}{\sin^2\frac{q}{2}}}}{\lambda}\right.$$
$$\left. + \ln\frac{1+\sqrt{1-\frac{\lambda}{2\sin^2\frac{q}{2}}}}{1-\sqrt{1-\frac{\lambda}{2\sin^2\frac{q}{2}}}} - \ln\frac{1+\sqrt{1-\frac{\lambda_0}{2\sin^2\frac{q}{2}}}}{1-\sqrt{1-\frac{\lambda_0}{2\sin^2\frac{q}{2}}}}\right]. \tag{5.16}$$

Assuming that $\lambda_0 < 2\sin^2 q/2$ we see that in the limit $\lambda \to \infty$ the imaginary part of phase ϕ_q goes to:

$$\Im\phi_q(\infty) = \pm\frac{2\pi}{\delta}\sin^2\frac{q}{2}. \tag{5.17}$$

So if δ is large enough then the instability cannot develop in time and the phase remains essentially real. In the opposite limit the fluctuations become large and we have to study the nonlinear regime of GP equations. More specifically the relation

$$|\xi_{0q}|e^{\Im\phi_q(\infty)} = 1 \tag{5.18}$$

defines the boundary between the regimes of small and large fluctuations. Using the estimate of initial fluctuations (see the next section for details)

$$\xi_{0q} \sim \frac{1}{\sqrt{N}} \tag{5.19}$$

we derive that the instability for a given momentum mode will evolve into a nonlinear regime given that

$$\delta \leq \frac{2\pi\sin^2\frac{q}{2}}{\ln N}. \tag{5.20}$$

This tells us that the interaction should indeed change slowly in time (at least near the onset of instability) and so justifies the adiabatic limit we used. The lowest energy mode corresponds to the momentum $q = 2\pi/M$ so the lower boundary for δ becomes:

$$\delta_1 = \frac{2\pi}{\ln N}\sin^2\frac{\pi}{M}, \tag{5.21}$$

and the upper boundary clearly is

$$\delta_2 = \frac{2\pi}{\ln N}. \tag{5.22}$$

If $\delta < \delta_1$ then all the modes have enough time to get into the nonlinear regime. On the contrary if $\delta > \delta_2$ then the fluctuations around GP state will remain small. In the intermediate regime $\delta_1 < \delta < \delta_2$ some of the momentum modes will exhibit small fluctuations and some will become strongly enhanced.

5.2 Quantum fluctuations

Here we will try to examine the role of quantum fluctuations. Before starting the technical calculations, let us give some qualitative discussion. As we mentioned before we are interested in the regime, where N is large and interactions are relatively weak $\lambda \ll \lambda_{SI} \sim N^2$ so that the system is far from the insulating transition and the quantum fluctuations are intrinsically small. This means that normally it is possible to use GP approach or at most the Bogoliubov's extension. However, this is not the case for our problem. Indeed, near the classical instability the starting point for the Bogoliubov's expansion of the uniform condensate becomes bad. The other way to describe this is to note, that the Bogoluibov's equations are nothing but the quantized version of linearized equations (5.9, 5.10), which can predict the onset of instability but fail to describe the nonlinear regime. On the other hand, we can anticipate that the quantum fluctuations will remain weak until we cross the instability point. After that they will force the system to evolve into the superposition of unstable classical trajectories and become unimportant again, when those trajectories will be relatively far from each other.

These ideas known as the truncated Wigner approximation [160] (TWA) have been recently successfully applied to the description of BECs [94, 142, 143, 144, 147]. The usual method of deriving this scheme is based on the Fokker-Planck equations of motion for the density matrix written in the Wigner representation. The main difficulty with these Fokker-Planck equations is that the third order derivative terms, which are responsible for the corrections to GP trajectories, make them practically untractable [147]. Another entirely different Keldysh technique can be also used to attack non-equilibrium problems [76]. Classical equations of motion appear there naturally as the saddle point of the action. However any attempt to include quantum

fluctuations immediately results in a path integral with a self-interacting classical field [76], which is practically impossible to evaluate. In the next chapter we will try to combine these two approaches justifying TWA and showing how to go beyond.

The whole idea of the TWA is that the expectation value of any given operator Ω at time t is equal to the corresponding classical observable $\Omega_{cl}(t)$ evaluated according to standard GP equations and averaged over an ensemble of initial conditions distributed according to the Wigner transform of the initial density matrix ρ_0 (see the next chapter for the details of the derivation)

$$\Omega(t) = \int d\psi_0^* d\psi_0 p(\psi_0, \psi_0^*) \Omega_{cl}(\psi(t), \psi^*(t), t), \tag{5.23}$$

where p is defined as:

$$p(\psi_0, \psi_0^*) = \int d\eta_0^* d\eta_0 \langle \psi_0 - \frac{\eta_0}{2} | \rho_0 | \psi_0 + \frac{\eta_0}{2} \rangle e^{-|\psi_0|^2 - \frac{1}{4}|\eta_0|^2} e^{\frac{1}{2}(\eta_0^* \psi_0 - \eta_0 \psi_0^*)}. \tag{5.24}$$

Note that if initially the system is in the pure state $|O\rangle$, then

$$\rho_0 = |O\rangle\langle O|. \tag{5.25}$$

In the equation (5.24) $|\psi_0 \pm \eta_0/2\rangle$ denote coherent states. We use the following measure

$$d\psi_0 d\psi_0^* \equiv \prod_\alpha \frac{d\Re\psi_{0\alpha}\, d\Im\psi_{0\alpha}}{\pi} \tag{5.26}$$

with the product taken over continuous or discrete spatial indices, which we suppressed in (5.23) and (5.24) to shorten the notations. The interpretation of $p(\psi_0, \psi_0^*)$ as a probability is not very precise, because the Wigner transform does not have to be positive. To get the function $\Omega_{cl}(\psi, \psi^*, t)$ we need to rewrite the quantum operator Ω in the fully symmetrized form and substitute field operators a and $a^\dagger$ by their classical counterparts ψ and ψ^*.[1] In particular, the relation between Ω_{cl} and a

[1]To avoid the confusion hereafter in this and the following chapters, except otherwise specified, by ψ we will understand the expectation value of a without rescaling by a factor of $\sqrt{N}$ as we did in the previous chapter (see the text above (4.9)).

more familiar version of the classical counterpart of the normal ordered operator Ω usually appearing in the functional integrals is:

$$\Omega_{cl} = \langle \Omega\left(\psi^* + \eta^*/2, \psi - \eta/2\right)\rangle, \tag{5.27}$$

where the average is taken over η with the weight $\exp(-|\eta|^2/2)$. Let us give a simple example of the operator Ω:

$$\Omega = a^\dagger a = \frac{1}{2}(a^\dagger a + a a^\dagger) - \frac{1}{2}. \tag{5.28}$$

According to (5.27) we have:

$$\Omega_{cl} = \langle \psi^* + \eta^*/2, \psi - \eta/2\rangle = \psi^*\psi - \frac{1}{2}, \tag{5.29}$$

We see that Ω_{cl} obtained from the normal-ordered Ω according to (5.27) is equivalent to substituting the symmetrized product of a and $a^\dagger$ by $\psi\psi^*$ in (5.28).

Let us now give general comments on validity of (5.23). If the Hamiltonian is non-interacting, then this expression is exact. So it includes the Bogoliubov's approximation and goes beyond. To recover the Bogoliubov's theory we just need to linearize the semiclassical (Gross-Pitaevskii) equations of motion while evaluating $\psi(t)$. This statement is not surprising since the noninteracting evolution is always classical [19, 53, 144]. If there are nonlinear interactions, then in general, there will be corrections to the equations of motion themselves. We will consider them in the next chapter. Let us only note here that for the two coupled condensates we showed in chapter 4 (see also Sec. 5.2) that the time where GP breaks down in the worst possible scenario with the least classical initial state having completely undefined phase is equal to $t_c \approx N/\lambda = J/U$. We expect that the scaling with N is generic[2] and therefore (5.23) should be valid at least for the times shorter than t_c. In next section we will see that if there are no sudden perturbations, so that a small fraction

[2]To get the unique classical limit at $N \to \infty$ we should keep λ, not U, to be independent of N.

of quantum levels is populated then the time scale of validity of TWA becomes much longer.

Two coupled condensates. Comparison with exact solution.

The main purpose of this section is to test the truncated Wigner approach on a simple example of two coupled condensates, where it is straightforward to obtain the exact solution. The two well version of the hamiltonian (4.1) reads:

$$\mathcal{H}(t) = -a_\alpha^\dagger \tau_x^{\alpha\beta} a_\beta + \frac{U(t)}{2} a_\alpha^{\dagger 2} a_\alpha^2, \tag{5.30}$$

where $\alpha, \beta = L, R$ denote left or right well respectively, $\tau_a^{\alpha\beta}$, $a = x, y, z$ are the Pauli matrices. As usually we imply the implicit summation over repeated indices. Let us choose

$$\Omega = \frac{1}{N^2}(a_\alpha^\dagger \tau_z^{\alpha\beta} a_\beta)^2 = \frac{1}{N^2} : (a_\alpha^\dagger \tau_z^{\alpha\beta} a_\beta)^2 : + \frac{2}{N}, \tag{5.31}$$

as an observable, which is nothing but the variance of the relative number distribution. We consider several examples of evolution: (i) the initial state is symmetric and the interaction increases with time, (ii) the initial state is antisymmetric and the interaction increases with time, and (iii) the initial state is the Fock state and the interaction does not change in time. Another example will be discussed in the next chapter. The situation (ii) is directly relevant to the "cat" state dynamics we consider in this chapter, but we also look to the other possibilities to check the validity of this approach in a more general case.

As we discussed before the operator Ω should be substituted by its classical counterpart Ω_{cl} (see (5.27)), which in our particular case reads:

$$\begin{aligned} \Omega_{cl}(\psi^*, \psi) &= \frac{1}{N^2}(\psi_\alpha^* \tau_z^{\alpha\beta} \psi_\beta)^2 + \frac{2}{N} - \frac{2}{N} - \frac{1}{8N^2} \\ &= \frac{1}{N^2}(\psi_\alpha^* \tau_z^{\alpha\beta} \psi_\beta)^2 - \frac{1}{8N^2}. \end{aligned} \tag{5.32}$$

The final step is to find the probability function $p(\psi_0, \psi_0^*)$ according to (5.24). This will depend on the details of the state $|O\rangle$, therefore we have to explicitly study different initial configurations.

Symmetric or antisymmetric initial state

Suppose that at $t = 0$ the interaction was negligible. Then the products of symmetric and antisymmetric wavefunctions give the ground and the most excited stationary states, respectively. They can be also represented as a superposition of products of the two coherent states with equal or shifted by π phases:

$$|O\rangle = (4\pi N)^{1/4} \mathrm{e}^{-N} \int \frac{d\theta}{2\pi} \mathrm{e}^{-2i\theta N} |\sqrt{N}\mathrm{e}^{i\theta}\rangle_L |\sqrt{N}\mathrm{e}^{i\theta + i\pi\sigma}\rangle_R, \tag{5.33}$$

where $\sigma = 0, 1$ for symmetric or antisymmetric state, respectively. The integral over the global phase θ ensures the particle number conservation. Before proceeding with further analysis let us look into a simpler example of just a product of the two coherent states, where the global phase symmetry is broken and θ takes some particular value, say zero. Then after straightforward calculation one can show that:

$$p(\psi_0, \psi_0^*) = 4\mathrm{e}^{-2\sum_\alpha |\psi_{0\alpha} - \sqrt{N}\mathrm{e}^{i\pi\sigma}|^2}. \tag{5.34}$$

We see that in this simple case the probability distribution of ψ_0 is a gaussian centered near the classical value with relative variance of fluctuations of the order of $1/\sqrt{N}$. This makes perfect sense and we indeed recover GP picture of a single initial state in the limit $N \longrightarrow \infty$. Now let us look closer to the true wavefunction (5.33). After simple calculation the final expression for the probability p reads:

$$p(\psi_0, \psi_0^*) = 4\mathrm{e}^{-|\psi_{0+}|^2 - |\psi_{0-}|^2} L_{2N}(2|\psi_{0+}|^2), \tag{5.35}$$

where $\psi_{0\pm} = \psi_{0L} \pm \psi_{0R}$ in the symmetric state and we should interchange ψ_{0+} and ψ_{0-} for the π state, $L_{2N}(x)$ is the Laguerre's polynomial. This expression is a

gaussian in terms of $|\psi_{0-}|$, however it has a nonlocal behavior as a function of $|\psi_{0+}|$. Moreover $p(\psi_0, \psi_0^*)$ is not positively defined. This leads to interesting consequences. For example, while the average of $|\psi_{0+}|^2$, computed with help of (5.35) gives the expected classical result, the variance of $|\psi_{0+}|^2$ is *negative*. In figure 5.1 we plot the normalized function $|\psi_{0+}|\, p(|\psi_{0+}|)$ for the situation with 8 bosons per well. The extra factor of $|\psi_{0+}|$ comes from the integral measure:

$$\int_0^\infty |\psi_{0+}| p(|\psi_{0+}|) d|\psi_{0+}| = 1, \tag{5.36}$$

For convenience we rescaled the fields $\psi_0 \to \sqrt{N}\psi$ so that the expectation value of $|\psi_{0+}|$ is 2. In the limit $N \to \infty$ we again recover the classical result (for the rescaled

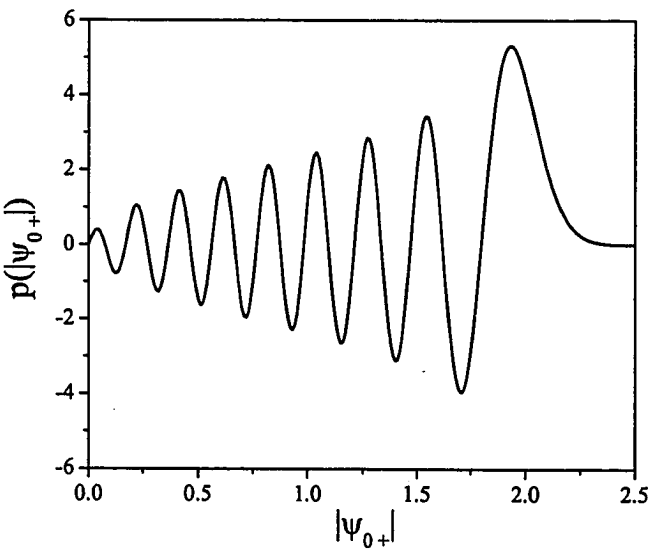

Figure 5.1: Distribution of the GP initial conditions versus $|\psi_{0+}|$ for the symmetric state with eight noninteracting bosons per well. The classical value of $|\psi_{0+}|$ is equal to two.

fields) $\psi_{0\,L,R} = 1$ or $|\psi_{0+}| = 2$, $|\psi_{0-}| = 0$, but in a peculiar way. The contributions to a given observable from $|\psi_{0+}| < 2$ will cancel each other because of the fast oscillations of p and those coming from $|\psi_{0+}| > 2$ will be exponentially suppressed,

so that only a small region around $|\psi_{0+}| = 2$ will determine the ultimate result. We might think, that if the observable is a smooth function of the initial parameters, then the details of the distribution $p(\psi_0, \psi_0^\star)$ are not important and we can substitute it by some gaussian function with appropriate mean and variance. However, as we pointed out before the variance given by the distribution (5.35) is negative, so at least this is not very straightforward to do.

Now let us assume that the interaction increases with time according to:

$$\lambda(t) = \frac{\tanh(\delta t)}{1 - \delta t}, \tag{5.37}$$

where $\delta \ll 1$ is the adiabatic parameter. This dependence is somewhat different from what we used in the previous section. But the resulting instability is still there, and besides the purpose of this section is to test our approximation scheme rather than to do some particular calculations. The resulting graphs for both symmetric and antisymmetric initial states are plotted in figures 5.2, 5.3. Note that even for the eight particles per well the agreement between the exact and the TWA solutions is remarkable. For the thirty two particles there is a small discrepancy for the intermediate value δ. Apparently the semiclassical curve does not capture the small oscillations very well. But both in the limit of large and small δ the oscillations disappear and the agreement becomes perfect. Notice that the steady state for the initial antisymmetric conditions is exactly the maximally entangled "Schrödinger cat" state, where all the bosons occupy either left or right well:

$$|\Psi_f\rangle = \frac{1}{\sqrt{2}}(|LLL\ldots\rangle + |RRR\ldots\rangle). \tag{5.38}$$

The ultimate reason for this is that as we mentioned above the π shifted state is at classical equilibrium for any interactions λ. This equilibrium though becomes unstable for $\lambda > \lambda_c$. So any fluctuation will cause a classical trajectory to end up either in the left or in the right well and the quantum zero point motion provides

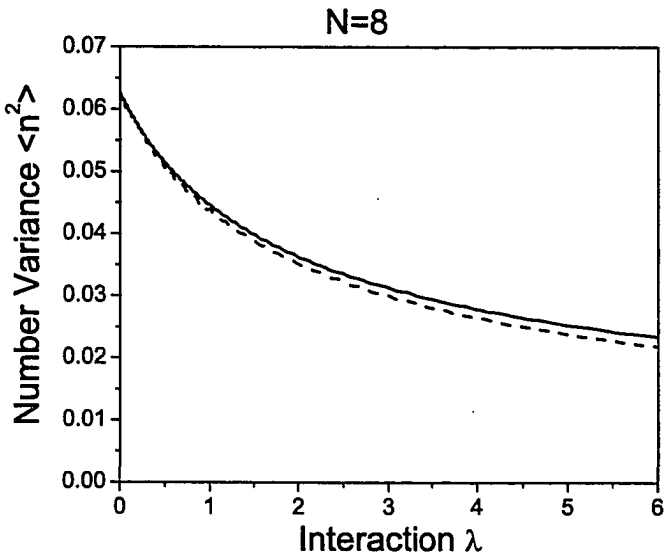

Figure 5.2: Dependence of the number variance as defined in (5.32) on the interaction changing with time according to (5.37) for initial symmetric state and 8 bosons per well. Dashed and solid lines show semiclassical and exact solutions, respectively.

us with these fluctuations. However, quantum mechanically we do not break the left-right symmetry, because it is the property of the full hamiltonian. The only way to reconcile these two results is to have the final configuration in the coherent superposition of the left and the right states, which can be also verified from the exact solution.

Initial number state

Here we revisit our results derived in the previous chapter, where the two condensates were initially uncoupled and their wavefunction was just the product of the number states. At $t = 0$ the tunnelling is suddenly turned on and the number variance starts to experience some oscillatory behavior. Repeating the same analysis as in the

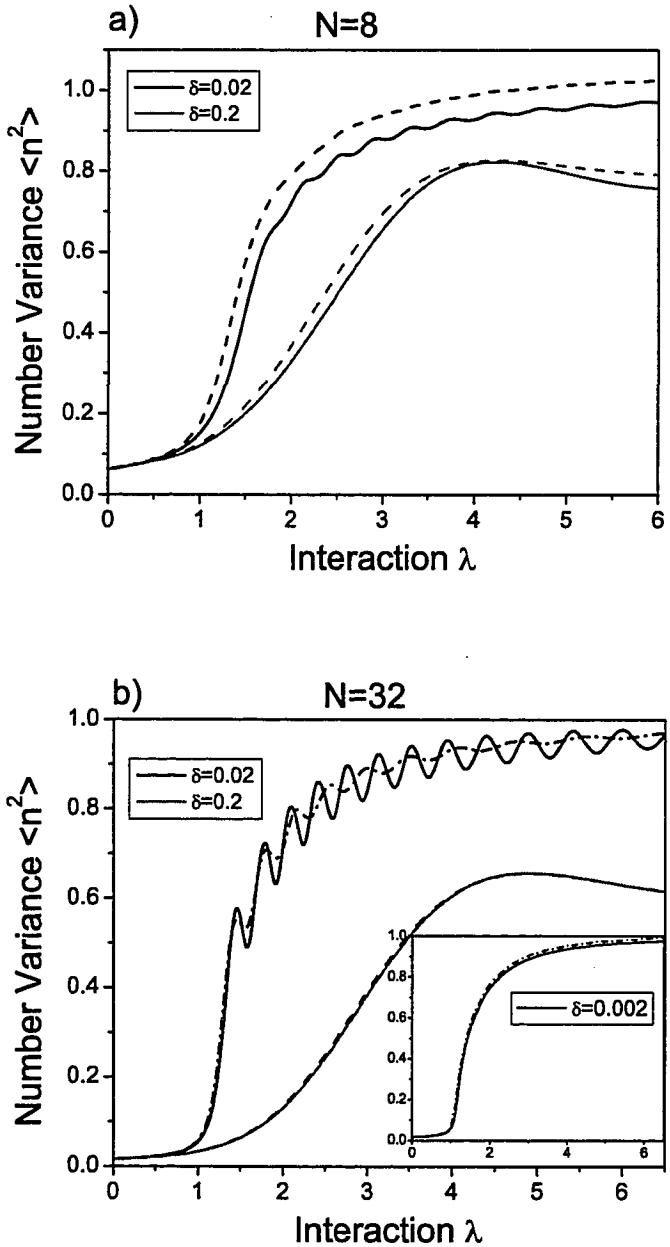

Figure 5.3: Same as in figure 5.2 but for initial antisymmetric state. The graphs (a) and (b) correspond to 8 and 32 bosons per well, respectively . The lower graphs correspond to a faster turning on the interaction. The inset in the graph (b) corresponds to the slowest evolution.

previous subsection we find:

$$\langle (a^\dagger_\alpha(t)\tau_z^{\alpha,\beta}a_\beta(t))^2\rangle = \int dn_L dn_R d\theta p_{num}(n_L)p_{num}(n_R)(\psi^*_\alpha(t)\tau_z^{\alpha,\beta}\psi_\beta(t))^2, \quad (5.39)$$

where $n_{L,R} = |\psi_{L,R}(t=0)|^2$, θ is the initial phase difference between ψ_L and ψ_R. So in the Fock state the phases in the two wells are indeed uncorrelated as we argued in chapter 4. However the number of bosons is distributed according to $p_{num}(n)$ given below and not fixed at $n = N$ as we might naively think. In 5.39 we ignored an additive $1/8N^2$ correction (see (5.32)). The probability of having initial occupation n in either well is [53]:

$$p_{num}(n) = 2e^{-2n}L_N(4n), \quad (5.40)$$

where as before $L_N(x)$ stands for Laguerre's polynomial of the order N. The function p_{num} is very similar to its counterpart defined in (5.35) in the sense that it has also an oscillatory behavior for $n < N$ and exponentially decays for $n > N$. Recall that the simple GP picture does not predict correctly the prefactor before the number variance (see Sec. 4.1) and it is valid for the finite amount of time shorter than some characteristic scale determined by interactions: $t < t_c \approx J/U = N/\lambda$. For longer times the GP result starts to strongly deviate from the exact solution due to the recurrence occurring in a quantum system. We might guess that the agreement between the semiclassical and the quantum pictures can be improved upon inclusion of quantum fluctuations at initial time according to (5.40). This is indeed the case for $t < t_c$, i.e. the discrepancy in the prefactor completely disappears. However, as we can see from the figure 5.4, these fluctuations do not affect the time t_c itself so that the correct result can be recovered only if we also include quantum scattering, or in other words deviations of the trajectories from the classical ones. We briefly conclude this section noting that the developed approach works very well if the external parameters change smoothly with time so we do not excite many quantum levels. In this case

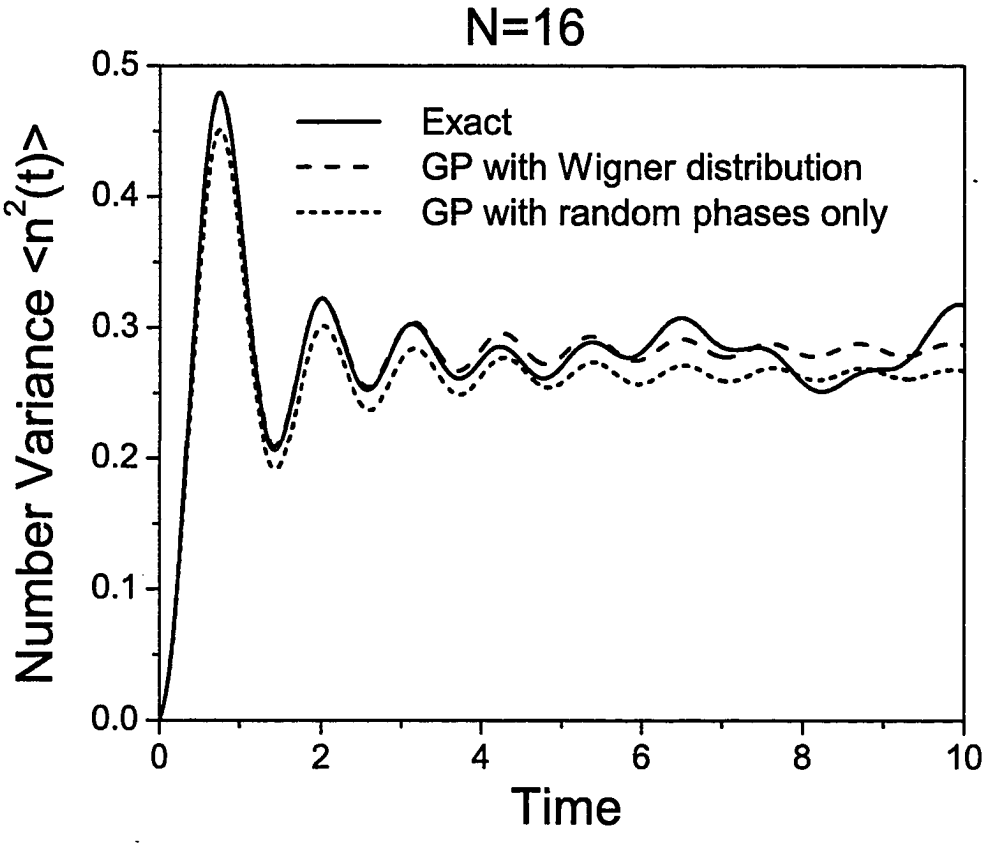

Figure 5.4: Time dependence of the number variance for the initial number state and 16 bosons per well. The interaction strength is $\lambda = 1$.

the quantum fluctuations enter only at initial time and the subsequent evolution is essentially classical. In the opposite limit when the parameters change fast the classical behavior is adequate for short times ($t < t_c$) and breaks completely for $t > t_c$ with the characteristic time t_c determined by the strength of interactions.

5.3 Numerical results for multiple wells

Having established the general framework and checked its validity let us move on to the main subject of the chapter. First, following the analysis given in Sec. 5.1, we

will study the temporal behavior in a periodic array of wells being initially in the π state. Then we will consider a case of a harmonic trapping potential.

Periodic array

The straightforward generalization of (5.33) for the π state in a periodic chain of coupled condensates of size M (we assume M to be even) is:

$$|0\rangle = (4\pi NM)^{\frac{1}{4}} \mathrm{e}^{-\frac{NM}{2}} \int \frac{d\theta}{2\pi} \mathrm{e}^{-i\theta NM} \prod_{j=1}^{M} |\sqrt{N}\mathrm{e}^{i\theta + i\pi j}\rangle_j, \tag{5.41}$$

where $|\ldots\rangle_j$ stands for the coherent state in the j-th well. This state is an eigenstate of the noninteracting hamiltonian and apart from the global phase, which conserves the total number of bosons, it is just a product of coherent states with alternating phases. Ignoring the integral over θ, results in a gaussian probability distribution of the initial state (compare with (5.34)):

$$p(\psi_0, \psi_0^*) = 2^M \prod_{j=1}^{M} \mathrm{e}^{-2|\psi_{0j} - \sqrt{N}\mathrm{e}^{i\pi j}|^2}. \tag{5.42}$$

while the correct result for (5.41) reads:

$$p(\psi_0, \psi_0^*) = 2^M \mathrm{e}^{-2M\sum_k |\hat{\psi}_{0k}|^2} L_{NM}(4M|\hat{\psi}_{00}|^2), \tag{5.43}$$

where $\hat{\psi}_{0k}$ stands for the discrete Fourier transform of ψ_{0j}:

$$\hat{\psi}_{0k} = \frac{1}{M} \sum_j \psi_{0j} \mathrm{e}^{-ikj} \tag{5.44}$$

Clearly as $M \to \infty$ the difference between (5.42) and (5.43) should vanish. Next let us define the operator Ω, which would be a good measure of the instability:

$$\Omega = \frac{1}{N^2 M(M-1)} \sum_j (a_j^\dagger a_j - N)^2. \tag{5.45}$$

Clearly Ω is equal to the normalized sum of number variances over the different wells. It is easy to verify that the classical counterpart of Ω is:

$$\Omega_{cl}(\psi^*, \psi) = \frac{1}{N^2 M(M-1)} \sum_j \left(\psi_j^* \psi_j - N - \frac{1}{2} \right)^2 - \frac{1}{4N^2(M-1)}. \qquad (5.46)$$

It is reasonable to expect that as the number of wells increases the global phase becomes less and less important and therefore (5.42) becomes more accurate. First let us take interaction to be monotonically increasing in time according to (5.37). In

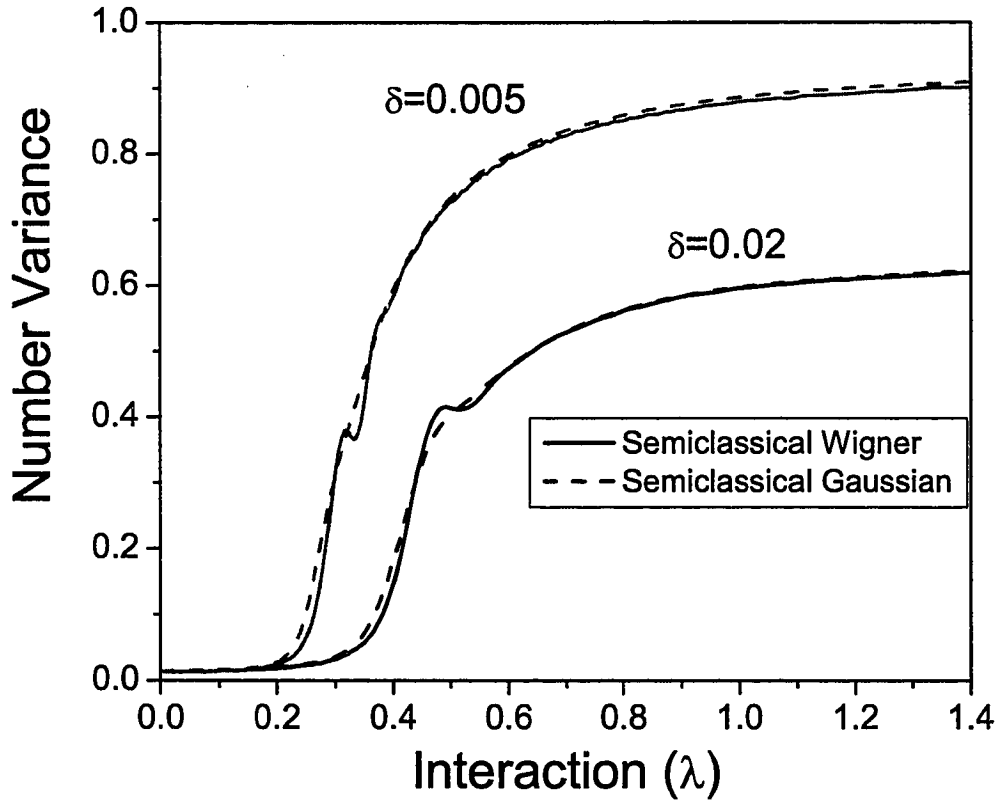

Figure 5.5: Number variance defined in (5.46) as a function of the interaction for the case of ten wells with eight bosons per well. The solid and the dashed lines correspond to the distributions given by (5.43) and (5.42), respectively. The upper curves correspond to a slower increase in interaction.

figure (5.5) we plot the resulting evolution of the state for the case of ten wells with

eight bosons per well in average. The solid and the dashed lines correspond to the probability distributions given by (5.43) and (5.42), respectively . Clearly there is no noticeable difference between them. Note that the upper curves corresponding to smaller δ, i.e. adiabatic limit, saturate at $\Omega \approx 1$, which shows that *all* the bosons appear in a single well, i.e. the resulting steady state $|F\rangle$ is:

$$|F\rangle = \frac{1}{\sqrt{M}}(|111\ldots\rangle + |222\ldots\rangle + \ldots |MMM\ldots\rangle). \tag{5.47}$$

The whole procedure of driving the system into the maximally entangled state described here is conceptually very similar to that recently suggested in [38], where the tunneling was assumed to decrease by the spatial drag of the double-well condensate through a beam splitter. The important difference however, is that here we are not limited by the double-well system and can consider larger arrays, so that our entangled "cat" occupies more than two macroscopic states.

There is an important issue, which was completely obscured in the preceding analysis. Indeed, studying the number variance alone it is impossible to distinguish the "cat" state from a collapsed condensate. While the collapse is often very well reproduced using GP equations, it is much harder to describe recovery within this framework. To examine this issue let us consider the interaction, which is periodic in time:

$$\lambda(t) = \lambda_0 \sin^2(\pi\delta t), \tag{5.48}$$

where the parameter δ determines the adiabaticity of the interaction. If δ is small then we expect complete restoration of the initial state after one period of oscillation $T = 1/\delta$. With decreasing period we gradually loose adiabatic limit and the evolution of the system is no longer expected to be periodic. Figure 5.6 summarizes this discussion and the graphs are in perfect agreement with our expectations. The

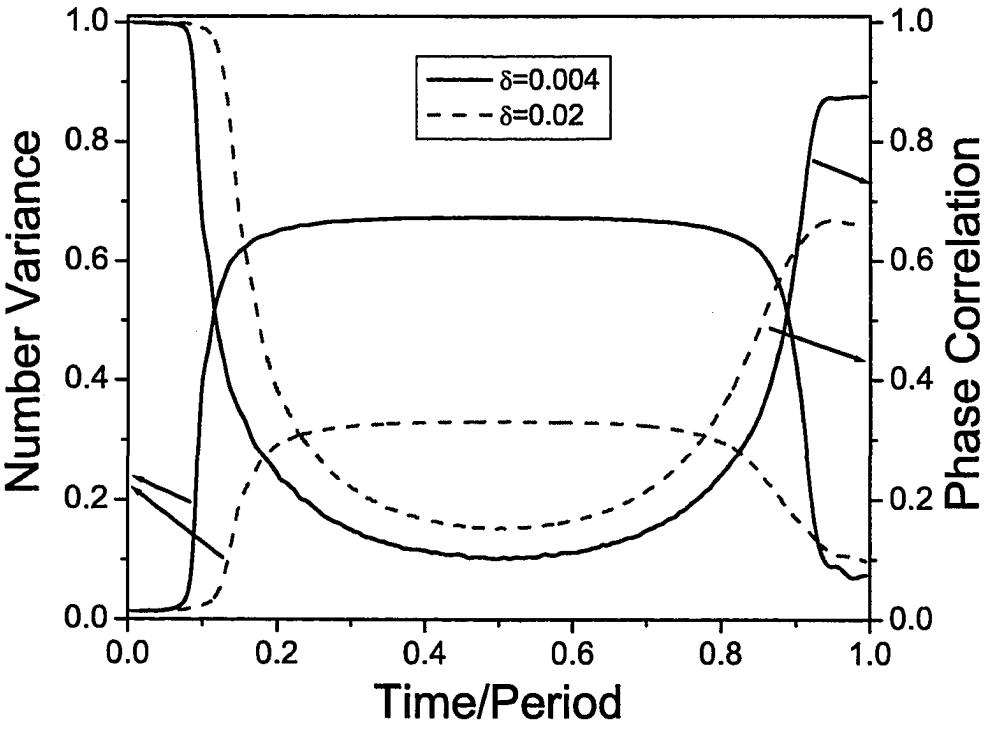

Figure 5.6: Number variance and the phase correlation as a function of time divided by the period of interaction ($T = 1/\delta$) for ten wells and eight bosons per well. The interaction changes with time according to (5.48) with $\lambda_0 = 2$. For smaller δ the phase restoration is almost complete, which proves the coherence of the dynamics.

phase coherence in this figure is defined in a usual way as

$$-\frac{1}{2NM}\sum_j \langle a_j^\dagger a_{j+1}\rangle + c.c$$

and the "−" sign is inserted for convenience because we start from the π-state.

So far we considered examples, where the initial state was a noninteracting π-phaseshifted condensate and then the interaction was slowly ramped up (or equivalently tunnelling was ramped down). This rather hypothetical situation is certainly suitable for the theoretical analysis, but hardly applicable to any real experimental realization, where the interactions between the bosons is always present. So the initial wavefunction is not a simple product of coherent states but a more compli-

cated object. One way to proceed with this issue is to write down an approximate wavefunction, which can be obtained using either Bogoliubov's hamiltonian (valid for $\lambda \ll N^2$) or variational methods, and then find its Wigner transform according to (5.24). This would be a tractable but lengthy calculation. Instead we can do a simple trick, demonstrating the advantage of the present approach. Namely, we can start from the simple noninteracting ground state, then adiabatically increase the interaction strength to the desired value, and finally apply the π-phaseshift and follow the subsequent evolution. In this scheme there is no need to do any additional analytic calculations, both the "fake" evolution to the interacting ground state and the subsequent real dynamics are described within the same scheme. Moreover the computational time does not increase much because of the extra "fake" evolution to the true ground state. Indeed, the classical motion is stable before the π-phaseshift is applied so that GP equations can be efficiently integrated. To be more specific, assume that we start from the interacting condensate with $\lambda = \text{const}(t)$, then at $t = 0$ suddenly apply a π phaseshift and follow the subsequent appearance of the "cat". Clearly if $\lambda > \lambda_c$ (see (5.7)) the system will become unstable and the quantum fluctuations will force it into the entangled state. Without any calculations, it is obvious that the final state will not be maximally entangled as described in figure 5.5 because of the energy conservation. Indeed, the state with all the bosons occupying one well costs a huge interaction energy which can not be compensated unless there is an external pumping resulting in the time dependence of the hamiltonian. From the same considerations it is obvious that the maximum possible entanglement within this scheme can be achieved at some intermediate values of λ. Thus if $\lambda < \lambda_c$, there is no instability to begin with and so no entanglement in the final state. On the other hand for the large λ any significant number fluctuations will cost a strong increase in the interaction energy, which can not be compensated by a limited decrease of the

hopping energy. We plot the resulting number variance as a function of time for the periodic array of ten wells in figure 5.7. The critical value of the interaction for this

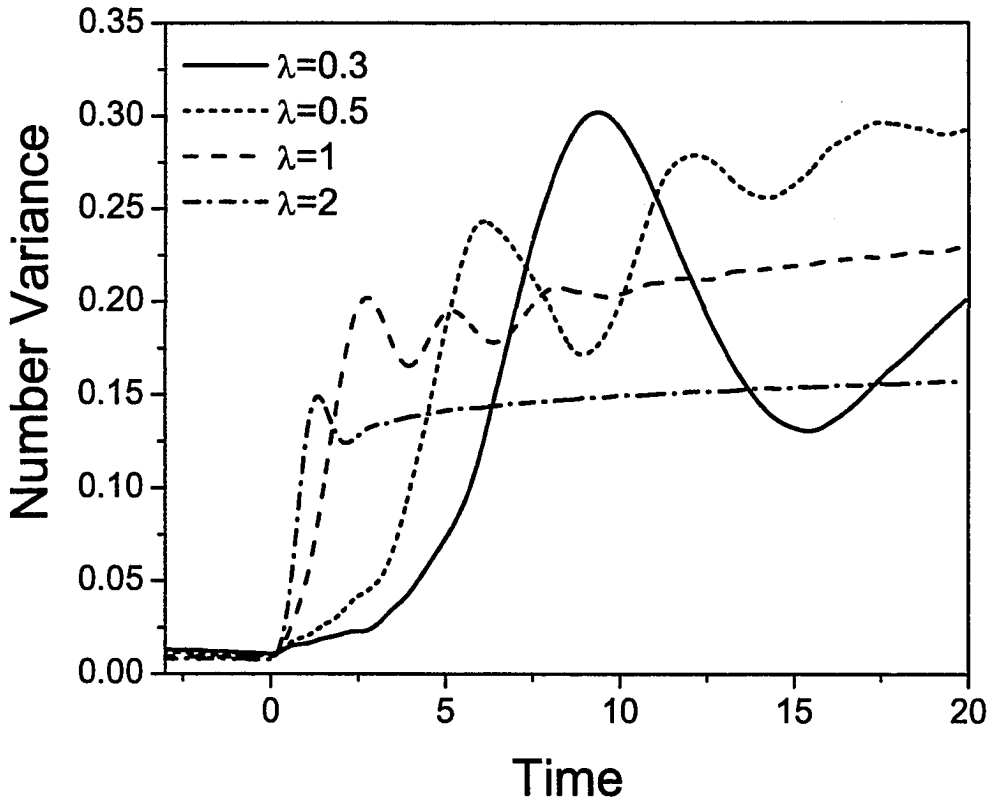

Figure 5.7: Number variance as a function of time for ten wells and eight bosons per well. The interaction remains constant in time in this example but at $t = 0$ a sudden π-phaseshift is applied to the system.

case is $\lambda_c = 2\sin^2(\pi/10) \approx 0.19$. Clearly for λ getting closer to λ_c the oscillations become slower and the steady state is achieved later. We would like to point out, that this type of dynamics certainly corresponds to a sudden perturbation discussed in Sec. 5.2. Therefore we expect a finite ergodic time for a full quantum solution and no true steady state for the finite number of bosons. So to achieve a stable stationary entangled state it is always preferable to drive the system adiabatically towards the

instability, i.e. apply a π-phaseshift at smallest possible λ and then slowly ramp up the interaction.

Harmonic trap

The effect of the harmonic trap can be mimicked by adding a quadratic potential term to the hamiltonian of the system see (4.1):

$$V_j = \frac{J\xi}{2} j^2 \equiv \frac{J\omega_t^2}{4} j^2, \tag{5.49}$$

where ω_t is the trapping frequency. As before let us assume that initially the interactions are suppressed and the system is in the ground state:

$$|O\rangle = \left(\sum_j \alpha_j a_j^\dagger \right)^N_{tot} |Vac\rangle, \tag{5.50}$$

where $|Vac\rangle$ denotes a vacuum state with no particles, N_{tot} is the total number of bosons in the system and

$$\alpha_j \approx \frac{\sqrt{2}}{(\pi\omega_t)^{\frac{1}{4}}} \mathrm{e}^{-\frac{\omega_t^2}{4} j^2} \tag{5.51}$$

is the ground state wave function of a single boson in the harmonic trap in the coordinate representation. This wavefunction can be written as:

$$|O\rangle = \int \frac{d\theta}{2\pi} \mathrm{e}^{i\theta(n_1+n_2+\cdots-N_{tot})} |\sqrt{N_{tot}}\alpha_1\rangle_c |\sqrt{N}_{tot}\alpha_2\rangle_c \ldots, \tag{5.52}$$

where as usual $|\alpha\rangle_c$ stands for the coherent state. If the number of populated wells is not small, then we can ignore the global phase and use an approximate expression

$$|O\rangle \approx \prod_j |\sqrt{N_{tot}}\alpha_j\rangle_c. \tag{5.53}$$

As in the previous discussion we assume that at initial time the phases in the adjacent wells were uniformly shifted by some phase θ. However, we will not assume that $\theta = \pi$, because the π phase shift in the nonuniform potential does not give a stationary

solution, although it still preserves inversion symmetry. Also the number variance is no longer a convenient measure of the instability, because the distribution is not uniform even in the initial state. Instead let us introduce two other quantities: coordinate of the center of mass and the condensate width:

$$X = \frac{1}{N}\langle \sum_j j a_j^\dagger a_j \rangle, \; W = \sqrt{\frac{1}{N}\langle \sum_j j^2 a_j^\dagger a_j \rangle - X^2}. \tag{5.54}$$

The semiclassical operators can be trivially obtained from (5.54). For example,

$$X_{cl} = \frac{1}{N}\langle \sum_j j \, (\psi_j^* \psi_j - 1/2) \rangle. \tag{5.55}$$

Let us assume that both the interaction and the trap frequency increase in time:

$$\lambda(t) = \frac{\tanh \delta t}{1 - \delta t}, \quad \omega_t^2(t) = \frac{\omega_t^2(0)}{1 - \delta t}. \tag{5.56}$$

We define λ according to (4.8) with $N = N_{tot}|\alpha_0|^2$ being the number of bosons in the central well. Note that with $\omega_t \neq 0$ there are two degrees of freedom: λ/J and ω_t/J. If we want to reflect the experimentally relevant case of vanishing tunnelling rather then increasing interaction we have to keep the ratio λ/ω_t^2 constant. Extra multiplier "$\tanh \delta t$" in the interaction term is taken only for convenience purposes and does not qualitatively change any of the results.

The two graphs in figure 5.8 show the condensate width and the center of mass position versus time for different initial phase imprints. Note that if the phaseshift is equal to π, there is no center of mass oscillation because of the left-right symmetry. On the other hand, the width oscillations are very large and pronounced. Clearly these oscillations die very fast away from the π phaseshift, however the steady state condensate width depends on θ rather smoothly. It is also interesting to point out that the center of mass oscillations decay faster for larger angles. This is in a direct agreement with the previous predictions of self-trapping [146]. We would like to point

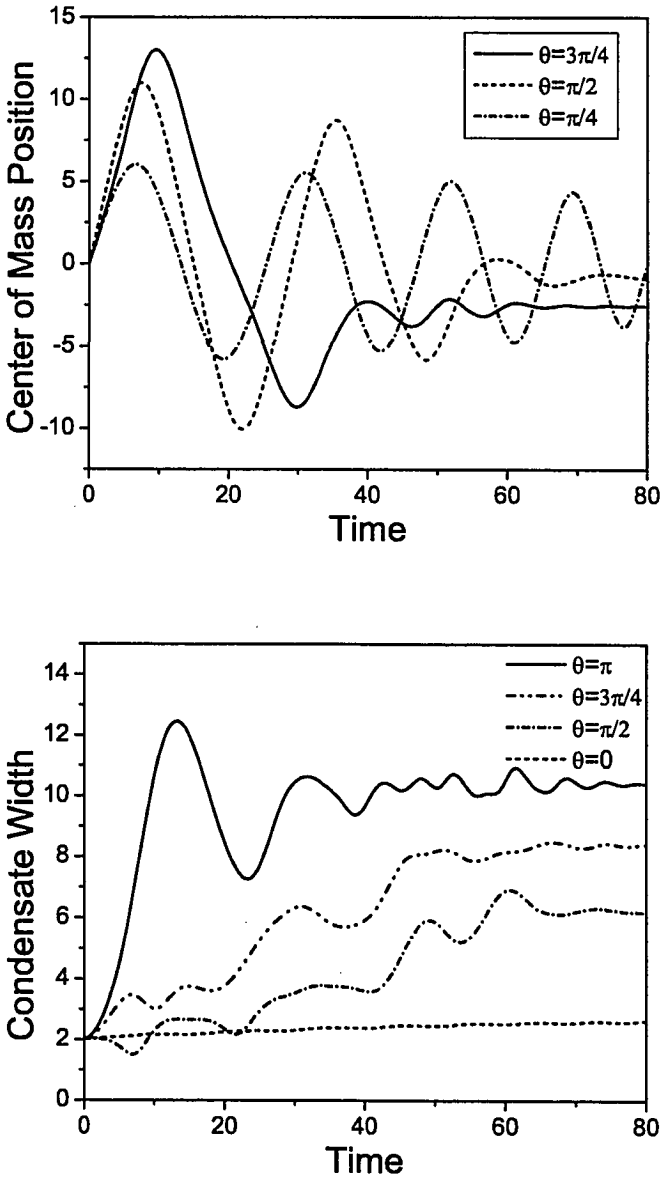

Figure 5.8: Center of mass position and the condensate width as a function of time for the interaction and trapping frequency increasing in time according to (5.56) with $\delta = 0.01$, $\omega_t^2(0) = 0.06$, and the total number of bosons $N_{tot} = 100$.

out that the trapping is real in our case because of the rapidly increasing interaction (or equivalently vanishing tunnelling).

There is, however, a major difference between the results for a periodic array and a harmonic trap. In the semiclassical limit the π state is an eigenstate in a periodic array for any strength of the interaction, therefore the motion is completely driven by the quantum-mechanical fluctuations, while in a harmonic trap the π state is semiclassically unstable (that is why we plot our observables versus interaction for the periodic array and versus time for the parabolic case). This makes quantum effects unimportant if the number of bosons is large. To further elucidate this point let us compare the results for a single Gross-Pitaevskii trajectory, i.e. simple classical limit, with the TWA result advocated here. The two dependences are shown in

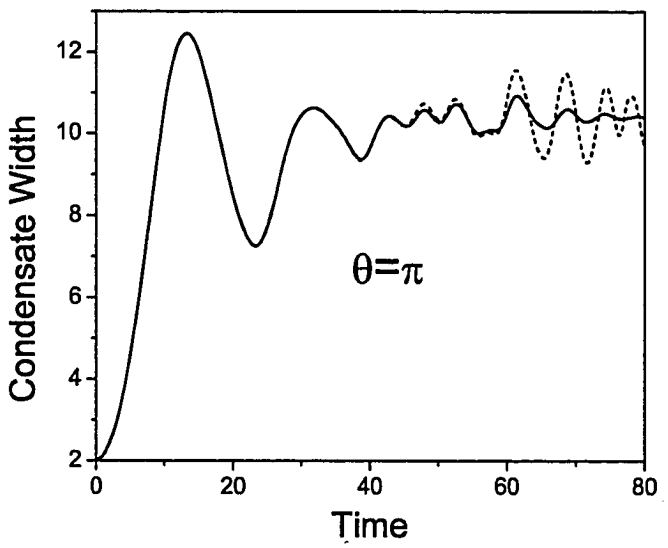

Figure 5.9: Condensate width as a function of time for the same conditions as in figure (5.8). The dashed line is the simple Gross-Pitaevskii result and the solid line is the improved calculation according to (5.23).

figure 5.9 and they are clearly very similar. This proves that the resulting instability has a simple classical nature and does not give a "cat" state, rather the condensate

simply has large amplitude breathing modes. Such an outcome should not be very surprising. In order to get to the macroscopic entanglement one has to prepare a classically equilibrium but unstable state, which can be driven away via quantum fluctuations. This can be achieved by a simple phase shift only in a uniform periodic lattice. We can also check the reversibility of the evolution for the periodic in time interaction (5.48). And clearly, see figure 5.10, the dynamics is completely

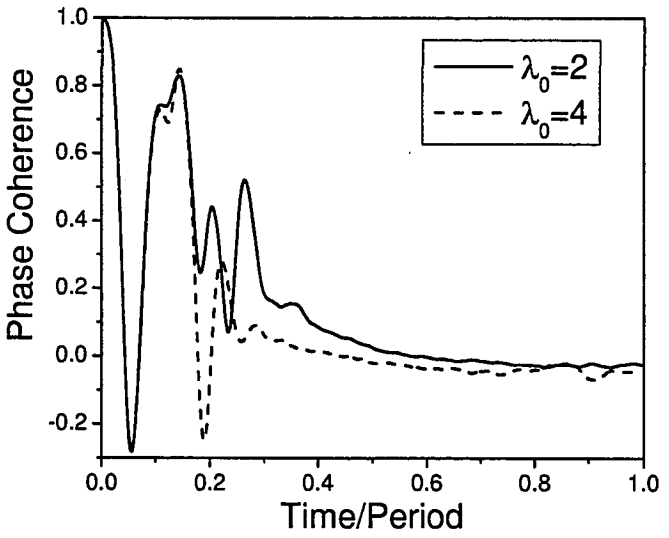

Figure 5.10: Phase coherence as a function of time for the periodic interaction (5.48) with $\delta = 0.004$. The total number of bosons $N_{tot} = 100$, the parabolicity $\omega_t^2 = 0.06$, and the initial phaseshift $\theta_0 = \pi$. Clearly the dynamics is completely irreversible as opposed to figure 5.6.

irreversible. This result is quite trivial given that the initial state is not stationary even without interactions, so the π phaseshift looks as a sudden perturbation applied at $t = 0$ and the even if the interactions changes with time slowly the system is not in the adiabatic regime.

5.4 Discussion

In the previous sections we adopted a reduced Wigner approximation allowing to treat classical instabilities due to quantum fluctuations. In this analysis we completely ignored the classical noise, which may come from various sources e.g. fluctuations of the laser intensity or wavelength, fluctuations of the magnetic field creating the harmonic trap, collisions with external atoms, triple interactions between the bosons leading to the loss of the atoms from the condensate, etc. All these sources are generally quite weak, otherwise no beautiful experiments would ever be possible. On the other hand the "cat"states are extremely fragile to any kinds of classical noise. For example, we know that in a double well in the equilibrium the noise required to destroy the coherence exponentially scales with the mass (or equivalently number of particles). So that heavy objects are always localized in one of the classical minima. However, this is not the case in our situation. Indeed, the system is far from the equilibrium and the "cat"state is not a ground state. Let us crudely estimate the limits on the noise. Assume that the classical fluctuations result in a random external potential with a usual correlator $\langle Y(t)Y(t')\rangle = Y_0\delta(t-t')$ and consider a case of two wells for simplicity. Then the relative phase flow with time due to fluctuations will be

$$\delta\theta \sim NY_0\sqrt{t}.$$

On the other hand the minimum time required to get to the cat state is (see (5.1)):

$$t \sim \frac{1}{\delta} \sim \ln N.$$

Requiring that the total phase accumulated during the evolution is less then 1 we get an upper bound for the noise which does not destroy the coherence :

$$Y_0 \sim \frac{1}{N\sqrt{\ln N}}.$$

This result is encouraging, because instead of an exponentional we get a much weaker scaling of the noise with the number of particles. Clearly, in the multi-well limit there will be an extra scaling with the number of wells and of course no cat state is possible in the thermodynamic limit. However, the scaling will be again weak and tractable. Another possibility to observe macroscopic "cat" states experimentally is to use modulated hopping between the sites in a large array effectively splitting the condensate into pairs of sites, so the effects of the classical noise become weaker.

The other two constraints used in our analysis that the number of bosons is large and the condensate is one-dimensional are also not essential. We used large number of bosons rather to satisfy the formalism then to explain the effect. The instability is there even in the fully quantum-mechanical treatment of the problem. The evolution of macroscopically entangled states with a large number of atoms are much more interesting from both theoretical and experimental points of view. Concerning higher dimensions we would like to point out that, although we did not performed actual calculations, it is extremely unlikely that any of the results will qualitatively change. The instability will clearly survive in any dimensions and the π state can be implemented, at least theoretically, in square lattices of arbitrary dimensionality.

To conclude this chapter, we showed that it is possible to create macroscopically entangled "Schrödinger cat" states in the bosonic systems in optical lattices with finite number of sites. We developed a formalism generalizing a simple GP approach by exact treatment of quantum fluctuations at initial and final times of the evolution. The resulting expressions were tested on a solvable model of two coupled condensates and found a very good agreement with the exact results. At the end we presented some numerical simulations for the multiple-well condensates and argued that it is possible to create a "cat" state with more than two possible outcomes.

Chapter 6

Quantum corrections to classical evolution

6.1 Overview

Motivated by the discussion given in the previous chapter we will try to justify the truncated Wigner approximation and see how it is possible to go beyond. The essence of this work is to try to develop a consistent expansion of the evolution equations in powers of $\hbar$. We will use Bose condensates as an example, though the results can be easily generalized. In this way the Gross-Pitaevskii equations describe the classical evolution. It is important to emphasize again that the Bogoliubov's approximation, which certainly goes beyond GP, nevertheless is not what we need. The ultimate reason is that there is an implicit assumption of smallness of both quantum and classical fluctuations. To justify it we need to require not only that initially the system is almost classical, but also that the subsequent classical evolution is stable, i.e. fully described by the linearized version of the GP equations. This is certainly not always a good assumption.

Before presenting the actual derivation let us review in some detail other techniques used to attack nonequilibrium problems. We will try to concentrate on their advantages and drawbacks and give the final justification for the present contribution.

6.1.1 Fokker-Planck equations and stochastic evolution

One of the possible approaches, which came from quantum optics [53, 160] is based on the Liouville equations for a density matrix written in the coherent basis. This technique was first adopted to BECs in [147]. The main idea is to rewrite a density matrix ρ in a coherent state representation and substitute into the corresponding evolution equation. Note that the coherent basis is overcomplete. In particular if

$$\rho = \int d^2\alpha d^2\beta \, P(\alpha,\beta) \frac{|\alpha\rangle\langle\beta^*|}{\langle\beta^*|\alpha\rangle}, \tag{6.1}$$

there is no way the function $P(\alpha,\beta)$ can be uniquely defined. However, we can always impose some additional requirements on the function P, so that the ambiguity disappears.

Glauber P-representation

One way to deal with (6.1) is to require $|\alpha\rangle = |\beta^*\rangle$ then we get

$$\rho = \int d^2\alpha \, P(\alpha)|\alpha\rangle\langle\alpha|. \tag{6.2}$$

The number $\langle\alpha|\alpha\rangle$ can be absorbed into the integral measure. It can be proven [160] that for any density matrix ρ, there is a unique function $P(\alpha)$, which is called the Glauber P-function.

With this representation it is particularly easy to write the averages of normally ordered products of creation and annihilation operators. Indeed,

$$\langle a^{\dagger m} a^n \rangle = \int d^2\alpha \, \alpha^{*m} \alpha^n P(\alpha). \tag{6.3}$$

Using the definition

$$|\alpha\rangle = \exp(-|\alpha|^2/2)\exp(\alpha a^\dagger)|0\rangle,$$

it is not hard to demonstrate [160] that

$$a\rho \leftrightarrow \alpha P(\alpha),\ a^\dagger\rho \leftrightarrow \left(\alpha^* - \frac{\partial}{\partial\alpha}\right)P(\alpha),\ \rho a \leftrightarrow \left(\alpha - \frac{\partial}{\partial\alpha^*}\right)P(\alpha),\ \rho a^\dagger \leftrightarrow \alpha^* P(\alpha). \tag{6.4}$$

These identities are sufficient to derive the time evolution of the distribution P from the standard equation for the density matrix:

$$i\frac{d\rho}{dt} = [\mathcal{H}, \rho]. \tag{6.5}$$

In particular, for the case of a single site with

$$\mathcal{H} = -\mu a^\dagger a + \frac{U}{2}a^\dagger a(a^\dagger a - 1) \tag{6.6}$$

the resulting master equation reads [147]:

$$i\frac{\partial P}{\partial t} = -\frac{\partial}{\partial\alpha}(-\mu\alpha + U|\alpha|^2\alpha)P + \frac{U}{2}\frac{\partial^2}{\partial^2\alpha}\alpha^2 P - \text{c.c.}. \tag{6.7}$$

Note that the classical equations of motion can be recovered as characteristics of (6.7) by simply ignoring the second order derivatives with respect to α and α^*. Also we would like to point out that absolutely the same equations will govern the time behavior of the positive P representation, which is obtained from (6.1) with the requirement that $P(\alpha, \beta)$ is positively defined. The only difference is that now instead of α^* we should use a new complex number β, which is independent of α. So $P(\alpha, \beta)$ is now a function of two complex or four real variables. The advantage of the positive P-representation is that the diffusion matrix in (6.7) becomes positive definite [160]. The price we pay is that the number of independent variables doubles.

It can be shown that a general Fokker-Planck equation with a positively defined diffusion matrix is equivalent to a system stochastic Langevin differential equa-

tions [54], in particular if

$$\frac{\partial F}{\partial t} = -\sum_j \frac{\partial}{\partial x_j} A_j(x,t)F + \frac{1}{2}\sum_{j,k} \frac{\partial^2}{\partial x_j \partial x_k} \left(\mathbf{B}(x,t)\mathbf{B}^{\mathsf{T}}(x,t)\right)_{jk} F \tag{6.8}$$

then

$$\frac{dx_j}{dt} = A_j(x,t) + B_{jk}(x,t)E_k(t), \tag{6.9}$$

where $\mathbf{E}$ is the real noise source with a standard correlator $\overline{E_j(t)E_k(t)} = \delta_{jk}\delta(t-t')$. So that for our particular case (6.7) is equivalent to [147]:

$$\begin{aligned} i\frac{d\alpha}{dt} &= (-\mu\alpha + U|\alpha|^2\alpha) + \sqrt{iU}\alpha\eta_1(t) \\ i\frac{d\alpha^*}{dt} &= -(-\mu\alpha + U|\alpha|^2\alpha) + \sqrt{-iU}\alpha^*\eta_2(t) \end{aligned} \tag{6.10}$$

Obviously even if initially α and α^* are complex conjugates, they evolve according to independent paths and have independent noise sources ($\eta_1(t)$ and $\eta_2(t)$). So the positive P-representation must be used for the stochastic reformulation of (6.7).

Let us also mention that recently similar stochastic equations describing evolution of interacting bosons were presented in [21, 22], where the authors showed that one can get stochastic evolution not only using the coherent state basis, which is identical to the positive P-representation as described above, but also using the Fock (or number) basis. The main difficulty with this approach is that it heavily relies on quartic interaction between the particles. This interaction does not yield higher than second derivatives in (6.7) allowing the exact stochastic reformulation.

Wigner representation

From the definition (6.2) it is appealing to identify the Glauber P-function with the classical probability. Indeed, as we already discussed the master equation (6.7) reduces to the classical GP equation in the limit, when we can neglect by nonlinear terms. However, it is possible to make a better classical approximation. As it is

obvious from (6.3), the Glauber P-function maps normal-ordered quantum operators into c-numbers, while the general principles of quantum mechanics require that the symmetrized versions of classical operators should be quantized [104].

Let us note that the P-representation can be also obtained as a Fourier transform of the normally ordered characteristic function [160]:

$$P(\alpha) = \frac{1}{\pi^2} \int d^2\eta \, \mathrm{e}^{\alpha\eta^* - \alpha^*\eta} \chi_N(\eta), \tag{6.11}$$

where

$$\chi_N(\eta) = \mathrm{Tr}\left\{\rho \mathrm{e}^{\eta a^\dagger} \mathrm{e}^{-\eta^* a}\right\}. \tag{6.12}$$

Instead we can define the symmetrized version of $\chi_N(\eta)$:

$$\chi(\eta) = \mathrm{Tr}\left\{\rho \mathrm{e}^{\eta a^\dagger - \eta^* a}\right\}, \tag{6.13}$$

and its Fourier transform:

$$W(\alpha) = \frac{1}{\pi^2} \int d^2\eta \, \mathrm{e}^{\alpha\eta^* - \alpha^*\eta} \chi(\eta). \tag{6.14}$$

The latter is nothing but a Wigner function written in the coherent state basis. It is easy to convince oneself that the symmetrized expectation values of operators correspond to the averaging of the classical numbers with the Wigner weight (comp. with (6.3)):

$$\langle \{a^{\dagger m} a^n\}_{sym} \rangle = \int d^2\alpha \, \alpha^{*m} \alpha^n W(\alpha). \tag{6.15}$$

The analogue of (6.4) becomes also symmetric:

$$a\rho \leftrightarrow \left(\alpha + \frac{1}{2}\frac{\partial}{\partial \alpha^*}\right) W(\alpha), \; a^\dagger \rho \leftrightarrow \left(\alpha^* - \frac{1}{2}\frac{\partial}{\partial \alpha}\right) W(\alpha) \tag{6.16}$$

and similarly for the hermitean conjugates. With these rules it is easy to obtain the final master equation describing the time evolution of the Wigner function:

$$i\frac{\partial W}{\partial t} = -\frac{\partial}{\partial \alpha}(-\mu\alpha + U|\alpha|^2\alpha)W + \frac{U}{4}\frac{\partial^3}{\partial^2\alpha\partial\alpha^*}\alpha W - \text{c.c.}. \tag{6.17}$$

The classical limit corresponds to $|\alpha| \gg 1$ because only in this regime it is possible to ignore the fact that the commutator $[a^\dagger, a]$ is not equal to zero. From this prospect it is clear that the nonlinear term in (6.17) is much smaller than that in (6.7). This term is precisely responsible for the deviations of trajectories from classical paths (which are just the characteristics of the linear in derivatives master equation). So if quantum fluctuations are small one can hope that the truncated Fokker-Plank equation for the Wigner function:

$$i\frac{\partial W}{\partial t} \approx -\frac{\partial}{\partial \alpha}(-\mu\alpha + U|\alpha|^2\alpha)W - \text{c.c.} \tag{6.18}$$

is much better than the corresponding version appearing in the P-representation. The main idea of this approximation is to leave quantum fluctuations at the initial time, determining $W(t = 0)$, but ignore their effect completely on the classical equations of motion. We will see in the next section that this can be also justified using the path integral derivation of the dynamics of the system. We note that this is precisely the approximation we used in the previous chapter to derive the "Schrödinger cat" evolution. The main drawback of (6.17) is that it is unknown how to go beyond GP dynamics. Contrary to (6.7) there is no simple stochastic representation of (6.17). On the other hand it is not necessary to make any assumptions about the precise form of the interaction. It is clear that the corrections to the classical trajectories must be perturbative. It turns out that they can be straightforwardly derived using functional integrals (see Sec.6.2).

6.1.2 Keldysh formulation of quantum dynamics

A very powerful approach to non-equilibrium system is based on the diagrammatic technique suggested by Keldysh [81]. The basic idea is that expectation of any

observable can be written as:

$$\langle \Omega(t) \rangle = \mathrm{Tr}\{ \rho(t)\Omega \}, \tag{6.19}$$

where

$$\rho(t) = T_{K\tau} \epsilon^{-i\mathcal{H}t} \rho e^{i\mathcal{H}t} \tag{6.20}$$

is the time-dependent density matrix with $T_{K\tau}$ being a time ordering operator along the Keldysh contour going from 0 to t and returning back to 0. Similarly to standard static problems [1], expression (6.19) can be rewritten in the path integral representation using the coherent state basis [109]. The main difference between static and dynamic cases comes from the fact that instead of one "forward" time evolution in the former, we clearly have to evolve the density operator from the initial time to the final and then come back. Instead, one can use a single time interval but define two operators $a_f(t)$ and $a_b(t)$, which live in the forward and backward contours respectively [76]. We will omit the details of the derivation here, because we essentially repeat all the necessary steps in the next section. We will just note that the final form for the noninteracting part of the action appearing in the Keldysh technique is [76]:

$$S(a_{cl}, a_q) = 2 \int_{t_0}^{t_f} \int_{t_0}^{t_f} dt_1 dt_2 (a^*_{cl}(t_1), a^*_q(t_1)) \begin{pmatrix} 0 & \left[\mathcal{D}^A\right]^{-1} \\ \left[\mathcal{D}^R\right]^{-1} & \left[\tilde{\mathcal{D}}^{-1}\right]^K \end{pmatrix}_{t_1,t_2} \begin{pmatrix} a_{cl}(t_2) \\ a_q(t_2) \end{pmatrix}. \tag{6.21}$$

Here $\mathcal{D}^{\cdots}$ denote noninteracting propagators (see [76] for the details), $a_{cl}(t) = 1/2(a_f(t) + a_b(t))$ and $a_q(t) = 1/2(a_f(t) - a_b(t))$ are the so called classical and quantum combinations. The names "classical" and "quantum" are not accidental since in the classical evolution all trajectories are uniquely defined and the backward path should be exactly identical to the forward one. So $a_q(t) \neq 0$ comes due to quantum fluctuations. We would like to point out that the initial density matrix is encoded in the Keldysh

propagator $\mathcal{D}^K$. The times t_0 and t_f are usually taken to be $-\infty$ and ∞ respectively, while Ω is evaluated at some finite t. This is very convenient for studying steady state properties, where the details of the initial density matrix ρ are completely forgotten, however quite impractical for describing the short time evolution.

The interacting part of the action also differs from the more conventional one. Thus for the quartic interaction it reads:

$$S_{int} = 2U \int_0^t dt_1 a_{cl}^*(t_1) a_q^*(t_1)(a_{cl}^2(t_1) + a_q^2(t_1)) + \text{c.c.}. \tag{6.22}$$

The classical equations of motion can be easily recovered as a saddle point of the action: $\delta S/\delta a_q^* = 0$ and $\delta S/\delta a_{cl}^* = 0$, which indeed results in the following solution: $a_q \equiv 0$ and $a_{cl} = a_{cl}(t)$ is the solution of the GP equations. We would like to point out, that even though GP equations naturally appear in the saddle-point approximation, it is somewhat misleading to identify them with the evolution of the classical field. Indeed, the GP equations make sense only if the initial conditions are specified, however recall that in the Keldysh formulation those are completely absorbed into the quantum propagator. Instead one has to compute the functional integral over *all* possible quantum fields with all possible boundary conditions. To recover the semiclassical limit it is necessary to integrate out quantum fluctuations in the linearized action, which results in [76]:

$$S_{cl}(a_{cl}) = 2 \int\int dt_1 dt_2 a_{cl}^*(t_1)(\mathcal{L}^A[a_{cl}]\mathcal{D}^A)[\mathcal{D}^K]^{-1}\mathcal{D}^R\mathcal{L}^R[a_{cl}])_{t_1,t_2} a_{cl}(t_2). \tag{6.23}$$

where $\mathcal{L}^{R,A}[a_{cl}]$ denote retarded or advanced (complex conjugate) versions of the GP differential operator. The only way to proceed with any calculations using (6.23) is to do a perturbation theory in the interactions, because only in the non-interacting case we can recover a tractable quadratic classical propagator. But this is not what we want. Our goal is to recover in the classical limit the dynamics governed by GP equations for *any* strength of interaction.

We will not go into further details of the Keldysh technique. It is a well developed area with many applications. The discussion above was aiming to point out, that as all diagramatic techniques, the Keldysh formulation is based on the Gaussian action, or equivalently on the smallness of interactions. It is extremely hard to obtain even simple GP dynamics there, because it would involve the summation over all classical vertexes [76], which is virtually impossible.

6.2 Quantum corrections to classical dynamics

This section is the key part for the this and preceding two chapters. Here we will develop a perturbative approach to the semiclassical evolution. We are not making any underlying assumptions on the classical equations of motion themselves: they can be either stable or unstable, can contain interactions with arbitrary space and time dependence, etc. The main result of this work is that the quantum corrections manifest themselves in two ways: (i) we find the the truncated Wigner approximation naturally arises in the path integral formulation of the problem, i.e. the short-time dynamics is asymptotically described by the classical equations of motion with the initial conditions distributed according to the Wigner transform of the initial density matrix; the classical observable is the symmetrized version of the quantum operator with fields substituted by c-numbers (see also discussion preceding (5.24)), (ii) there are quantum scattering processes, which are represented as a nonlinear response of the observable to the infinitesimal transform of the field along its classical trajectory. For many situations it is sufficient to ignore quantum scattering completely, considering only the evolution along multiple classical paths. We would like to emphasize that any harmonic action (in particular Bogoliubov's approximation) is completely described by the truncated Wigner approximation, i.e. by classical dynamics with

appropriate initial conditions. Moreover to recover Bogoliubov's approximation it is sufficient to linearize classical GP equations around the stationary solution. As we saw in the previous chapter this linearization is not adequate for problems with unstable dynamics. Quantum scattering actually modifies the semiclassical trajectories themselves. But this modification is conceptually simple. In the first approximation there is only one scattering event (although distributed over the whole time of evolution), i.e., one has to add a small perturbation only once (for a local in time interaction) during the classical evolution and calculate the (nonlinear) response of the observable at the end of the classical evolution. In the second order of perturbation theory there are two scattering events, etc. The whole picture thus resembles the perturbative approach to the ordinary scattering problem in the Feynman path integral representation. Although in this chapter we mostly concentrate on the problem of interacting bosons, the results are very general. They are applicable to any type of evolution, where the classical equations of motion arise as the saddle point of the action. Let us also note that the classical evolution with distributed initial conditions is equivalent to taking into account *all* classical vortices in the conventional Keldysh technique [76]. Each quantum scattering event is equivalent to adding a quantum vortex. The perturbative approach we develop here should be recovered also in the Fokker-Planck master equation for the Wigner function (6.17). However, to obtain nonlinear response of the observable, one must consider corrections to the distribution function in terms of functional derivatives with respect to the fields, so that the response is recovered upon integrating by parts the product of the distribution function and the observable. While this must be certainly possible to do, we will see that the functional integral derivation gives a very simple and elegant way of deriving the desired equations. Finally we would like to point out that similar ideas were recently developed by Filinov *et all* in the context of interacting fermions [43, 44, 45].

Let us assume that the system is described by some Hamiltonian: $\mathcal{H}(a_j^\dagger, a_j, t)$, which in general depends on time and is expressed as a polynomial in boson operators $a^\dagger$ and a. It does not matter whether a is continuous in space or a discrete field sitting on a lattice. We also assume that the initial state of the system is given by a density matrix ρ_0:

$$\rho_0 = \sum_\chi P(\chi)\,|\chi\rangle\langle\chi|, \tag{6.24}$$

where $|\chi\rangle$ represents some basis and $P(\chi)$ is the probability to be in a particular state (this P should not be confused with the Glauber P-function, because the basis we use here is quite arbitrary). If the initial state is pure, the sum contains only one term. While the precise form of $\mathcal{H}$ is not important, we will keep in mind the boson-Hubbard model for the specific illustrations. Then the classical limit is obtained as the number of bosons per site N tends to infinity. So we will develop an expansion in terms of $1/N$. The time dependent average of any operator is given according to the standard quantum mechanical formulas:

$$\Omega(t) = \sum_\chi P(\chi)\,\langle\chi|\mathrm{T}_{K\tau} e^{i\int_0^t \mathcal{H}(\tau)d\tau}\Omega \mathrm{e}^{-i\int_0^t \mathcal{H}(\tau)d\tau}|\chi\rangle \tag{6.25}$$

Note that contrary to (6.19) we ascribe dynamics to the operator Ω rather then to the density matrix ρ. In the coherent state basis (6.25) reads:

$$\Omega(t) = \int Da_f Da_b\,\langle a_{b0}|\rho_0|a_{f0}\rangle\,\mathrm{e}^{-a^*_{f0}a_{f0}+a^*_{f0}a_{f1}+i\mathcal{H}(a_{f0},a^*_{f1})\Delta\tau}\ldots\mathrm{e}^{-a^*_{fQ}a_{fQ}}$$
$$\Omega(a^*_{fQ}, a_{bQ}, t)\mathrm{e}^{a^*_{fQ}a_{bQ}}\mathrm{e}^{-a^*_{bQ}a_{bQ}+a^*_{bQ}a_{bQ-1}-i\mathcal{H}(a_{bQ},a^*_{bQ-1})\Delta\tau}\ldots\mathrm{e}^{-a^*_{b0}a_{b0}}, \tag{6.26}$$

where $\Delta\tau = t/Q$ and $Q \to \infty$. Here $\mathcal{H}(a_{f,b}, a^*_{f,b}, \tau)$ is the normal ordered hamiltonian $\mathcal{H}$ with operators a and $a^\dagger$ substituted by complex numbers $a_{f,b}$ and $a^*_{f,b}$ respectively. The expression above is intentionally written in the discrete form, since we want to take special care of the boundary effects. Instead of the fields a_f and a_b propagating forward and backward in time, it is convenient to introduce their classical (ψ) and

quantum (η) combinations: $a_f = \psi + \eta/2$, $a_b = \psi - \eta/2$. Note that the definitions of ψ and η are slightly different from those of a_{cl} and a_q used in [76] (see also the text after 6.21). But the key thing that the in the classical limit $\eta(\tau) = 0$ and $\psi(\tau)$ coincides with the classical field is unaffected by the particular choice. After taking the limit $\Delta\tau \to 0$ in (6.26) we derive:

$$\langle\Omega(t)\rangle \approx \int D\eta(\tau)D\psi(\tau)\,\langle\psi_0 - \frac{\eta_0}{2}|\rho|\psi_0 + \frac{\eta_0}{2}\rangle\,\Omega(\psi(t)^* + \frac{\eta(t)^*}{2}, \psi(t) - \frac{\eta(t)}{2})$$
$$\mathrm{e}^{-|\psi_0|^2 - \frac{1}{4}|\eta_0|^2 - \frac{1}{2}|\eta(t)|^2}\mathrm{e}^{\frac{1}{2}(\eta_0^*\psi_0 - \eta_0\psi_0^*)}\mathrm{e}^{\int_0^t d\tau\,\eta^*(\tau)\mathcal{L}[\psi,\psi^*,\tau] - \eta(\tau)\mathcal{L}^*[\psi,\psi^*,\tau]}$$
$$\exp\left(i\int_0^t d\tau \sum_{n\geq 1}\sum_{m=0}^{2n+1} \frac{\partial^{2n+1}\mathcal{H}(\psi,\psi^*,\tau)}{\partial\psi^m\psi^{*2n+1-m}} \frac{\eta^m\eta^{*2n+1-m}}{2^{2n}m!(2n+1-m)!}\right), \qquad (6.27)$$

where $\mathcal{L}(\psi,\psi^*,\tau)$ stands for the classical (GP) differential operator acting on the field $\psi(t)$:

$$\mathcal{L}_j[\psi,\psi^*,\tau] \equiv \frac{d\psi_j}{d\tau} + i\frac{\delta\mathcal{H}(\psi(\tau),\psi^*(\tau))}{\delta\psi_j(\tau)}. \qquad (6.28)$$

Note again that the operator $\mathcal{L}$ as well as fields ψ and η contain spatial indices which we suppressed in (6.27) to simplify notations. Equating (6.28) to zero gives the classical equations of motion. In particular, if $\mathcal{H}$ is given by the normal ordered version of (4.1) with a_j and $a_j^\dagger$ substituted by ψ_j and ψ_j^* respectively, then the equation $\mathcal{L}_j[\psi,\psi^*,\tau] = 0$ is equivalent to the Gross-Pitaevskii equation (4.36). Let us explain now in some detail how we arrive from (6.26) to (6.27). There are several different contributions to the exponent in (6.26), which we call S. The first one comes from the terms, which do not involve hamiltonian $\mathcal{H}$:

$$\begin{aligned} S_1 &= \sum_{q=1}^{Q-1}(a_{fq}^*(a_{fq+1} - a_{fq}) - a_{bq}^*(a_{bq} - a_{bq-1})) + a_{f0}^*a_{f1} - a_{f0}^*a_{f0} \\ &- a_{fQ}^*a_{fQ} - a_{bQ}^*a_{bQ} + a_{bQ}^*a_{bQ-1} - a_{b0}^*a_{b0} + a_{fQ}^*a_{bQ}. \end{aligned} \qquad (6.29)$$

Here q denotes the discrete time, while the spatial indices are suppressed. The first sum in the continuum limit transforms to the integral:

$$\sum_{q=1}^{Q-1} a_{fq}^*(a_{fq+1} - a_{fq}) - a_{bq}^*(a_{bq} - a_{bq-1}) \to \int_0^t d\tau\left(a_f^*(\tau)\frac{\partial a_f(\tau)}{\partial\tau} - a_b^*(\tau)\frac{\partial a_b(\tau)}{\partial\tau}\right), \qquad (6.30)$$

which under substitutions $a_f \to \psi + \eta/2$, $a_b \to \psi - \eta/2$ and integrating by parts becomes:

$$\int_0^t d\tau \left(\eta^\star(\tau) \frac{\partial \psi(\tau)}{\partial \tau} - \eta(\tau) \frac{\partial \psi^\star(\tau)}{\partial \tau} \right) + \psi^\star(t)\eta(t) - \psi_0^\star \eta_0. \tag{6.31}$$

The boundary term in (6.29) in the continuum limit becomes:

$$a_{fQ}^\star(a_{bQ} - a_{fQ}) - a_{b0}^\star a_{b0} = -|\psi_0|^2 - \frac{|\eta_0|^2}{4} + \frac{1}{2}(\psi_0^\star \eta_0 + \eta_0^\star \psi_0) - \psi^\star(t)\eta(t) - \frac{|\eta(t)|^2}{2}. \tag{6.32}$$

Combining all these terms we derive:

$$S_1 = \int_0^t d\tau \left(\eta^\star(\tau) \frac{\partial \psi(\tau)}{\partial \tau} - \eta(\tau) \frac{\partial \psi^\star(\tau)}{\partial \tau} \right) - |\psi_0|^2 - \frac{|\eta_0|^2}{4} - \frac{|\eta(t)|^2}{2} + \frac{1}{2}(\eta_0^\star \psi_0 - \psi_0^\star \eta_0). \tag{6.33}$$

The second contribution to the exponent of (6.26) comes from the terms containing hamiltonian. However, since all of them are proportional to $\Delta\tau$ the continuum limit becomes trivial and does not give any additional boundary terms:

$$S_2 = \int_0^t d\tau (\mathcal{H}(a_f(\tau), a_f^\star(\tau), \tau) - \mathcal{H}(a_b(\tau), a_b^\star(\tau), \tau)) = \int_0^t d\tau$$
$$\left(\mathcal{H}(\psi(\tau) + \frac{\eta(\tau)}{2}, \psi^\star(\tau) + \frac{\eta^\star(\tau)}{2}, \tau) - \mathcal{H}(\psi(\tau) - \frac{\eta(\tau)}{2}, \psi^\star(\tau) - \frac{\eta^\star(\tau)}{2}, \tau) \right). \tag{6.34}$$

Finally, the last step in our derivation is the expansion of the expression above in powers of η:

$$\mathcal{H}(\psi + \frac{\eta}{2}, \psi^\star + \frac{\eta^\star}{2}, \tau) - \mathcal{H}(\psi - \frac{\eta}{2}, \psi^\star - \frac{\eta^\star}{2}, \tau) = \frac{\partial \mathcal{H}(\psi, \psi^\star)}{\partial \psi} \eta + \frac{\partial \mathcal{H}(\psi, \psi^\star)}{\partial \psi^\star} \eta^\star$$
$$+ \sum_{n \geq 1} \sum_{m=0}^{2n+1} \frac{\partial^{2n+1} \mathcal{H}(\psi, \psi^\star, \tau)}{\partial \psi^m \psi^{\star\, 2n+1-m}} \frac{\eta^m \eta^{\star\, 2n+1-m}}{2^{2n} m!(2n+1-m)!}. \tag{6.35}$$

We purposely separated the terms linear in η and $\eta^\star$ because they enter classical equations of motion and the higher powers contribute quantum corrections. Combining (6.29), (6.34), and (6.35) we indeed recover (6.27).

Let us discuss how quantum fluctuations enter the classical dynamics. From equation (6.27) we see there are three different contributions. The first one comes from

integrating out $\eta(t)$ and results only in the modification of the observable operator:

$$\Omega_{cl} = \langle \Omega\,(\psi^\star + \eta^\star/2, \psi - \eta/2)\rangle. \tag{6.36}$$

Here the average is taken over η with the measure $\exp(-|\eta|^2/2)$. Note that the original operator Ω must be written in the normal ordered form. It is easy to check that integrating out fluctuations according to (6.36) is equivalent to rewriting Ω in the symmetrized form and substituting a and $a^\dagger$ by ψ and $\psi^\star$ as we discuss in the text above and below (5.27). The second contribution originates from the field η_0 corresponding to the initial time. Because of the coupling to ψ_0, this fluctuation introduces a probability distribution for the classical initial conditions:

$$p(\psi_0, \psi_0^\star) = \int d\eta_0^* d\eta_0 \langle \psi_0 - \frac{\eta_0}{2}|\rho|\psi_0 + \frac{\eta_0}{2}\rangle \mathrm{e}^{-|\psi_0|^2 - \frac{1}{4}|\eta_0|^2}\, \mathrm{e}^{\frac{1}{2}(\eta_0^*\psi_0 - \eta_0\psi_0^*)}, \tag{6.37}$$

Note that $p(\psi_0, \psi_0^\star)$ is nothing but a Wigner transform of the density matrix in the coherent state representation [53, 160] and therefore it is not a positively defined quantity. Sometimes $p(\psi_0, \psi_0^\star)$ has a weird nonlocal behavior and the semiclassical limit is achieved in a somewhat nonintuitive way [53], see also the discussion given in the previous chapter. If we ignore corrections to the classical equations of motion coming from higher powers of the quantum field η, then the time dependence of the observable Ω will be given simply by (5.23), which because of its importance we write down again:

$$\Omega(t) = \int d\psi_0^* d\psi_0 p(\psi_0, \psi_0^\star) \Omega_{cl}(t, \psi_0, \psi_0^\star), \tag{6.38}$$

where $\Omega_{cl}(t, \psi_0, \psi_0^\star)$ is evaluated on the classical field which is subject to a given initial condition $\psi(0) = \psi_0$. This expression constitutes so called truncated Wigner approximation frequently used in quantum optics [160].

The third most complicated contribution of quantum fluctuations comes from the last multiplier in (6.27) and represents quantum scattering processes. Clearly this

term is nonzero only if there is an interaction between the bosons, i.e. $\mathcal{H}$ contains terms of the order of three or higher in the boson fields a and $a^\dagger$. For simplicity, let us restrict the following analysis only on the case of a two particle short range interaction. After the construction is clear, the generalization on other cases becomes trivial. Then

$$\mathcal{H}_{int} = \frac{U(t)}{2} \sum_j a_j^\dagger a_j (a_j^\dagger a_j - 1) \tag{6.39}$$

with j being a discrete or continuous coordinate. The quantum scattering part of the action reads:

$$S_q = \int_0^t d\tau \frac{U(\tau)}{4} \left(\psi^\star(\tau)\eta(\tau) + \psi(\tau)\eta^\star(\tau)\right) |\eta(\tau)|^2. \tag{6.40}$$

Because S_q contains third (or higher) power of the quantum field η we can treat it perturbatively so that:

$$\begin{aligned}\Omega(t) = \int d\psi_0^\star d\psi_0 p(\psi_0, \psi_0^\star) \Bigg[1 - i \sum_j \int_0^t d\tau \frac{U(\tau)}{4} \left(\psi_j^\star(\tau) \frac{\partial^3}{\partial^2 f_j^\star(\tau) \partial f_j(\tau)} - \text{c.c.} \right) \\ + \frac{(-i)^2}{2} \sum_{j,k} \int_0^t \int_0^t d\tau d\tau' \frac{U(\tau)U(\tau')}{16} \left(\psi_j^\star(\tau) \frac{\partial^3}{\partial^2 f_j^\star(\tau) \partial f_j(\tau)} - \text{c.c.} \right) \\ \times \left(\psi_k^\star(\tau') \frac{\partial^3}{\partial^2 f_k^\star(\tau') \partial f_k(\tau')} - \text{c.c.} \right) + \ldots \Bigg] \Omega_{cl}(f, f^\star, t)\Big|_{f \equiv 0},\end{aligned} \tag{6.41}$$

where $f_j(\tau)$ is the infinitesimal perturbation applied to the classical trajectory ψ_j at time τ:

$$\psi_j(\tau) \to \psi_j(\tau) + f_j(\tau), \; \psi_j^\star(\tau) \to \psi_j^\star(\tau) + f_j^\star(\tau). \tag{6.42}$$

Let us briefly describe how we arrive to this representation. Expanding (6.27) in powers of η gives the following integrals:

$$\int d\eta_\tau^* \eta_\tau^{*m} e^{\eta_\tau^* (\psi(\tau+\delta\tau) - \psi(\tau) + iH(\psi^*(\tau), \psi(\tau), \tau))}, \tag{6.43}$$

where H is the classical Hamiltonian of the nonlinear Schrödinger (or GP) equation, not to be confused with $\mathcal{H}$. Next we use the change of variables:

$$\psi(\tau_q) = \psi(\tau_{q-1}) - iH(\psi(\tau_{q-1}), \tau_{q-1}) + f(\tau_q) = \psi_{cl}(\tau_q) + f(\tau_q) \tag{6.44}$$

and a simple identity:

$$\int x^m e^{i\alpha x} dx = -2\pi i^m \delta^{(m)}(\alpha). \tag{6.45}$$

Note that the transform from $\psi(\tau_q)$ to $f(\tau_q)$ is linear and gives no Jacobian for *any* interaction. The exactly same idea can be used to integrate out η_τ. From the structure of (6.41) it is obvious that each term in the expansion gives an extra prefactor of $1/N$, which is the classical parameter for the boson Hubbard model. So the first quantum correction to the trajectory appears as a nonlinear response to the displacement of the classical field at an arbitrary moment of time (and space) integrated over time (space). The classical equations of motion themselves need not be linear. It is trivial to generalize (6.41) for the interaction nonlocal in space or time. The only difference is that the field ψ and its derivatives over f and f^* would carry different spatial or time indices. The variables f and f^* in (6.41) are treated independently. In numerical evaluations it is more convenient to use:

$$\frac{\partial}{\partial f} = \frac{1}{2}\frac{\partial}{\partial \Re f} - \frac{i}{2}\frac{\partial}{\partial \Im f}, \quad \frac{\partial}{\partial f^*} = \frac{1}{2}\frac{\partial}{\partial \Re f} + \frac{i}{2}\frac{\partial}{\partial \Im f}. \tag{6.46}$$

Then (6.41) becomes:

$$\Omega(t) = \int d\psi_0^* d\psi_0 p(\psi_0, \psi_0^*) \left[1 - \frac{1}{16}\sum_j \int_0^t d\tau U(\tau) \left(\frac{\partial^2}{\partial \Re f_j^2(\tau)} + \frac{\partial^2}{\partial \Im f_j^2(\tau)}\right)\right.$$
$$\left. \times \left(\Im\psi_j(\tau)\frac{\partial}{\partial \Re f_j(\tau)} - \Re\psi_j(\tau)\frac{\partial}{\partial \Im f_j(\tau)}\right) + \ldots\right] \Omega_{cl}(f, f^*, t)\Big|_{f\equiv 0}. \tag{6.47}$$

We would like to make a few comments about equations (6.41) and (6.47). In our specific example we used the number of bosons per well N as a dimensionless semi-classical parameter. Clearly each term in the expansion in those equations brings an extra factor of $1/N$. The absence of $\hbar$ anywhere, may be confusing since the classical limit certainly corresponds to $\hbar \to 0$. However, this should not be surprising since here and quite often in the atomic physics the Planck's constant is either completely absorbed into energies, which are measured in Hz, or into time. In conventional

units $\hbar^{-1}$ appears as a prefactor in the action justifying the saddle-point or the classical approximation. In the same way the number of bosons per site N appears as a prefactor in the exponent of (6.27) after rescaling $\psi \to \sqrt{N}\psi$ and $\eta \to \sqrt{N}\eta$. So in general any expansion in powers of η is in fact the expansion in powers of $\hbar$. The other important remark is that at small times the deviation from the classical dynamics due to the quantum scattering behaves as $O(f(t)/N)$, where $f(t)$ is some function of time, which vanishes at $t \to 0$. This proves that the truncated Wigner approximation, where the quantum scattering is completely ignored gives the *exact* short-time asymptotical behavior of the full quantum dynamics. This very remarkable result is to be contrasted with those obtained within the Keldysh technique, where the short time scales are usually unaccessible.

To illustrate the current approach let us consider a couple of exactly solvable examples. Suppose there are two condensates with a unit tunneling amplitude and a modulated in time strength of interaction (see eq. (5.30)): $U(t) = N^{-1}\sin(2t)$ (or equivalently $\lambda(t) = \sin(2t)$) and $U(t) = -N^{-1}\sin^2(t)$ ($\lambda(t) = -\sin^2(t)$). The factor of $1/N$ is inserted to get a unique classical limit at $N \to \infty$ (see chapter 4). Let us also assume that the bosons are initially in the noninteracting ground (i.e. symmetric) state. In the simple GP picture nothing is going to happen with time in both cases, because classically the initial state is the ground state for any strength of interaction. However, quantum mechanically this is not true, so we expect that the system will evolve in time exciting some bosons into the higher energy levels. Note that although $U(t)$ becomes negative for certain periods of time, the semiclassical symmetric state is always stable. The instability appears only for a stronger interaction $\lambda < -1$ (see chapter 5). Thus the examples mimic the evaporation, or loss of atoms from the condensate to the higher excited states. In the first one we have a kind of parametric resonance with no average interaction, while in the second example we

also introduce a mean attractive U. As an observable we will use the number variance defined in (5.31). We omit the details of the calculation here since they are identical to those performed in Sec. 5.2. The resulting evolution for the case of eight bosons per site is plotted in figures 6.1 and 6.2.

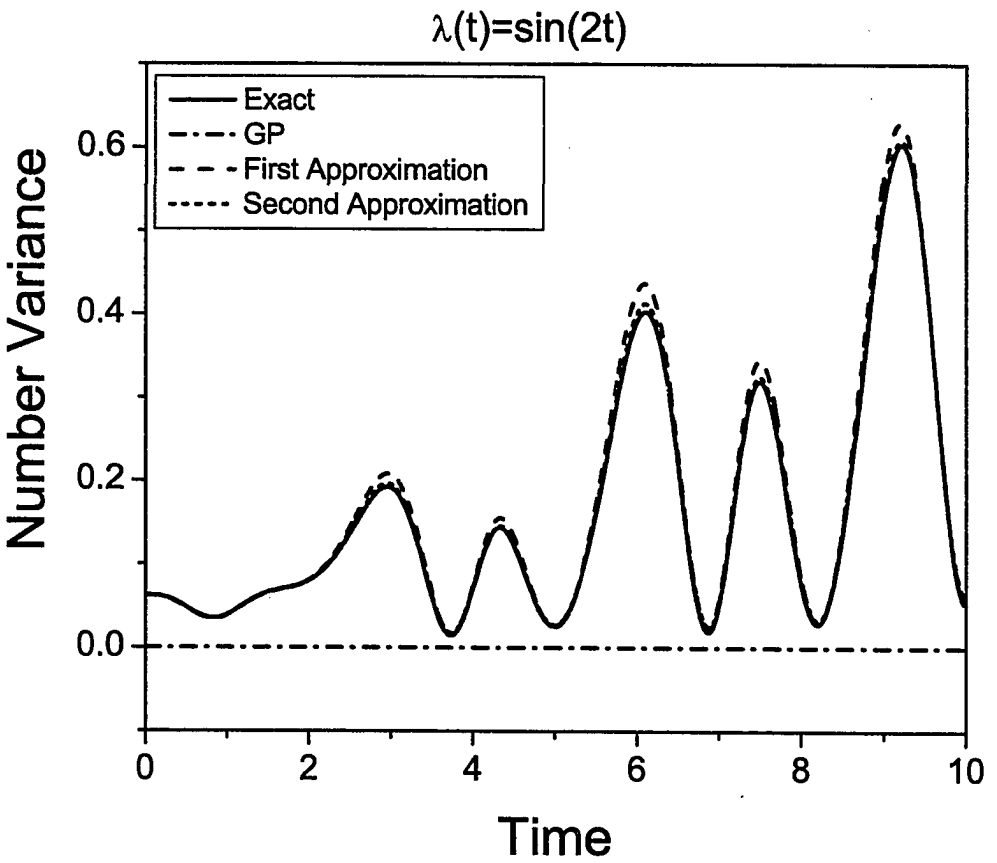

Figure 6.1: Number variance as a function of time for the case of eight bosons per site. The GP result gives identically zero. The first approximation includes only fluctuations at the boundaries of the time domain as described in the text and is equivalent to TWA. The second approximation includes also a single quantum scattering event. It is hard to distinguish by eye the difference between the exact result and the first approximation in the graph.

Clearly the GP approximation is completely wrong for both examples. However, a purely classical dynamics with the appropriate (Wigner) distribution of initial

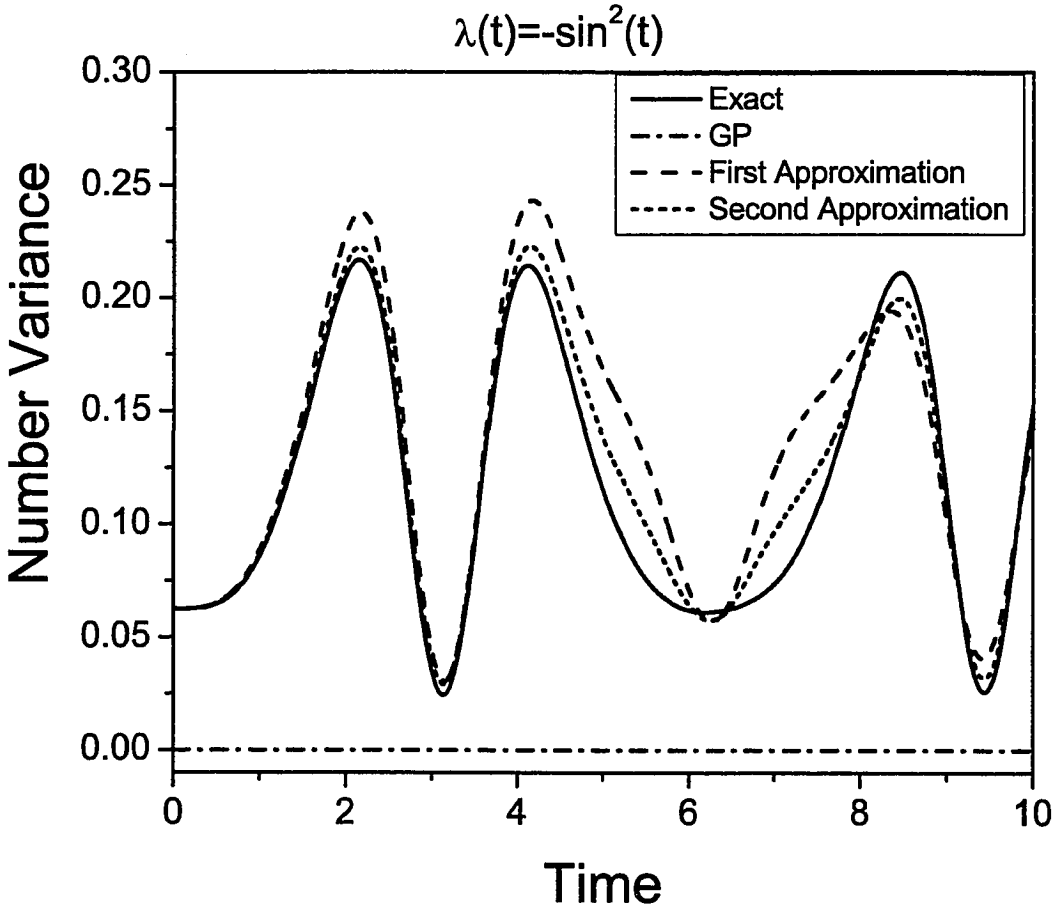

Figure 6.2: Same as in figure 6.1, but for a different dependence of the interaction on time.

conditions gives a very good result for the first example and a reasonable one for the second. Since the number variance is not small in both cases, the Bogoliubov's approximation is not justified. If we include one quantum scattering event then the agreement with the exact result becomes remarkably better showing that the perturbative scheme presented here indeed works.

Let us now summarize and discuss the derived results. We developed a perturbation theory to the classical equations of motion. We found the two types of corrections. The first one (which is equivalent to the truncated Wigner approximation)

does not affect the evolution equations themselves but requires to take an average over the ensemble of trajectories with the initial conditions distributed according to the Wigner transform of the initial density matrix. The observable is the classical counterpart of the symmetrized quantum operator. The second type of corrections are quantum scattering processes, which manifest themselves as a nonlinear response to the infinitesimal change of the fields along their classical evolution (see (6.41)). We would like to point out again that the widely used Bogoliubov's approximation, or more generally any expansion of the action up to second order in fields is entirely contained in the TWA. Moreover, as we saw in the previous chapter, the truncated Wigner approximation is more powerful then the Bogoliubov's description of the dynamics.

Although we never discussed here the coupling to the thermal bath (or more generally to the external noise), it is very easy and straightforward to incorporate this into our picture. For example, in the simple representation of the bath as a set of harmonic oscillators, one obtains a dissipative term, which can be directly added to the GP equations and a quadratic term in the quantum fields, which is equivalent to a random force with a Gaussian distribution [19]. In general, there will be other terms in the action as well, but all of them can be treated perturbatively in the same way as we explained irrespective of their origin. So they will result in some kinds of nonlinear responses to the classical, now stochastic, evolution. Note also, that the effects of dissipation or random forces will wash out all the quantum scattering processes which occur a long time (longer then the relaxation time) prior to the observation. Clearly the response to an infinitesimal perturbation will decay with time if we have such processes. So the theory can be easily extended to describe the evolution to steady states. One have to be cautious though in the low temperature limit, because generically all the relaxation processes are frozen out and the time

scale for the scattering leading to equilibrium goes to infinity. This implies that as $T \to 0$ more and more quantum scattering events have to be considered to correctly describe the equilibrium. So this theory would give some kind of high temperature expansion. If one is interested in non-equilibrium dynamics, then the limit of the applicability of the perturbative expansion of the given order will be set either by the time of evolution or by the scattering time in a bath, whatever is shorter. Certainly further careful analysis of this approach for the systems interacting with the bath is required and it is a subject of the future work.

Finally let us spend a few words on the numerical implementation of the calculations. The solution of the classical equations themselves is very straightforward. The averaging over the initial conditions can be easily done with Monte-Carlo methods and the convergence time either slowly increases with the size of the system or saturates depending on the particular problem. But in any case it does not grow exponentially in size as would be the case for the full quantum solution. The quantum scattering part requires evaluating nonlinear response, which might be tricky for a nonlinear system of differential equations, but this part is also straightforward and well controlled numerically. We would like to point out that contrary to exact stochastic schemes, this method starts directly from the classical equations of motion, which may be very complicated themselves and shows how to add quantum corrections step by step. So it certainly must be very efficient if the quantum fluctuations are relatively weak. Thus the description of the unstable "cat" dynamics considered in the previous chapter, which is very straightforward in the present scheme can be hardly efficiently achieved using stochastic equations. We believe this method is a competing alternative both to the schemes based on the conventional diagrammatic technique, which is not very suitable for strongly interacting systems, and to the stochastic methods, which can usually deal with a limited number if degrees of

freedom.

Chapter 7

Summary and future extensions

This work consists of two major parts focusing on scattering of quasiparticles in cuprate superconductors and on the properties of the dynamics of the interacting boson system. Despite apparent distinctions they are not completely disconnected. It is widely accepted that the underlying model describing HTSc superconductors is precisely the Hubbard model, only with fermions instead of bosons. Currently interacting atoms with Fermi statistics are actively studied both theoretically [66, 106] and experimentally [34, 60, 139, 152]. Because fermions with small repulsive or attractive interactions can condense to produce BCS-like or conventional boson superfluids [106], there are many similarities between the behavior of Fermi and Bose systems at low temperatures. Dynamics of interacting fermion systems is certainly an interesting extension of the present work. Now it looks that both theoretical and experimental research on ultra cold fermions in optical lattices is the way to resolve the paradigm that the superconductivity in cuprates arises from the doping of a half-filled Mott insulator described by the fermion Hubbard model in two dimensions. Another connection between high-temperature superconductors and interacting Bose system emerges in the description of magnetic vortices in terms of the boson Hubbard

model [93, 110]. The vortices can either form traditional Abrikosov's lattices or be placed into artificial periodic arrays of columnar pins [18]. In the latter case their hopping from one pin two another is exactly mapped to the imaginary time dynamics of the boson Hubbard model [93] with possibly non-hermitean hopping. If both vortex and quasiparticle degrees of freedom are taken into account, then the problem becomes particularly interesting.

In the context of the present work we addressed rather specific issues which were related to particular experiments. Thus we showed that the Kondo effect in cuprates can give a consistent explanation of the experimentally observed oscillations of the electron density of states [114]. We also showed that the observed period four modulation of the density of states near vortices or isolated defects [64, 65] can be directly related to the dynamic period eight spin-density waves and suggested some tests which would either confirm or contradict to this proposal. The study of the dynamics of interacting bosons was also motivated by the experiments [154]. We gave an explanation of the restoration of the coherence after the bosons were suddenly allowed to tunnel between different sites. However, the work motivated by those experiments have risen interesting theoretical issues. Thus we developed a mean-field theory of the Kondo effect in the systems with vanishing density of states and showed that the large N calculations give a picture consistent with sophisticated numerical renormalization group studies even for the spin one half, where $N = 2$. But because of its simplicity, the mean field approach allowed us to solve the problem with non-local spin-spin coupling and realistic band-structure. Such calculations are either not accessible or extremely involved for the exact computational methods. The study of the dynamics of interacting bosons revealed other problems of the applicability of the classical GP equations. From comparison with exactly solvable model we found out that the time scale becomes a very important issue of the validity of the classical

equations of motion. This lead us to further investigation of the effect of quantum fluctuations on time evolution. We showed that the natural extension of the classical dynamics requires averaging of the observable over multiple classical trajectories with initial conditions distributed according to the Wigner transform of the initial density matrix. This approach gives asymptotically exact behavior of the observable at small times but eventually breaks down. The time scale when it happens depends on the details of the evolution and is shorter if many quantum states are excited, which is the case for a sudden perturbation. The further corrections appear as quantum scattering events in the same spirit as in the conventional scattering problem of free particles. These corrections modify trajectories, which are no longer classical.

The natural extension of the work on the time evolution would be to include bath degrees of freedom. The issues of relaxation and decoherence are of the primary importance in real systems. They are ultimately responsible for bringing the system into the thermal equilibrium. A very successful approach to attack this problem is to represent the bath as a continuum of harmonic oscillators linearly coupled to the system and then integrate them out [19]. Such procedure introduces a dissipative term and fluctuating forces into the classical equations of motion. The main current theoretical difficulty with the emerging Langevin equations is that they directly applicable only to the noninteracting system of harmonic oscillators. If there are intrinsic interactions then one has to face a problem of adding internal quantum fluctuations as we saw in the Chapter 6. As long as this point is understood it becomes straightforward to reformulate dynamics for the open interacting systems. It would be certainly an important extension of the current work. While the exact picture is still to appear, it is intuitively clear that the quantum scattering events will be important if the time scale associated with them (which is essentially independent of temperature) becomes larger then either the time of observation or the relaxation

time due to the thermal bath. So the classical picture should be generically valid either for finite time or at sufficiently high temperatures. It would be very important to quantify these vague ideas. Ultimately the competition between quantum and classical scattering processes is responsible for the decoherence of the quantum states. Understanding the details of the loss of coherence at finite time scales is a primary task for the field of quantum computing.

Non-equilibrium dynamics near the classical limit suggests other natural extensions whenever the mean field solution adequately describes static properties. For example the formation of the Kondo screening, behavior of the superconducting gap under a sudden perturbation, dynamics of Josephson junctions, etc. belong to this class of problems. While the standard approach relies on dynamical self-consistent equations of a specific order parameter, it is usually very hard to justify this approximation and to go beyond. The method developed here seems to be particularly suitable to attack these problems. Another challenging task would be extrapolation of the nonequilibrium dynamics to the imaginary time evolution, or to equilibrium problems, where quantum effects are relatively weak. One straightforward way to access at least the ground state of the interacting system is to adiabatically evolve a ground state of an exactly solvable model, e.g. noninteracting limit, to the desired regime of parameters using the approach developed here.

We mentioned only several possible future directions, while there are certainly more of them. I would be extremely happy if the results presented here will have further applications and will help to attack even few of problems which condensed matter and atomic community are currently facing.

Appendix A

Mean field ground state of the boson lattice system in a harmonic potential

The problem of the Mott insulator transitions for infinite arrays of bosons have been extensively studied during the last decade, see for example [46, 52, 131]. It was shown [131] that the mean filed calculation qualitatively captures the two possible phases and gives a good estimate for the phase boundary. Recently, using quantum Monte-Carlo methods, an exact ground state for the system of bosons in a parabolic potential was found [13]. It was shown that near the expected transition, the global compressibility does not vanish due to the spatial inhomogeneity. However, still the bosons form local insulating domains separated by narrow superfluid regions. The Monte Carlo approach, though very powerful, is incapable to solving the problem with many bosons per well. Therefore we think that for qualitative understanding of the ground state as a function of the interaction strength, it is worthwhile to do a mean field calculation.

The details of the derivation of the mean field equations can be found in Ref. [131]. Here we will only outline the principal steps.

The mean field Hamiltonian obtained from (4.1) is

$$\mathcal{H}_{mf} = -\sum_j J(b_j a_j^\dagger + b_j^* a_j) + (V_j - \mu) a_j^\dagger a_j + \frac{U}{2} a_j^\dagger a_j (a_j^\dagger a_j - 1), \qquad \text{(A.1)}$$

where μ is the chemical potential. The variational free energy is that of $\mathcal{H}_{mf}$ plus additional contributions which depend upon the complex variational parameters b_j [131]. Minimizing this free energy, yields the optimum values of b_j:

$$b_j = \frac{\langle a_{j+1} + a_{j-1} \rangle}{2}, \qquad \text{(A.2)}$$

where the average is taken over the density matrix (or the ground state in the zero temperature limit) of (A.1). We also define the order parameter

$$\rho = \sum_j b_j^* b_j. \qquad \text{(A.3)}$$

The self consistent evaluation of the superfluid mean field b_j is straightforward, and the resulting order parameter is plotted in fig A.1 for $T = 0$. The graph (a) corresponds to few bosons per lattice site. If the interaction (U) is strong enough, then the order parameter forms a domain structure similar to that predicted in [13]. For a large number of bosons per well, the quantum fluctuations start playing a role when the ratio of the interaction U and the hopping J becomes of the order of the number of bosons in the central well ($N \approx \mu/U$), and the smooth GP shape of boson density (ρ) breaks down. For very strong interactions, the actual profile of ρ becomes sensitive to small variations of the mean density of bosons per central well (see figure A.1).

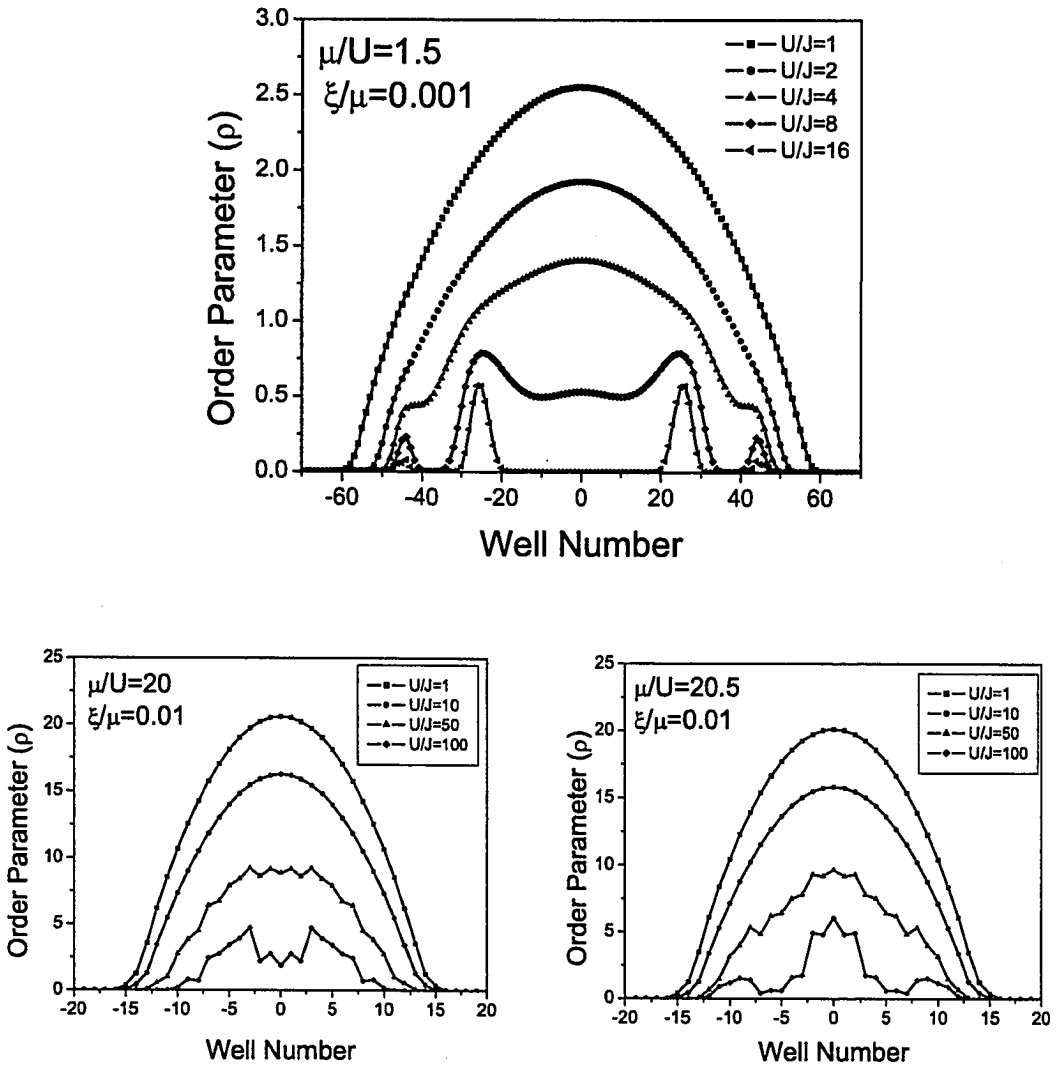

Figure A.1: Mean field order parameter for different interactions in a parabolic potential ($V_j = \xi j^2/2$) at $T = 0$. Graph (a) corresponds to few bosons per site and the other two graphs to many bosons.

Bibliography

[1] A.A. Abrikosov, L.P. Gorkov, and I.E. Dzyaloshinski, *Methods of quantum field theory in statistical physics*, Englewood Cliffs, New Jersey (1963).

[2] E. Altman and A. Auerbach, Phys. Rev. B **65**, 104508 (2002).

[3] E. Altman and A. Auerbach, Phys. Rev. Lett. **89**, 250404 (2002).

[4] L. Amico and V. Penna, Phys. Rev. B **62**, 1224 (2000).

[5] M.H. Anderson, J.R. Ensher, M.R. Matthews, C.E. Wieman, and E.A. Cornell, Science **269**, 198 (1995).

[6] P.W. Anderson, Phsyica Scripta **T102**, 10 (2002).

[7] P.W. Anderson, J. Phys. C **3**, 2436 (1970).

[8] P.W. Anderson, Science, **235**, 1196 (1987).

[9] J.R. Anglin and A. Vardi, Phys. Rev. A **64**, 013605 (2001).

[10] D.P. Arovas, A.J. Berlinsky, C. Kallin, and S.-C. Zhang, Phys. Rev. Lett. **79**, 2871 (1997);

[11] W.A. Atkinson, P.J. Hirschfeld and A.H. MacDonald, Phys. Rev. Lett. **85**, 3922 (2000).

[12] A.V. Balatsky, M.I. Salkola, and A. Rosengren, Phys. Rev. B **51**, 15547 (1995)

[13] G.G. Batrouni, V. Rousseau, R.T. Scalettar, M. Rigol, A. Muramatsu, P.J.H. Denteneer, and M. Troyer, Phys. Rev. Lett **89**, 117203 (2002).

[14] J.G. Bednorz and K.A. Müller, Z. Phys. **64**, 198 (1986).

[15] J. Bobroff, W.A. MacFarlane, H. Alloul, P. Mendels, N. Blanchard, G. Collin, and J.F. Marucco, Phys. Rev. Lett. **83**, 4381 (1999).

[16] J. Bobroff, H. Alloul, W.A. MacFarlane, P. Mendels, N. Blanchard, G. Collin, and J.F. Marucco, Phys. Rev. Lett. **86**, 4116 (2001).

[17] M. Bosch, W. van Saarloos, and J. Zaanen, Phys. Rev. B **63**, 092501 (2001);

[18] R.C. Budhani, M. Suenaga, and S.H. Liou, Phys. Rev. Lett. **69**, 3816 (1992).

[19] A.O. Caldeira, A.J. Leggett, Physica **121A**, 587 (1983).

[20] L. Capriotti, D.J. Scalapino, and R.D. Sedgewick, cond-mat/0302563 (2003).

[21] I. Carusotto, Y. Castin, and J. Dalibard, Phys. Rev. A **63**, 023606 (2003).

[22] I. Carusotto and Y. Castin, cond-mat/0209135 (2002).

[23] C.R. Cassanello and E. Fradkin, Phys. Rev. B **53**, 15079 (1996).

[24] C.R. Cassanello and E. Fradkin, Phys. Rev. B **56**, 11246 (1997).

[25] A.H. Castro Neto, Phys. Rev. B **64**, 104509 (2001).

[26] K. Chen, C. Jayaprakash, J. Phys.: Condensed Matter **7**, L491 (1995).

[27] A.A. Clerk, S.M. Girvin, and A.D. Stone, cond-mat/0211001 (2002).

[28] A.A. Clerk, unpublished.

[29] S.L. Cornish, N.R. Claussen, J.L. Roberts, E.A. Cornell, and C.E. Wieman, Phys. rev. Lett. **85**, 1795 (2000).

[30] E. Dagoto, Rev. Mod. Phys. **66**, 763 (1994).

[31] K. Damle, S. Majumdar, and S. Sachdev, Phys. Rev. A **54**, 5037 (1996).

[32] K. Damle, T. Senthil, S. Majumdar, and S. Sachdev, Europhys. Lett. **36**, 7 (1996).

[33] K.B. Davis, M.O. Mewes, M.R. Andrews, N.J. van Druten, D.S. Durfee, D.M. Kurn, and W. Ketterle, Phys. Rev. Lett. **75**, 3969 (1995).

[34] B. DeMarco and D.S. Jin, Science **285**, 1703 (1999).

[35] D. DeMille, Phys. Rev. Lett. **88**, 067901 (2002).

[36] E. Demler, S. Sachdev, and Y. Zhang, Phys. Rev. Lett. **87**, 067202 (2001).

[37] E.A. Donley, N.R. Claussen, S.L. Cornish, J.L. Roberts, E.A. Cornell, and C.E. Wieman, Nature **412**, 295 (2001).

[38] U. Dorner, P. Fedichev, D. Jaksch, M. Lewenstein, and P. Zoller, quant-ph/0212039 (2002).

[39] R.A. Duine and H.T.C. Stoof, cond-mat/0211514 (2002).

[40] J. Dziarmaga, A. Smerzi, W.H. Zurek, and A.R. Bishop, Phys. Rev. Lett. **88**, 167001 (2002).

[41] N. Elstner and H. Monien, Phys. Rev. B **59**, 12184 (1999).

[42] A.L. Fetter and J.D. Walecka, *Quantum Theory of Many-Particle Systems*, McGraw-Hill, New York (1971).

[43] V.S. Filinov, Mol. Phys. **88**, 1517 (1996).

[44] V.S. Filinov, Yu.E. Lozovik, A.V. Filinov, I.E. Zacharov, and A.M. Opartin, Physica Scripta **58**, 297 (1998).

[45] V.S. Filinov, P. Thomas, I. Varga, T. Meier, M. Bonitz, V. Fortov, and W.S. Koch, Phys. Rev. B **65**, 165124 (2002).

[46] M.P.A. Fisher, P.B. Weichman, G. Grinstein, and D.S. Fisher, Phys. Rev. B **40**, 546 (1989).

[47] A.M. Finkelstein, V.E. Kataev, E.F. Kukovitskii, and A.M. Teitelbaum, Physica C **168**, 370 (1990).

[48] M.E. Flatté, Phys. Rev. B **61**, R14920 (2000).

[49] H.F. Fong, P. Bourges, Y. Sidis, L.P. Regnault, J. Bossy, A. Ivanov, D.L. Milius, I.A. Aksay, and B. Keimer, Phys. Rev. Lett. **82**, 1939 (1999);

[50] M. Franz and Z. Tesanovic, Phys. Rev. B **63**, 064516 (2001);

[51] R. Franzosi and V. Penna, cond-mat/0205209 (2002).

[52] J.K. Fredericks and H. Monien, Europhys. Lett. **26**, 545 (1994).

[53] C.W. Gardiner, *Quantum Noise*, Springer-Verlag, Berlin Heidelberg (1991).

[54] C.W. Gardiner, *Handbook of Stochastic Methods*, Springer-Verlag, Berlin (1985).

[55] A. Georges, G. Kotliar, W. Krauth, and M. Rozenberg, Rev. Mod. Phys. **68**, 13 (1996).

[56] L.I. Glazman and M. Pustilnik, cond-mat/0302159 (2003).

[57] C. Gonzalez-Buxton and K. Ingersent, Phys. Rev. B **57**, 14254 (1998).

[58] M. Greiner, O. Mandel, T. Esslinger, T.W. Hänsch, and I. Bloch, Nature, **415**, 39 (2002).

[59] M. Greiner, O. Mandel, T.W. Hänsch, and I. Bloch, Nature, **419**, 51 (2002).

[60] Z. Hadzibabic, C.A. Stan, K. Dieckmann, S. Gupta, M.W. Zwierlein, A. Grlitz, and W. Ketterle, Phys. Rev. Lett. **88**, 160401 (2002).

[61] J.H. Han and D.H. Lee, Phys. Rev. Lett. **85**, 1100 (2000);

[62] A.C. Hewson, *The Kondo Problem to Heavy Fermions*, Cambridge University Press, Cambridge (1997).

[63] P. Hirschfeld, P. Wölfle, and D. Einzel, Phys. Rev. B **37**, 83 (1988).

[64] J.E. Hoffman, E.W. Hudson, K.M. Lang, V. Madhavan, H. Eisaki, S. Uchida, and J.C. Davis, Science **295**, 466 (2002).

[65] J.E. Hoffman, K. McElroy K, D.H. Lee, K.M. Lang, H. Eisaki, S. Uchida, and J.C. Davis, Science **297**, 1148 (2002).

[66] W. Hofstetter, J.I. Cirac, P. Zoller, E. Demler, and M.D. Lukin, Phys. Rev. Lett. **89**, 220407 (2002).

[67] C. Howald, H. Eisaki, N. Kaneko, M. Greven, and A. Kapitulnik, Phys. Rev. B **67**, 014533 (2003).

[68] C. Howald, H. Eisaki, N. Kaneko, and A. Kapitulnik, cond-mat/0201546 (2002).

[69] C. Howald, R. Fournier, and A. Kapitulnik, Phys. Rev. B **64**, 100504 (2001).

[70] B.L. Hu, J.P. Paz, and Y. Zhang, Phys. Rev. D **47**, 1576 (1993).

[71] E.W. Hudson, S.H. Pan, A.K. Gupta, K.W Ng, J.C. Davis, Science **285**, 88 (1999).

[72] E.W. Hudson, K.M. Lang, V. Madhavan, S.H. Pan, H. Eisaki, S. Uchida, and J.C. Davis, Nature **411**, 920 (2001).

[73] K. Ingersent and Q. Si, cond-mat/9810226 (1998).

[74] D. Jaksch, C. Bruder, J.I. Cirac, C.W. Gardiner, and P. Zoller, Phys. Rev. Lett. **81**, 3108 (1998).

[75] M.-H. Julien, T. Fehér, M. Horvatic, C. Berthier, O.N. Bakharev, P. Ségransan, G. Collin, and J.-F. Marucco , Phys. Rev. Lett. **84**, 3422 (2000).

[76] A. Kamenev, cond-mat/0109316 (2001).

[77] R. Kanamoto, H. Saito, and M. Ueda, Phys. Rev. A, **67**, 013608 (2003).

[78] V.A. Kashurnikov, N.V. Prokof'ev, and B.V. Svistunov, Phys. Rev. A **66**, 031601 (2002).

[79] M. Kasevich, private communication.

[80] G.M. Kavoulakis, Phys. Rev. A **67**, 011601 (2003).

[81] L.V. Keldysh, Zh. Eksp. Teor. Fiz. **47**, 1515 (1964); (Sov. Phys. JETP **20**, 1018 (1965)).

[82] B. Khaykovich, Y.S. Lee, S. Wakimoto, K.J. Thomas, R. Erwin, S.-H. Lee, M.A. Kastner, and R.J. Birgeneau, Phys. Rev. B **66**, 014528 (2002).

[83] B. Khaykovich, R.J. Birgeneau, F.C. Chou, R.W. Erwin, M.A. Kastner, S.H. Lee, Y.S. Lee, P. Smeibidl, P. Vorderwisch, and S. Wakimoto, Phys. Rev. B **67**, 054501 (2003).

[84] R. Kilian, S. Krivenko, G. Khaliullin, and P. Fulde, Phys. Rev. B **59**, 14432 (1999).

[85] J.I. Kishine, P.A. Lee, and X.-G. Wen, Phys. Rev. Lett. **86**, 5365 (2001).

[86] S.A. Kivelson, E. Fradkin, V. Oganesyan,I.P. Bindloss, J.M. Tranquada, A. Kapitulnik, and C. Howald, cond-mat/0210683 (2002).

[87] S.A. Kivelson, E. Fradkin, and V.J. Emery, Nature **393**, 550 (1998);

[88] M. Krämer, L. Pitaevskii, and S. Stringari, Phys. Rev. Lett. **88**, 180404 (2002).

[89] B. Lake, G. Aeppli, K.N. Clausen, D.F. McMorrow, K. Lefmann, N.E. Hussey, N. Mangkorntong, M. Nohara, H. Takagi, T.E. Mason, and A. Schröder, Science **291**, 1759 (2001).

[90] B. Lake, H.M. Rønnow, N.B. Christensen, G. Aeppli, K. Lefmann, D.F. McMorrow, P. Vorderwisch, P. Smeibidl, N. Mangkorntong, T. Sasagawa, M. Nohara, H. Takagi, and T.E. Mason, Nature **415**, 299 (2002).

[91] L.D. Landau and E.M. Lifshitz, *Statistical Physics*, Pergamon, London (1980).

[92] A.J. Leggett, Rev. Mod. Phys. **73**, 307 (2001).

[93] R.A. Lehrer and D.R. Nelson, Phys. Rev. B, **58**, 12385 (1998).

[94] C. Lobo, A. Sinatra, and Y. Castin, cond-mat/0301628 (2003).

[95] M.D. Lukin, M. Fleischhauer, R. Cote, L.M. Duan, D. Jaksch, J.I. Cirac, and P. Zoller, Phys. Rev. Lett. **87**, 037901 (2001).

[96] S.-k. Ma, *Modern Theory of Critical Phenomena*, Benjamin Cummings, Reading (1976).

[97] W.A. MacFarlane, J. Bobroff, H. Alloul, P. Mendels, N. Blanchard, G. Collin, and J.F. Marucco, Phys. Rev. Lett. **85**, 1108 (2000).

[98] A.V. Mahajan, H. Alloul, G. Collin, and J.F. Marucco, Eur. Phys. J. B **13**, 457 (2000).

[99] G.D. Mahan, *Many-Particle Physics*, Plenum, New York (1990).

[100] I. Martin and A.V. Balatsky, Physica C **341**, 125 (2000).

[101] I. Martin I, A.V. Balatsky, and J. Zaanen, Phys. Rev. Lett. **88**, 097003 (2002).

[102] K. McElroy, R.W. Simmonds, J.E. Hoffman, D.H. Lee, J. Orenstein, H. Eisaki, S. Uchida, and J.C. Davis, Nature **422**, 592 (2002).

[103] P. Mendels, J. Bobroff, G. Collin, H. Alloul, M. Gabay, J.F. Marucco, N. Blanchard, and B. Grenier, Europhys. Lett. **46**, 678 (1999).

[104] A. Messiah, *Quantum Mechanics*, North-Holland, Amsterdam (1965).

[105] G.J. Milburn, J. Corney, E.M. Wright, and D.F. Walls, Phys. Rev. A **55**, 4318 (1997).

[106] J.N. Milstein, S.J.J.M.F. Kokkelmans, and M.J. Holland, Phys. Rev. A **66**, 043604 (2002).

[107] N. Nagaosa and P.A. Lee, Phys. Rev. Lett. **79**, 3755 (1997).

[108] N. Nagaosa and P. A. Lee, Phys. Rev. B **45**, 966 (1992);

[109] J.W. Negele and H. Orland, *Quantum many-particle systems*, Addison-Wesley, Redwood City (1988).

[110] D.R. Nelson and H.S. Seung, Phys. Rev. B, **39**, 9153 (1989).

[111] M.R. Norman and C. Pepin, cond-mat/0302347 (2003).

[112] C. Orzel, A. K. Tuchman, M. L. Fenselau, M. Yasuda, and M. A. Kasevich, Science **291**, 2386 (2001).

[113] J. Pachos and P.L. Knight, quant-ph/0301084 (2003).

[114] S.H. Pan, E.W. Hudson, K.M. Lang, H. Eisaki, S. Uchida S, and J.C. Davis, Nature **403**, 746 (2000).

[115] K. Park and S. Sachdev, Phys. Rev. B **64**, 184510 (2001).

[116] C. Pépin and P.A. Lee, Phys. Rev. Lett. **81**, 2779 (1998).

[117] D. Podolsky, E. Demler, K. Damle, B.I. Halperin, cond-mat/0204011 (2002).

[118] A. Polkovnikov, S. Sachdev, and M. Vojta, Phys. Rev. Lett. **86**, 296 (2001).

[119] A. Polkovnikov, S. Sachdev, M. Vojta, and E. Demler, Int. J. Mod. Phys. **16**, 3156 (2002).

[120] A. Polkovnikov, M. Vojta, and S. Sachdev, Phys. Rev. B **65**, 220509 (2002).

[121] A. Polkovnikov, S. Sachdev, and M. Vojta, Physica C **388-389**, 19 (2003).

[122] A. Polkovnikov, Phys. Rev. B **65**, 064503 (2002).

[123] A. Polkovnikov, S. Sachdev, and S.M. Girvin, Phys. Rev. A **66**, 053607 (2002).

[124] A. Polkovnikov, cond-mat/0303629 (2003).

[125] A. Polkovnikov, cond-mat/0303628 (2003).

[126] *The Quantum Hall Effect*, ed. by R.E. Prange and S.M. Girvin, Springer, Heidelberg (1987).

[127] S. Raghavan, A. Smerzi, S. Fantoni, and S. R. Shenoy, Phys. Rev. A**59**, 620 (1999).

[128] N. Read and D. Newns, J. Phys. C **16**, 3273 (1983).

[129] N. Read and S. Sachdev, Phys. Rev. Lett. **62**, 1694 (1989).

[130] A.M. Rey, K. Burnett, R. Roth, M. Edwards, C.J. Williams, and C.W. Clark, cond-mat/0210550 (2002).

[131] S. Sachdev, *Quantum Phase Transitions*, Cambridge University Press, Cambridge (1999).

[132] S. Sachdev, Phys. Rev. B **45**, 389 (1992);

[133] S. Sachdev, Phys. Rev. B **59**, 14054 (1999).

[134] S. Sachdev, C. Buragohain, and M. Vojta, Science **286**, 2479 (1999);

[135] S. Sachdev, K. Sengupta, and S.M. Girvin,Phys. Rev. B **66**, 075128 (2002).

[136] S. Sachdev and N. Read, Int. J. Mod. Phys. B **5**, 219 (1991).

[137] M.I. Salkola, A.V. Balatsky, and D.J. Scalapino, Phys. Rev. Lett. **77**, 1841 (1996).

[138] M.I. Salkola, A.V. Balatsky, and J.R. Schrieffer, Phys. Rev. B **55**, 12648 (1997).

[139] F. Schreck, L. Khaykovich, K.L. Corwin, G. Ferrari, T. Bourdel, J. Cubizolles, and C. Salomon, Phys. Rev. Lett. **87**, 80403 (2001).

[140] T. Senthil and M.P.A. Fisher, Phys. Rev. B **60**, 6893 (1999).

[141] Y. Sidis, P. Bourges, H.F. Fong, B. Keimer, L.P. Regnault, J. Bossy, A. Ivanov, B. Hennion, P. Gautier-Picard, G. Collin, D.L. Millius, and I.A. Aksay, Phys. Rev. Lett. **84**, 5900 (2000).

[142] A. Sinatra, Y. Castin, and C. Lobo, J. of Mod. Optics **47**, 2629 (2000).

[143] A. Sinatra, C. Lobo, and Y. Castin, Phys. Rev. Lett. **87**, 210404 (2001).

[144] A. Sinatra, C. Lobo, and Y. Castin, cond-mat/0201217 (2002).

[145] D.L. Sisson, D. Doettinger, A. Kapitulnik, R. Liang, D.A. Bonn, and W.N. Hardy, Phys. Rev. B **61**, 3604 (2000).

[146] A. Smerzi, A. Trombettoni, P.G. Kevrekidis, and A.R. Bishop, Phys. Rev. Lett., **89**, 170402 (2002).

[147] M.J. Steel, M.K. Olsen, L.I. Plimak, P.D. Drummond, S.M. Tan, M.J. Collet, D.F. Walls, and R. Graham, Phys. Rev. B **58**, 4824 (1998).

[148] H.T.C. Stoof, J. of Low Temp. Phys., **114**, 11 (1999).

[149] B.M. Terhal, M.M. Wolf, and A.C. Doherty, Physics Today, **56** (4), 46 (2003).

[150] E. Tiesinga, B.J. Verhaar, and H.T.C. Stoof, Phys. Rev. A **47**, 4114 (1993).

[151] A. Trombettoni, A. Smerzi, and A.R. Bishop, Phys. Rev. Lett. **88**, 173902 (2002).

[152] A.G. Truscott, K.E. Strecker, W.I. McAlexander, G.B. Partridge, and R.G. Hulet, Science **291**, 2570 (2001).

[153] H. Tsunetsugu, M. Troyer, and T.M. Rice, Phys. Rev. B **51**, 16456 (1995).

[154] A. Tuchman, S. Dettmer, M. Fenselau and M. Kasevich, to be published.

[155] M. Vojta, R. Bulla, Phys. Rev. B **65**, 014511 (2002).

[156] M. Vojta, R. Zitzler, R. Bulla, and T. Pruschke, Phys. Rev. B **66**, 134527 (2002).

[157] M. Vojta, Phys. Rev. Lett. **87**, 097202 (2001).

[158] M. Vojta, C. Buragohain, and S. Sachdev, Phys. Rev. B **61**, 15152 (2000).

[159] M. Vojta and S. Sachdev, Phys. Rev. Lett. **83**, 3916 (1999).

[160] D.F. Walls and G.J. Milburn, *Quantum Optics*, Springer-Verlag, Berlin (1994).

[161] Q.-H. Wang and D.-H. Lee, Phys. Rev. B **67**, 020511 (2003).

[162] Z. Wang and P.A. Lee, Phys. Rev. Lett. **89**, 217002 (2002).

[163] S.R. White and D.J. Scalapino, Phys. Rev. Lett. **80**, 1272 (1998); Phys. Rev. B **61**, 6320 (2000).

[164] K.G. Wilson, Rev. Mod. Phys. **47**, 773 (1975).

[165] D. Withoff and E. Fradkin, Phys. Rev. Lett. **64**, 1835 (1990).

[166] B. Wu and Q. Niu, Phys. Rev. A **64**, 061603, (2001).

[167] A.G. Yashenkin, W.A. Atkinson, I.V. Gornyi, P.J. Hirschfeld, and D.V. Khveshchenko, Phys. Rev. Lett. **86**, 5982 (2001).

[168] A. Yazdani, C.M. Howald, C.P. Lutz, A. Kapitulnik, and D.M. Eigler, Phys. Rev. Lett. **83**, 176 (1999).

[169] J. Zaanen and A.M. Oles, Ann. Phys. **5**, 224 (1996).

[170] O. Zachar, S.A. Kivelson, and V.J. Emery, Phys. Rev. B **57**, 1422 (1998).

[171] O. Újsághy, J. Kroha, L. Szunyogh, and A. Zawadowski, Phys. Rev. Lett. **85**, 2557 (2000).

[172] D. Zhang and C.S. Ting, Phys. Rev. B **67**, 100506(R) (2003).

[173] G.M. Zhang, H. Hu, and L. Yu, Phys. Rev. Lett. **86**, 704 (2001).

[174] Y. Zhang Y, E. Demler, and S. Sachdev, Phys. Rev. B **66**, 094501 (2002).

[175] J.X. Zhu and C.S. Ting, Phys. Rev. B **64**, 060501 (2001).

[176] J.X. Zhu and C.S. Ting, Phys. Rev. B **63**, 020506(R) (2001).

[177] K. Ziegler, M.H. Hettler, and P.J. Hirschfeld, Phys. Rev. Lett. **77**, 3013 (1996).